SHOCK WAVE PROPAGATION THROUGH THE PRESSURE TUBES OF A CANDU-TYPE NUCLEAR REACTOR

by

SUBHASH CHANDRA SUTRADHAR,
B.E., Grad.Dip., M.Eng.

A Thesis

Submitted to the School of Graduate Studies

in Partial Fulfilment of the Requirements

for the Degree

Doctor of Philosophy

SHOCK WAVE PROPAGATION THROUGH THE PRESSURE TUBES OF A CANDU-TYPE NUCLEAR REACTOR

DOCTOR OF PHILOSOPHY (1985)
(Nuclear Engineering)

McMaster University
Hamilton, Ontario

TITLE: Shock Wave Propagation through the Pressure Tubes of a CANDU-Type Nuclear Reactor

AUTHOR: Subhash Chandra Sutradhar,

B.E. (Gauhati University, India)

Grad.Dip. (Indian Inst. Tech., Madras)

M.Eng. (McMaster University)

SUPERVISOR: Dr. J. S. Chang

NUMBER OF PAGES: xvi, 207.

ABSTRACT

The propagation of weak shock waves through a horizontal stratified two-phase system has been investigated both theoretically and experimentally to demonstrate the various facets of its interaction with the phases, fuel bundles and flow network branches. Two types of shock tubes are used: a lucite shock tube is utilized in monitoring the mechanism at the interface of the phases by high speed photography and the other one is an aluminum shock tube of 101.6 mm inner diameter with flow network branches is used in investigating the shock wave behaviour inside a pressure tube during blow-down and loss of coolant accidents.

This dissertation can be divided in to three broad categories. First, the inclusion of the interfacial roughness factor in the analysis of the shock wave propagation through a two-phase system inside a pressure tube weakens the strength of the shock waves, because of the energy loss due to frictional resistance at the interface. The interface is subjected to a combined effect of the waves propagating both in the gas and liquid phases of the system. High speed photography of the interface is considered to estimate the parameters pertaining to the generation of the ripples at the interface and the coupling of this parameter to a quasi-steady energy balance for the system can provide the values of the magnitude of the overpressures in the system.

Secondly, the interaction of weak shock waves with three different types of fuel bundles used in CANDU reactors is presented. Depending on the percentage of the flow area available, different fuel bundles produce different magnitudes of the overpressure. For the

transmitted waves, the choking is markedly observed even for moderate range of the shock waves. Presence of liquid phase enhances the strengths of overpressure for the reflected and transmitted waves. Inside the fuel bundles, the shock waves cause unusual vibrational effects which may be detrimental to the life of the fuel elements.

Around the network, the two-phase propagation velocity is observed to be same as the gas phase propagation velocity. Though tap and distilled water exhibit variations in the maximum overpressures, the time averaged magnitude under these two systems agree very well everywhere in the network branches. The vertical pressure profiles in the tap water has dispersive and high oscillatory nature whereas in the distilled water the rise in overpressure is dispersive, but smooth in nature. In distilled water, the pre-pulses moving under a free surface travel at the speed of sound in water and for those in tap water, this velocity is influenced by the presence of air bubbles in the tube walls.

ACKNOWLEDGEMENTS

I wish to express my sincere gratitude and appreciation to my supervisor Dr. J.S. Chang for his constant inspiration and support throughout the course of my study and other endeavours. I also like to thank my supervisory committee members, Dr. G.A. Irons and Dr. D.S. Weaver for their time and attention to this research.

I am grateful to Dr. H. Yoshida of Chiba University, Japan for providing valuable information and ideas during the early stage of this work. I also like to acknowledge the help of Mr. E.C. Morala for the basic understanding of the electronic equipments at the beginning of this research.

The warm and cordial friendship of the students in Thermohydraulics group of NRB will always be remembered. I wish to thank the staff of the Science Word Processing Centre for their assistance in the final preparation of this dissertation.

Finally, it is my wife Ulka, without whose constant inspiration with spirit and hope, this dissertation might have been not undertaken by me; And my daughter Priyanka, whose jocular notion of using the lucite shock tube as an aquarium for the gold fish might have consoled her to bear with my absence from home during many pleasant evenings.

TABLE OF CONTENTS

TABLE OF CONTENTS (Continued)

TABLE OF CONTENTS (Continued)

LIST OF FIGURES

LIST OF FIGURES (Continued)

LIST OF FIGURES (Continued)

LIST OF FIGURES (Continued)

LIST OF TABLES

NOMENCLATURE

Symbols	Descriptions
a	speed of sound
A	cross-sectional area
B	resistance of fuel bundle
c	specific heat
C	velocity of wave
C_i	width of interface
d	diameter
D	tube distensibility
e	internal energy /or porosity of fuel bundle
E	modulus of elasticity /or total energy
f	friction factor
F	friction force
$\dot{F}$	body force
G	critical flow rate
h	height of liquid
K	compressibility /or slip factor (dynamic property)
L	length in axial direction
$\dot{m}$	mass flux
M	Mach number
n	normal vector
p	pressure
q	heat flux
Q	body heating
Re	Reynolds number
S	perimeter

NOMENCLATURE (continued)

Symbols	Descriptions
S	perimeter
t	time
T	temperature /or shear stress per unit length
T_p	duration of a pulse
$\overline{T}$	stress tensor
u	fluid velocity
v	specific volume
$\overline{v}$	velocity vector
V	volume of fluid
w	velocity of a wave
x	mass fraction
y	co-ordinate direction perpendicular to tube axis
z	co-ordinate direction along the tube axis

Greek Symbols

α	void fraction
γ	ratio of specific heats
ϵ	roughness parameter
λ	wave length
μ	ratio of mass of gas to mass of liquid
ρ	density
τ	time period
ϕ	velocity potential
χ	circular wave number
ω	circular frequency

NOMENCLATURE (continued)

Symbols	Descriptions
Subscripts	
0	ambient condition
1	incident shock condition
2	reflected shock condition
3	transmitted shock condition
g	gas phase
i	interface
l	liquid phase
k	any phase k
T	two-phase system
w	parameter pertaining to wall

CHAPTER 1

INTRODUCTION

1.1 Problem Definition

The interaction of both shock waves and pressure waves (weak shock waves) occur in many industrial plants where the instantaneous release of chemical or mechanical energy generates high speed shock waves and a change in the fluid properties of the system is brought about by the excursion of these waves. Besides industrial sectors, the shock waves have tremendously wide variety of their generation, such as from the high energy bomb explosion down to the exhaust of the internal combustion engines. Similarly, the strengths of the shock waves also vary from high hypersonic to the near sonic types of flows. In the study of the shock waves, the compressibility of the medium into which these waves are propagating, is of primary importance for the determination and the analysis of the aftermath of the wave propagation. Although shock waves can occur in solid, liquid and gaseous substances, it is the gas phase medium, which is held responsible for the physical changes in many modern industrial systems.

The complications associated with the shock wave propagation through a two-phase gas-liquid system have called for the thorough

investigation and understanding of the problem from the perspectives of the nuclear reactor safety analysis. In nuclear reactors, particularly in CANDU-type reactors, where the horizontal pressure tubes comprise the main part of the Primary Heat Transport (PHT) system, the coolant flows through these pressure tubes under pressure to remove the heat from the fuel elements. In the event of Loss of Coolant Accidents (LOCA) the pressure waves may be generated in the system and the propagation of these pressure waves through the fuel bundles, different pipe connections and other sophisticated flow measuring devices may induce a lot of complicated effects inside the pressure tubes. Once the coolant from the pressure tubes has been drained off, then part of the hot fuel bundles is exposed to the hot steam. At that time, the Emergency Core Cooling (ECC) water (or fluid) coming in contact with the hot steam or fuels, generates pressure waves in the pressure tubes. These pressure waves propagating through the fuel bundles produce unstable pressure fluctuations that may cause the dislodgement of the fuel elements from the bundle assembly. The extent of the vibrational effects are the measure in the design for the durability of the fuel bundles under fast transient conditions.

Referring the works of Borisov et al (1965) and Sutradhar et al (1983), the propagation of the shock waves in stratified two-component fluid flow systems is observed to generate high degree of instability at the interface. The energy imparted to the wavy interface by the high energy gas flow behind the pressure waves causes the flow regime of the system to change drastically [Sutradhar et al (1983)]. The shock waves through the heavier phase propagating at a faster speed suffer multiple

reflections from the surface as well as from the solid boundary at the bottom. This mechanism induces perturbations at the smooth interface producing low amplitude ripples spread over the interface. The presence of incompressible liquid phase tends to enhance the shock wave strengths due to the reduction of the compressible phase of the system. The non-linear increase in the strengths of the shock waves with the increase in the liquid level will produce stronger shock waves upon their reflections from the fuel bundles or any other flow monitoring objects stationed inside the pressure tubes [Sutradhar and Chang (1985b)]. The details of these effects are attempted for the investigation in this work, and are categorically mentioned in the next section.

1.2 Organisation of the Thesis

In Chapter 1, the basic shock wave dynamics are discussed in detail. These classical results are important for the compressibility effects of the fluids under consideration. In two-phase stratified horizontal flows, the compressibility of the gas phase plays a very important role as compared to that of the liquid phase. In a stratified system, the propagation speed of a pressure or shock wave is controlled by the compressible parameters of the gas phase. The equations for the particle velocities induced by a shock in both the gas and liquid phases are also provided in this chapter.

In Chapter 2, the literature review pertaining to the work in this thesis is presented. This includes the works done in the branched pipe systems in the single phase as well as in the two-phase systems.

Both symmetric and asymmetric 'TEE' cases are considered. In both the cases, the emphasis is put on the experimental analysis than the theoretical evaluation for the pressure rise around the branched systems. The works of many researchers have shown that in the case of shock propagation through the junctions, the multi-dimensional flow phenomena near the junctions render the theoretical evaluation an incomplete piece of work. The literature review relating the two-phase phenomena is also discussed in Chapter 2 where a thorough estimation of the early works as well as the present day works have been reviewed. The latest works of Morioka and Matsui (1975) and Stone (1982) are also discussed here. The approach followed in this work is different from that of the above authors. In this work the interfacial phenomena are emphasized rather than the mathematical analysis of the wave propagation. The energy shared by the gas and the liquid phases and that lost at the interface due to the frictional effects is the basis for the mathematical model in estimating the magnitudes of the overpressures in the system. The turbulence generated by the shock waves moving through a two-phase system has been observed by Borisov et al (1965) and this turbulence is apparently held responsible for the flow regime change in the system.

The experimental method and related topics, such as the data acquisition, facility, methods, etc. are discussed in Chapter 3. The use of the APPLE-IIe micro-computer in the process of data acquisition and analysis has also been discussed. The tube distensibility, if admissible, will affect the magnitude of the overpressure developed in the phases under consideration. The effect of distensibility in the pressure tube is also discussed in this chapter.

The theoretical and the experimental works pertaining to the estimation of the interfacial friction parameter and pre-pulses through the liquid phase are presented in Chapter 4. The phase and group velocities are estimated for a wave propagating through a liquid bounded by a free and a solid surface. The distribution of the ripples at the interface is also confirmed using a high speed photography in a lucite duct. The overpressure in the gas and the liquid phases are theoretically estimated and compared with the experimental results obtained using the deaerated water for different liquid levels inside the pressure tube. The pressure profiles from the experimental observations in the lucite shock tube are also presented in this section for many different conditions of the experimental observations.

In Chapter 5, the shock wave interactions with the fuel bundles of different porosities in both single (gas) and two-phase systems are illustrated. Inside the fuel bundles, the pressure traces show oscillatory behaviour with the sharp peaks at various liquid levels. A model is developed to estimate the strengths of the reflected and transmitted shock waves for weak incident shock waves in a single (gas) phase system. The presence of the liquid inside the pressure tube also increases the strengths of the reflected shock waves for different fuel bundles.

In Chapter 6, the shock wave propagation through the branched pipe having single (gas) and two-phase systems is discussed from the experimental point of view. The enhancement of the pressure peaks due to the presence of the air bubbles in the ordinary tap water also shown

experimentally. In the last chapter, the conclusions and the scope of the future works in the analysis and application of the shock waves in nuclear reactor safety systems have been discussed. Finally, the references and the appendices are also provided to complete the work in this thesis.

1.3 Shock Wave Dynamics

1.3.1 Steady-State Shock Waves

The fluid compressibility, which is a measure of the fractional change in volume of the fluid element per unit change in the pressure has extensive application in modern high speed fluid dynamics. Compressible flow is routinely defined as 'variable density flow' [Anderson (1982)]; this is in contrast to the incompressible flow, where the density is assumed to be constant throughout the flow. The decrease in specific volume, dv for an infinitesimal increase in pressure, dp is related by a parameter, called the compressibility of the fluid, K and it is defined as

$$K = -\frac{1}{v}\frac{dv}{dp} = \frac{1}{\rho}\frac{d\rho}{dp} \qquad (1.1)$$

where the fluid density, ρ is the inverse of specific volume, v.

The fluid compressibility is associated with the rise in temperature of the fluid. The isothermal compressibility is estimated

at constant temperature and the isentropic compressibility is calculated under adiabatic condition neglecting the effects of viscosity and diffusion mechanisms. A measure of the compressibility of a fluid provides the information about the speed of sound wave in the medium under isentropic condition. In general, the speed of sound is specified as

$$a^2 = \frac{1}{\rho K} \tag{1.2}$$

In the case of a flowing fluid, the speed of sound is a significant measure of the effects of compressibility. The dimensionless parameter, Mach number M is a measure of the ratio of the speed of fluid to the local speed of sound in the medium i.e. M = u/a. So the speed of sound of a fluid depends on two properties of the fluid - one is the compressibility and other is the inertia, characterized by the specific density. The compressibility of fluid is also dependent on the temperature of the fluid. For gases, the adiabatic compressibility decreases with the increase in temperature, however, all liquids, including water, become less compressible the more they are compressed. The basic properties of air and water under normal conditions are provided in Table 1.1 below.

Table 1.1 Properties of Air and Water

	Air	Water
Compressibility (Sq.m/N)	1.0E-05	5.0E-10
Density (Kg/Cu.m)	1.21	1000.0
Speed of Sound (m/sec)	340.0	1450.0

Shock wave is a natural process in a supersonic (Mach number greater than unity) flow system and it offers an unique solution to the perplexing problems having to do with the propagation of disturbances in the flow. A shock wave is a discontinuity of very thin region (thickness is usually of the order of few molecular mean free paths, typically one-tenth of a micro-metre for air at standard conditions). To establish a shock wave in a flow, the flow velocity relative to the laboratory conditions must be supersonic and depending on the downstream conditions, a shock wave will be established in the flow. For a stationary shock wave, the total temperature remains unchanged and the other properties such as pressure and density are observed to increase downstream of the shock. After the shock wave, the velocity decreases and the flow becomes subsonic behind it. The standard relations, which are useful in the treatment of the shock wave may be available from the standard books on Gas Dynamics, for example, Liepmann and Roshko (1957), Shapiro (1953) etc.

In Figure 1.1, the fluid conditions upstream and downstream of a shock wave are represented using the suffixes 0 and 1 respectively. A measure of the overpressure p_1 is important from the experimental point of view as well as for the theoretical evaluation of the shock strength in terms of Mach number as follows.

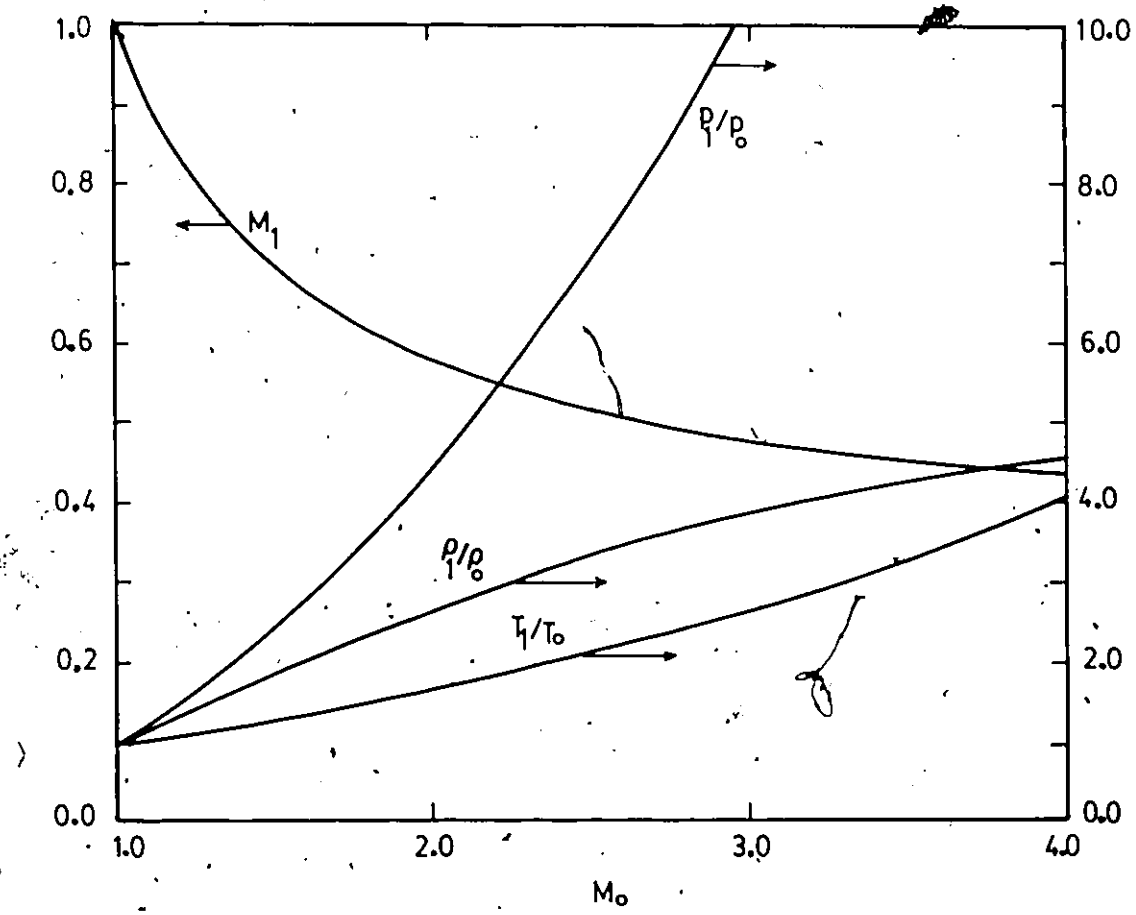

Fig. 1.1: Properties behind a normal shock wave as a function of upstream Mach number [Anderson (1982)].

$$M_0^2 = \frac{1+\gamma}{2\gamma}\frac{P_1}{P_0} - \frac{1-\gamma}{2\gamma} \tag{1.3}$$

where γ is the ratio of the specific heats of the fluid under consideration, and M_0 is the upstream Mach number.

Since the shock waves are the discontinuities of infinitely thin region and there is a significant change in the velocity across the shock wave, then a dissipative mechanism must be present within the shock wave structure. Hence, in flowing through a shock wave, a fluid particle passes from one state of equilibrium to another state of equilibrium. The available energy after a shock wave is less than that before the shock wave and therefore, in the absence of any heat transfer to the surroundings, an increase in the entropy must occur. Referring the work of Liepmann and Roshko (1957), it is noticed that across a shock wave, the entropy increases as the cube of the strength of the shock wave. The ratio

$$\frac{P_1 - P_0}{P_0} \tag{1.4}$$

is often used to define the strength of the shock wave. This ratio may also be expressed in terms of the Mach number as follows

$$\frac{P_1 - P_0}{P_0} = \frac{2\gamma}{1+\gamma}(M_0^2 - 1) \tag{1.5}$$

If the shock strength is less than 0.5 [Lighthill (1978)], the shock wave in this case is termed as the weak shock wave and under such circumstances, the entropy change across the shock waves are negligible. The total temperature across a stationary shock wave does not change, however, the shock wave is a non-isentropic process and this total pressure loss, if required, can be obtained in terms of the upstream Mach number of the flow.

1.3.2 Shock Waves in Water-like Substances

The behaviour of the shock wave in water-like substances is very different than that in the ideal gases and this situation is extensively dealt by Seeger and Polachek (1951) in their works. The mode of changes in the properties of a real gas undergoing a polytropic process is different from that of the water-like substances. In general, a gas undergoing such a specialized set of changes, however, does not fulfill the general requirements for a water-like substance. A weak shock wave when interacting with a water-like substance, exhibits both qualitatively and quantitatively different behaviour from those in ideal gases undergoing polytropic changes. The analysis forwarded by Seeger and Polachek (1951) indicates that most shock waves are comparatively weak after interacting with any water-like substance i.e. the changes in the overpressure and the entropy due to the shock wave are negligibly small. This statement can also be realized due to the fact of very low compressibility of the water as shown in Figure 1.2. The material or the particle velocity, which is a function of the overpressure, has negligible change under this condition.

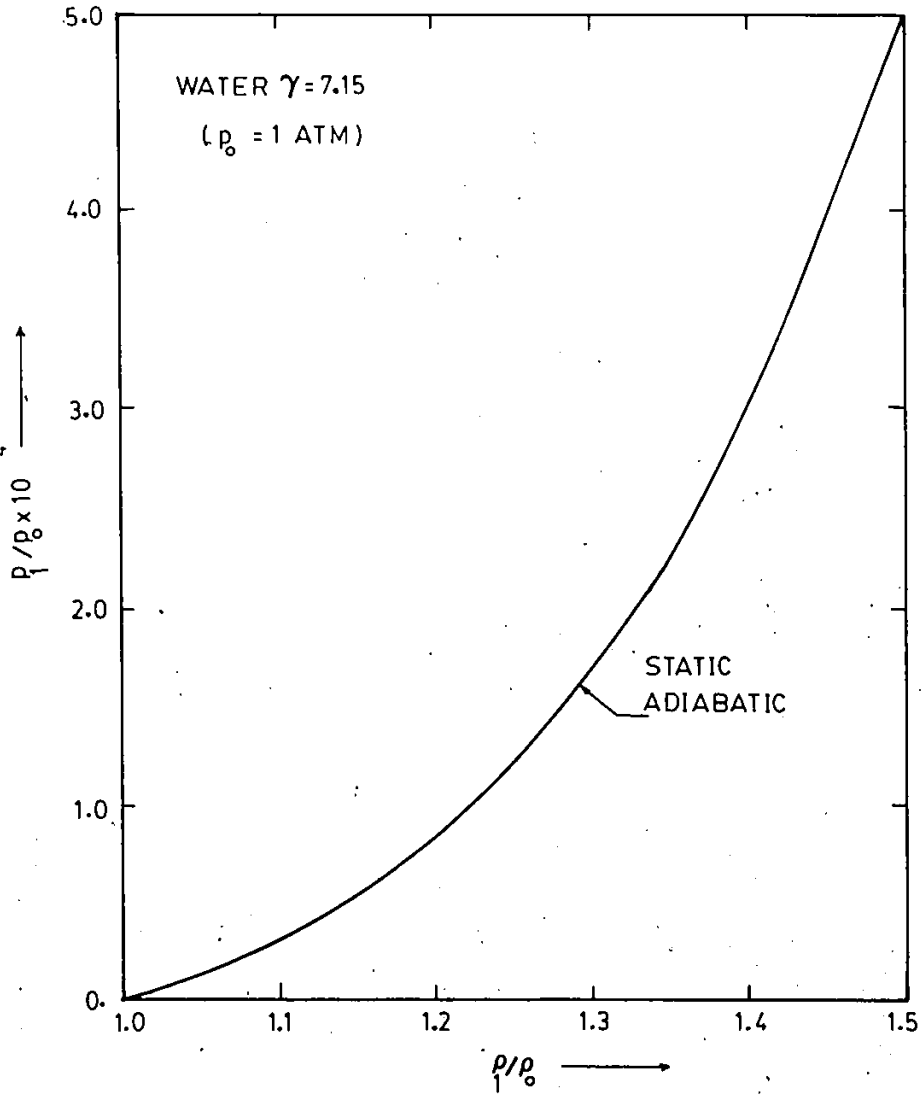

Fig. 1.2: Pressure density chart for water [Seeger and Polachek (1951)].

1.3.3 Unsteady Shock Waves

The basic mechanism about a stationary shock wave, fixed in space, is already discussed in the previous section of this chapter. However, when the wave is described as a physical disturbance in the flow, it propagates by the molecular collisions. Thus a shock wave has definite speed of propagation and this speed is usually higher than the speed of sound (supersonic) in the medium. In contrast to the steady flow, the unsteady flow is associated with the changes of variables with respect to space and time, that is, the flow parameters can be specified as $p = p(z,t)$, $u = u(z,t)$ and so on. The unsteady one-dimensional wave motion usually is studied in the shock tubes, as sketched in Figure 1.3. This is simply a tube which is divided by a diaphragm into two chambers of high (driver) and low (driven) pressures. Once the diaphragm is broken suddenly, thus releasing high energy in a very short time, a shock or compression wave is set off in the system, which moves in the low pressure chamber, and simultaneously, an expansion wave system starts moving in the opposite direction in the high pressure chamber. For a small pressure difference, the shock wave equations are approximated by the acoustic wave theory. The shock wave moving into the quiescent gas induces a mass motion, also called the fluid or particle velocity behind it in the direction of the motion of the wave. Referring Liepmann and Roshko (1957) and Lighthill (1978), it is found that the particle velocity is a function of the excess pressure produced in the system. In the absence of any heat transfer, the equations of mass and momentum for one-dimensional unsteady flows are

$$\frac{\partial \rho}{\partial t} + \nabla \cdot (\rho u) = 0 \tag{1.6}$$

$$\rho \frac{Du}{Dt} + \nabla p = 0 \tag{1.7}$$

where ρ, u and p are the fluid density, velocity and pressure respectively; and t and z are the time and space coordinates. The solution of these equations suggest that the speed of propagation, w of the acoustic wave with respect to the laboratory coordinates can be specified as

$$w = a_0 + \frac{\gamma+1}{2} u \tag{1.8}$$

and here a_0 is the sonic velocity in the undisturbed fluid and u, as mentioned earlier, is the particle velocity induced by the shock wave in the direction of the wave propagation. Most of the shock wave properties can be correlated to the magnitude of the overpressure generated by the shock wave and in view of the present day approach, these relations are extensively used in all the fields of shock wave research. The particle velocity in region (1) of the unsteady motion in Figure 1.3 is given as

$$u = a_0 \left(\frac{p_1}{p_0} - 1\right) \left[\frac{2/\gamma}{(1+\gamma)\ (p_1/p_0) + (\gamma-1)}\right]^{1/2} \tag{1.9}$$

The wave speed in terms of the overpressure is

$$w = a_0 \left[1 + \frac{\gamma+1}{2\gamma}(p_1/p_0 - 1)\right]^{1/2} \tag{1.10}$$

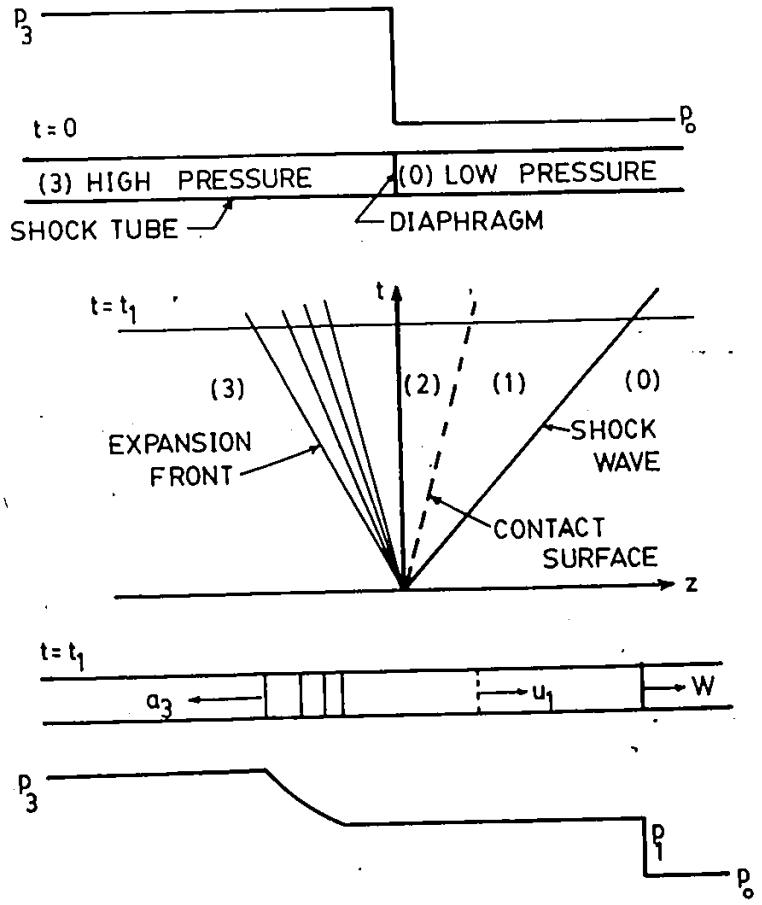

Fig.1.3: Motion in a Shock Tube [Liepmann and Roshko (1957)].

The changes in the other properties of the fluid undergoing a compression due to the shock wave may be found in the work of Liepmann and Roshko (1957), Shapiro (1953), and many other standard text books on Gas Dynamics. In a compressible flow, the change in the density due to the shock wave propagation as a function of pressure ratio is given as

$$\frac{\rho_1}{\rho_0} = \frac{(\gamma-1) + (\gamma+1)\ (p_1/p_0)}{(\gamma+1) + (\gamma-1)\ (p_1/p_0)} \tag{1.11}$$

The fundamental difference between a steady and an unsteady wave motion is that the stagnation properties across the shock waves in these two cases are not same. In the unsteady wave motion, the dynamic pressure term of the quiescent gas has no contribution in the determination of the stagnation properties for the gas phase into which the wave is propagating. Similarly, the magnitudes of the total pressures across the shock waves in both the cases have different magnitudes. Unsteady wave motion when considered in an incompressible fluid, which behaves more or less like a solid medium, the speed of sound in such a fluid has a very high value due to the low compressibility of the medium. The wave formation and its subsequent propagation is linear and as such the induced mass motion is insignificant. From Equations (1.4) and (1.5), neglecting the products of small quantities, the linearized equations of mass and momentum for an incompressible medium are

$$\frac{\partial \rho}{\partial t} + \rho \frac{\partial u}{\partial z} = 0 \tag{1.12}$$

$$\rho \frac{\partial u}{\partial t} + \frac{\partial p}{\partial z} = 0 \tag{1.13}$$

Assuming an irrotational potential flow and for small flow velocities, the wave motion induces a very gradual change of the fluid properties, then as per Lighthill (1978), from the above continuity and momentum equations, it can be shown that the magnitude of the induced overpressure due to the wave propagation may be stated as follows

$$p - p_0 = \rho_0 a_0 u \tag{1.14}$$

where p is the pressure due to the wave motion, ρ_0 is the density at a reference pressure p_0, a is the speed of sound and u is the corresponding particle velocity.

CHAPTER 2

LITERATURE SURVEY

2.1 Single-phase Straight and Branched Pipes

Shock waves, as discussed in the previous chapter, are the surfaces of discontinuity, across which the states of the fluids change abruptly; however, there is a flow of fluid matter through these surfaces of discontinuity. Shock waves in single phase compressible media have the origin in connection to the high speed flows, such as in the fields of aerodynamics and ballistics engineering. Numerous books and papers are published on the theory and applications of the shock waves in these areas of modern technology. The magnitudes of the changes of the fluid properties can now be evaluated unquestionably using the classical relations presented in any of the standard books of gas dynamics [Liepmann and Roshko (1957) and Shapiro (1953)]. It seems redundant to write more words in elaborating the basic principles of shock wave dynamics working with any compressible medium.

The study of shock waves in branched system is useful in the analysis of the propagation of blast waves in mine tunnels, in the exhaust pipes of reciprocating engines, and the structural failure of the pressure vessels. However, the work done until now regarding the

shock wave propagation in branched duct system under single phase flow conditions is very limited. The work is carried out in branched pipes with 'T' shape, 'L' shape and side branches having different angular orientations with respect to the main pipe assembly. In all the cases, both subsonic and supersonic flow behind the shock waves have to be considered, and this is also indicated by Hammitt and Carpenter (1964). The situation is depicted in Figure 2.1 where the conditions of incident shock wave, interaction of the shock wave with the junction producing subsonic and supersonic flow velocities behind the shock waves are respectively presented. For a subsonic flow velocity, a shock wave reflecting from the open end generates a system of expansion waves that move upstream of the shock tube and thus influencing the flow properties initiated by the principal incident wave - while at the same time, at locations 2 and 3 (Figure 2.1) two weak shock waves of different strengths start moving downstream of the junction. The theoretical solution at the junction itself is very complicated and poses a problem involving equations having three-dimensional parameters. Although many researchers are contented in visualizing the flow pattern around the junction using some optical techniques, however, to estimate the strength of the shock waves in the branches a quasi-steady flow phenomenon a few diameters downstream of the junction is considered by them with suitable loss coefficients of the junction. As per Hammitt and Carpenter (1964) the pressure losses at the junction are estimated from the steady incompressible flows, which for at least subsonic flow ranges agree well with the experimental results. In this respect, Deckker and Male (1967a,1967b) in their works followed the hydraulic analogy in order to estimate the losses in the junction using an incompressible

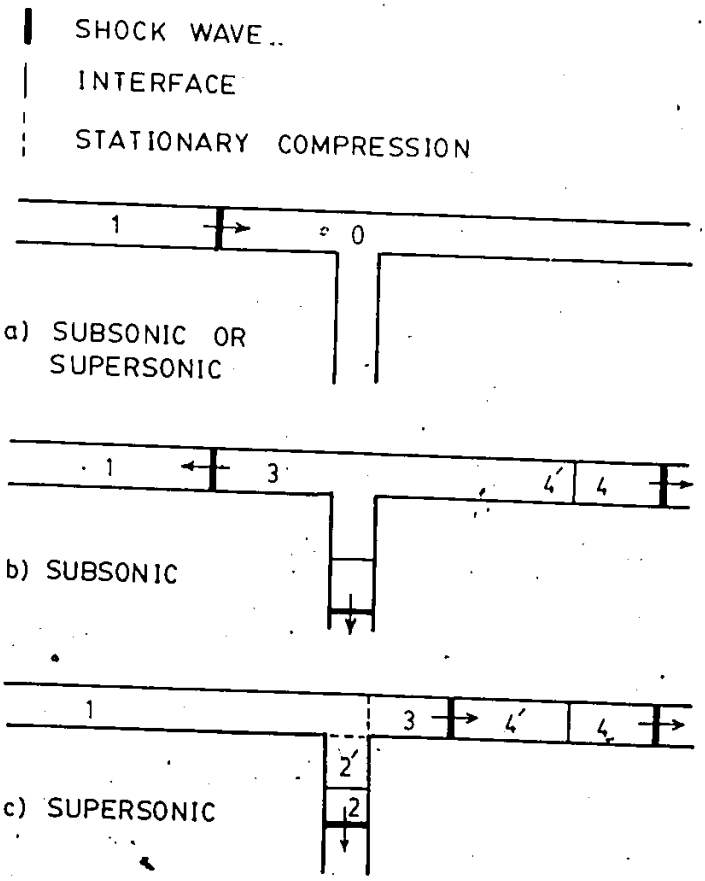

Fig.2.1: Wave motion in 'TEE' junction [Hammitt and Carpenter (1964)].

flow condition. The losses calculated in this way are then coupled to the conservative equations. However, the results obtained by Deckker and Male do not agree satisfactorily with the experimental results - even in some cases the results showed an opposite trend (Figure 2.2) than those predicted by the theory of the authors. The authors concluded that in the study of the flow around a junction, the best way to estimate the losses is to resort to an experimental procedure rather than to follow any theoretical evaluation. Also when the flow behind the shock wave is supersonic, the degree of disagreement found to be quite remarkable than that in the subsonic cases.

The failure of any theoretical analysis near the junction of an asymmetric 'T' may be realized due to the complexity of the waves at the junction (Figure 2.3). It is observed that the shock wave approaching the junction from left to right and after incident, the wave a b c is about to move in the side and main branches. Another expansion wave is generated at the junction and observed to move in the upstream direction. Next, as the waves move further into the branches, a bow shock wave k l m is generated at the corner of the junction, simultaneously another expansion wave is reflected from the wall of the main duct. Finally a finite shock wave is observed to be moving in the main branch and in the upstream direction of the junction. The pressure measured very near the junction does not provide any clear cut indication about the strength of the shock wave and as seen from the flow visualization system, an attempt in the theoretical evaluation may prove a futile exercise. Another idea of using the concept of stagnation pressure loss at the junction is also forwarded by Deckker and

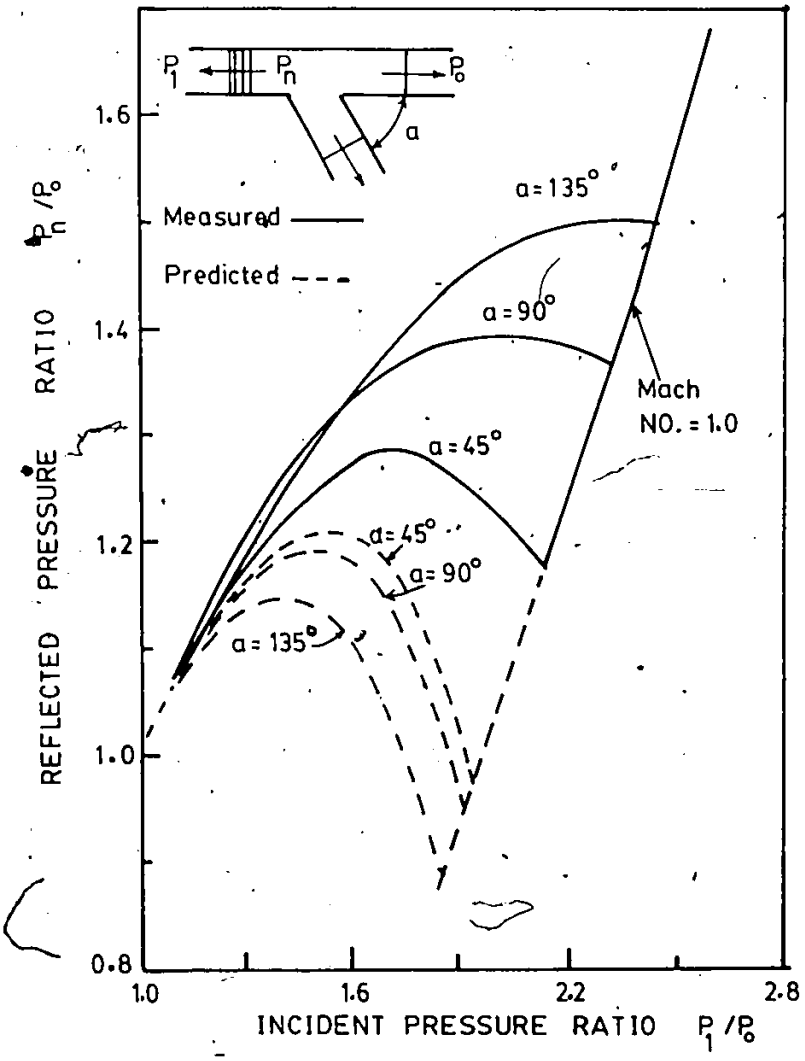

Fig.2.2: Pressure variation at junction entrance [Deckker and Male (1967a)].

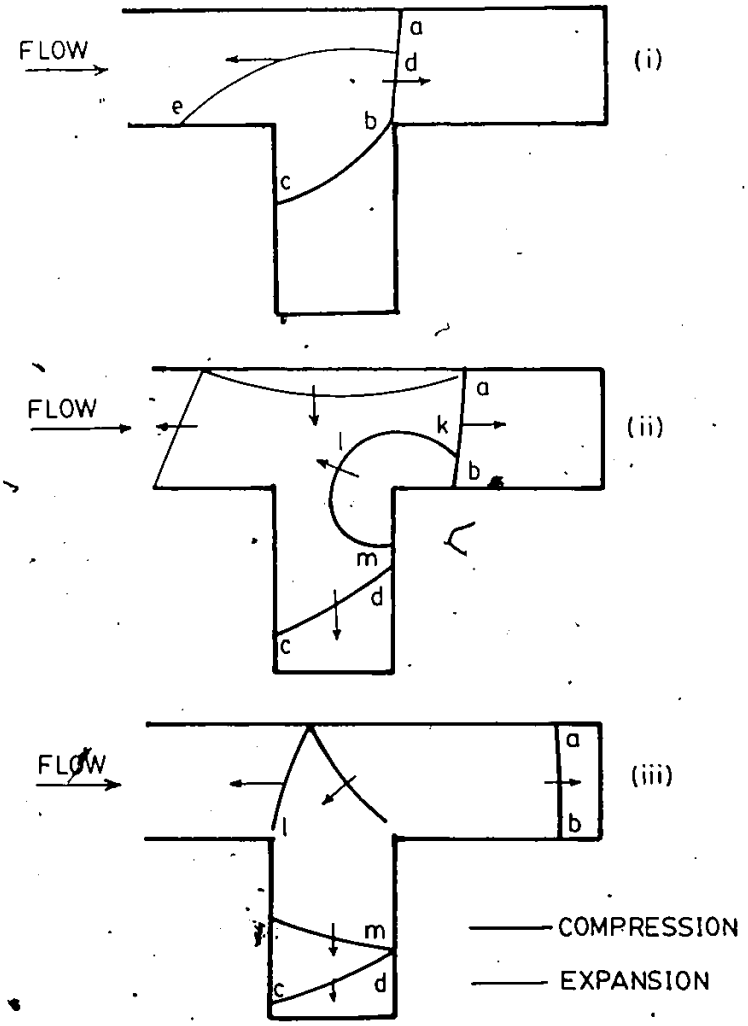

Fig.2.3: Flow development in an Asymmetric 'TEE' junction [Deckker and Male (1967b)].

Male (1967b), but the measurement of the stagnation pressure using any probe inside the shock tube may create some disturbanches in the flow stream. Also the method using the value of static pressure may not be accurate for the stronger shock waves interacting with the junction. On the other hand, for rarefaction wave, the work of Male et al (1969) shows better agreement between the predicted and experimental results. For rarefaction waves,however the system is assumed to be reversible adiabatic and the losses in the junction may be estimated from the hypothesis of an incompressible flow around the junction.

The re-orientation of 'T' junction i.e. to allow the shock wave to move along the perpendicular legs of the 'T' creates a similar type of problem in the evaluation of overpressure in the legs of the tube. The work of Wu and Ostrowski (1976) where the flow visualization technique is used to analyze the shock wave behaviour around a 90-degree turn, shows the complications associated with the theoretical treatment of the wave propagating through a bend. As shown in Figure 2.4, the multiple reflections of the compression waves at the junction generate a series of waves travelling upstream and other side branches of the tube. Summarizing the work of Wu and Ostrowski it can be stated that the essential features of the flow are: (1) diffraction of the incident wave, (2) formation of a vortex in the side branch, (3) reflection of incident and diffracted waves influenced by the reflection and diffraction processes. The diffraction and formation of vortex associated with the shock interaction at a corner are extensively studied by Skews (1967a,1967b). The strength of the transmitted shock wave in the side branch, according to the work of Sloan and Nettleton

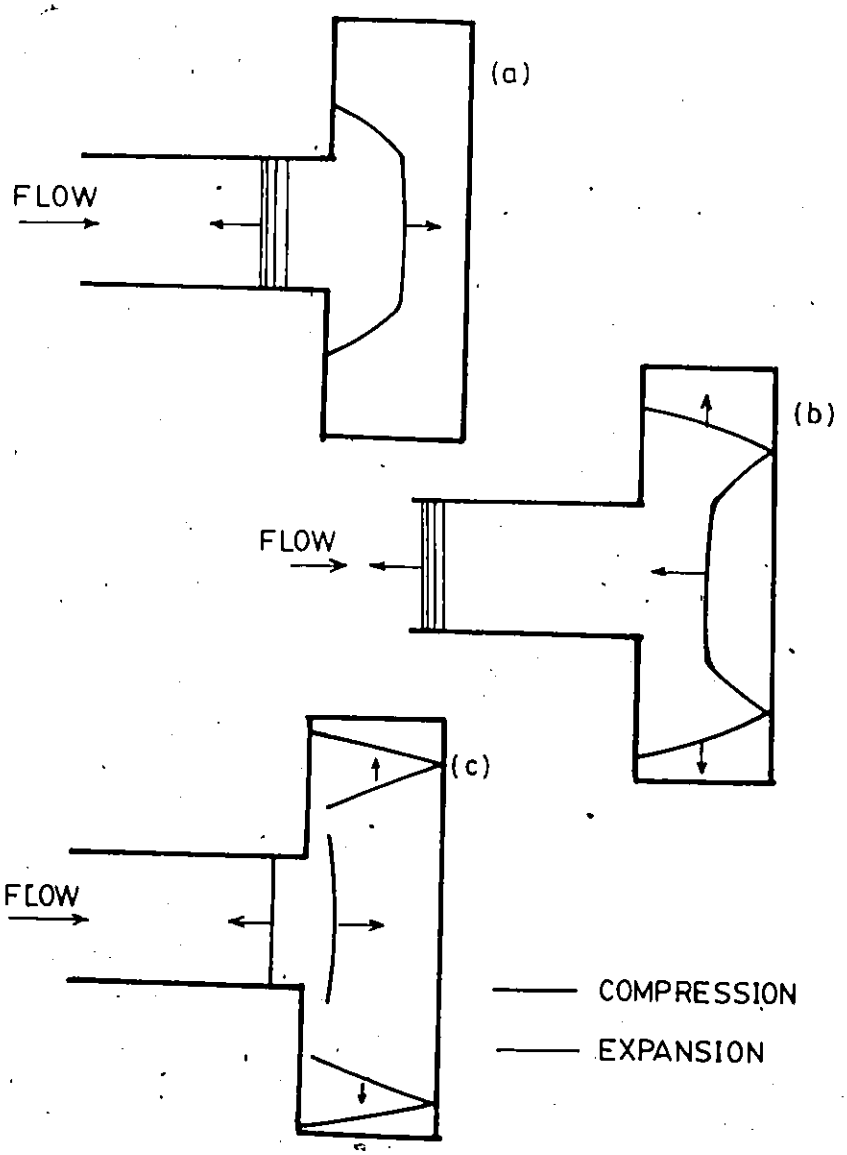

Fig.2.4: Flow development in a Symmetric 'TEE' junction [Wu and Ostrowski (1976)].

(1971), could vary considerably with the distance travelled by the shock wave.

2.2 Two Phase Straight and Branched Pipes

The very early work done in measuring the speed of sound in two-phase flow is due to Mallock in 1910 where the author evaluated the sonic speed in a liquid containing gas bubbles. Tangren et al (1949) mentioned the works of Ackeret (1930), Heinrich (1942), Charyk (1943) and Zwicky (1944) in connection with the measurement of the velocity of sound in a gas-liquid mixture. The work of Tangren et al contains valuable information of the propagation speed in gas-liquid mixture. The speed of sound in a homogeneous mixture is given by [Tangren et al (1949)]

$$a^2 = (\Gamma p/\rho_g)\ [\mu/(1+\mu)]\ [(1+\delta)/\delta]^2 \qquad (2.1)$$

where

$$\Gamma = (\mu c_p + c_f)/(\mu c_v + c_f)\ ;\ \delta = \mu\rho_f/\rho_g$$

p is the pressure , ρ_f and ρ_g are the fluid and gas mass densities respectively, c's are the specific heats. Campbell and Pitcher (1958) also inferred similar results using a vertical shock tube experiment with a diaphragm and air-water mixture. The sonic speed in this case is stated as

$$a^2 = (p/\rho)/[1- \rho/(1+\mu)\ \rho_f] \qquad (2.2)$$

where ρ is the mixture density, μ is the ratio of the mass of gas to the mass of fluid. It is also shown that the variation in pressure difference across the diaphragm of the shock tube has no significant effect on the propagation speed of the wave through the mixture.

Subsequent researchers such as Isbin et al (1957), Levy (1965), Moody (1965), Henry (1966), D'Arcy (1971), Dejong and Firey (1968), Henry and Fauske (1971), Mori et al (1975) and Evans et al (1970) have done extensive work about the sound wave propagation through two-phase homogeneous as well as separated mixtures. Though most of the work was directed towards the liquid containing gas bubbles and liquid containing dust particles, only a few have directed their attention to the case of separated flow systems. When both compression as well as expansion waves pass through a homogeneous steam-water mixture, Dejong et al (1968) noticed that for rarefaction wave, the energy transfer processes occur prior to or within the wave and consequent vapour condensation or liquid evaporation takes place at least partially (Figure 2.5). However, in case of compression waves the energy transfer processes and subsequent condensation of evaporation do not take place until the wave has travelled a large distance. Dejong could not succeed in predicting the critical flow rate at other working pressures than the experimental pressure. Henry (1970) deduced some important analytical solution for the sound speed in a homogeneous model as follows

$$a_{TP}/a_{HT} = 1.035 + 1.671\ \alpha \qquad (2.3)$$

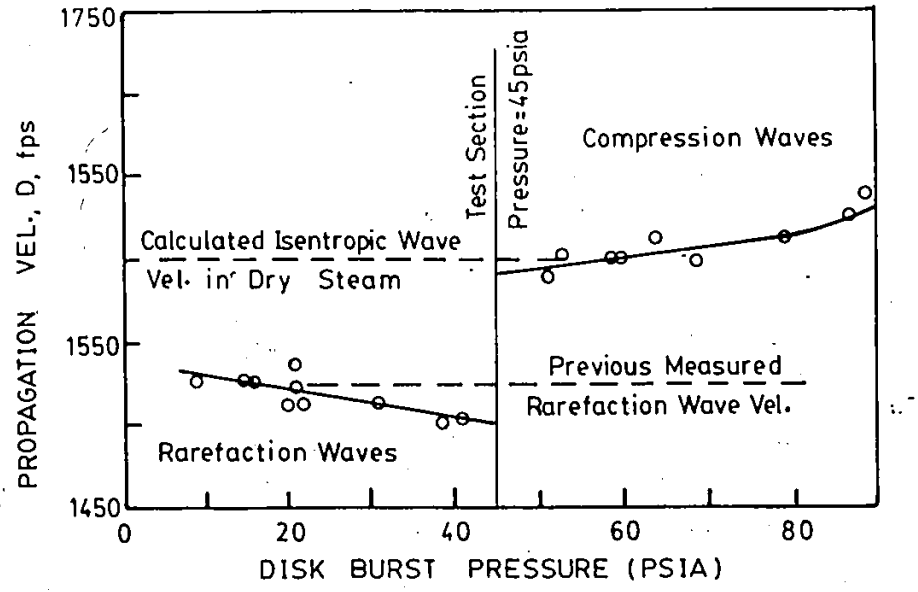

Fig.2.5: Compression and Rarefaction wave velocities in vapour-continuous, steam-water mixtures of 0.5 quality [Dejong and Firey (1968)].

where a_{TP} is the sound speed in two-phase model, a_{HT} is the sound speed in homogeneous isothermal model and α is the void fraction. This equation is compared with the results of earlier researchers and found to agree to a reasonable accuracy (Figure 2.6). Moody (1969) tried to develop a flow model where the vapor phase was at the centre of the liquid phase - a slip factor was defined as the ratio of the velocity of vapour to the velocity of liquid. A separated flow model was also tried with the inclusion of the slip factor. In Moody's work for separated flow model, it is noted that an adiabatic model with uniform liquid and vapour properties everywhere in the system is assumed. An unequal gas and liquid velocity has been assumed in the analysis. The dynamic property K is found to be related to the thermodynamic properties such as enthalpy, mass fraction etc. Considering the momentum and energy conservations across the pressure pulse for an isentropic case, the following relationships for critical flow and sonic velocity for a separated two-phase model may be presented. The critical flow rate [Moody (1969)]

$$G_{cs}^2 = (g/k_s) \left[\alpha^3/x^2 v_g + (1-\alpha)^3/(1-x)^2 v_l\right] \qquad (2.4)$$

and the sonic velocity is

$$a_s^2 = (g/k_s) \left[\alpha\, v_g + (1-\alpha)\, v_l\right] \qquad (2.5)$$

where the adiabatic compressibility is defined as

$$k_s = \left[(\alpha-1)/v_l\right] (\partial\, v_l/\partial p) - (\alpha/v_g)\, (\partial v_g/\partial p) \qquad (2.6)$$

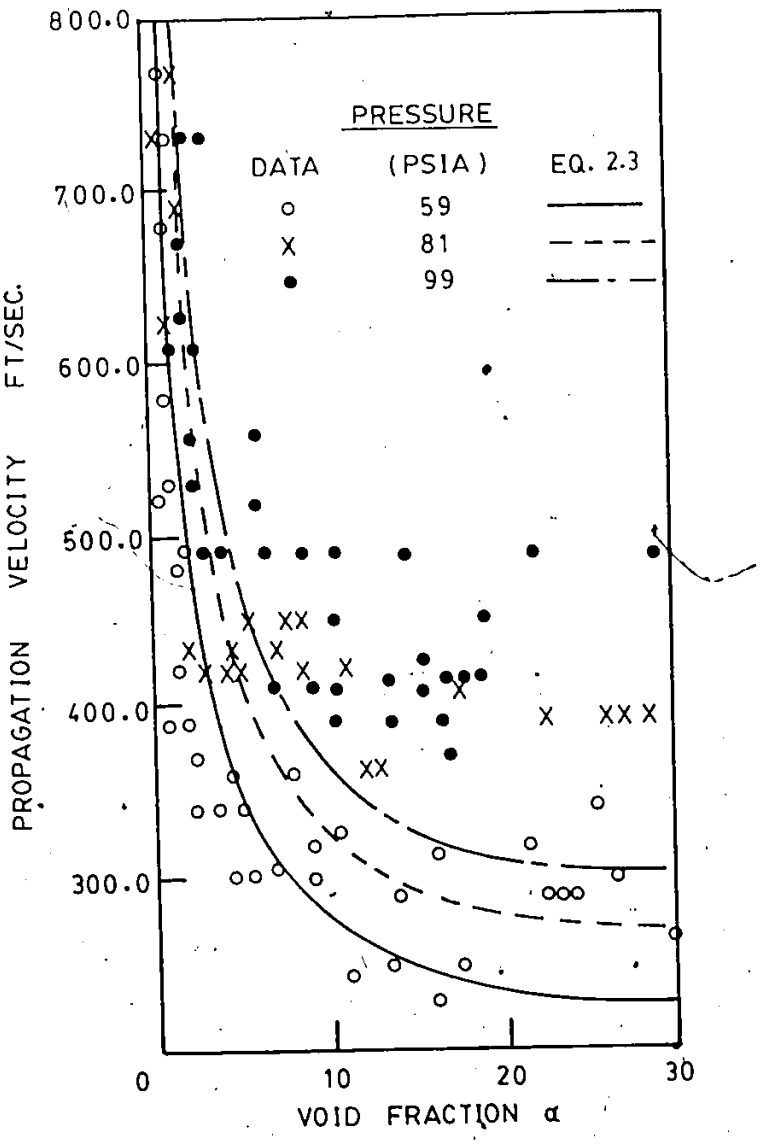

Fig.2.6: Comparison of propagation velocity as a function of void fraction with experimental data [Henry (1970)].

In the above equations a, x, v_g and v_l are the void fraction, mass fraction, specific volume of gas and specific volume of liquid respectively. Also for a separated flow model the derivative of dynamic property K with respect to pressure p is not equal to zero; whereas in case of a homogeneous model K=1, and the derivative of dynamic property with respect to pressure p is equal to zero. For steam-water flow model the above analysis shows that the critical flow rates are lowest for homogeneous phase pattern. Both the homogeneous and separated models are found to converge at the mass fraction of unity and toward the critical pressure of 3200 psi. The velocity ratio does not strongly affect the critical flow rate of the separated flow system. In contrast, the sonic velocity strongly depends on phase pattern. It is found to decrease with pressure in homogeneous pattern - however, in separated model it is affected by velocity ratio at low qualities. The discussion of Fauske and Grolmes in Moody's paper (1969) is also presented in Figure 2.7. D'Arcy also followed the single phase theory to evaluate the pressure pulse and arrived at similar results for separated flow model. It is found that there are different modes of propagation of disturbances at low and high void fractions.

In recent years, the works of Morioka and Matsui (1975), Matsui (1975), Stone (1983) and Sūtradhar et al (1983) show that the shock waves propagate one-dimensionally, but the transverse structure of the wave differs in gas and liquid phases and changes during the course of propagation. Morioka and Matsui (1975) have worked on the propagation of pressure waves through a stratified air-water system in a constant area rectangular duct where they used the complicated Laplace-Fourier trans-

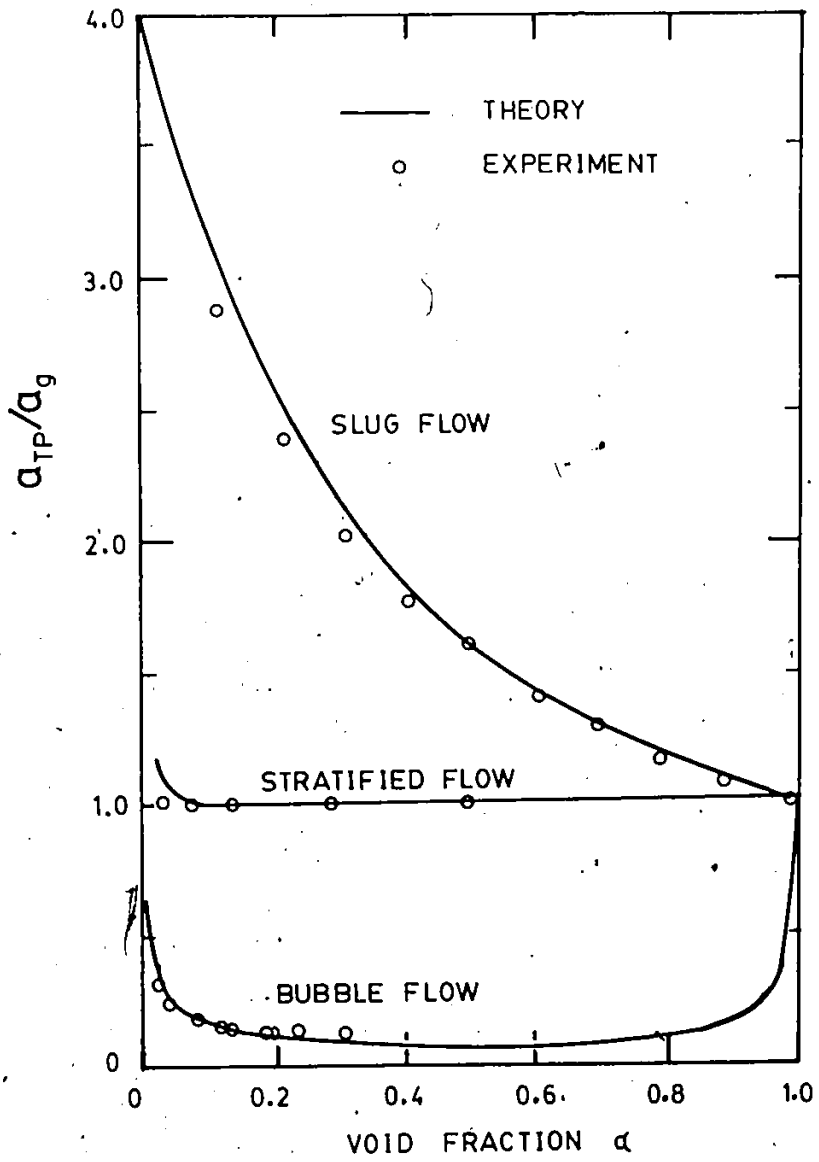

Fig.2.7: Measured and calculated pressure wave propagation velocities in air-water mixture at 25 psia [Moody (1965)].

form technique to solve the linearized two dimensional unsteady equations to show the dispersion structure of the wave in the liquid phase. It has been successfully shown by the authors that the weak pressure waves in this system are dispersive, possessing multiple modes which depend on the densities, thicknesses and the sound speeds of the phases. It is also suggested by them that a disturbance propagating through a separated gas-liquid system may consist infinite number of modes. Morioka and Matsui (1975) started with the following non-dimensional set of equations for each phase.

$$\frac{\partial}{\partial t}(\rho_k) + \frac{\partial}{\partial z}(\rho_k u_k) + \frac{\partial}{\partial y}(\rho_k v_k) = 0 \qquad (2.7)$$

$$\frac{\partial}{\partial t}(u_k) + u_k \frac{\partial}{\partial z}(u_k) + v_k \frac{\partial}{\partial y}(u_k) = -\frac{1}{\gamma \rho_* \rho_k} \frac{\partial}{\partial z}(p_k) \qquad (2.8)$$

$$\frac{\partial}{\partial t}(v_k) + u_k \frac{\partial}{\partial z}(v_k) + v_k \frac{\partial}{\partial y}(v_k) = -\frac{1}{\gamma \rho_* \rho_k} \frac{\partial}{\partial y}(p_k) \qquad (2.9)$$

$$\frac{\partial}{p_g}(p_k) = \gamma \rho_* a_*^2 \frac{\partial}{\rho_k}(\rho_k) \qquad (2.10)$$

where k represented either gas or liquid phase, ρ_* is the ratio of liquid to gas densities, a_* is the ratio of sound speeds in liquid to gas phases, u and v are the horizontal and vertical components of the velocity and p is the pressure in the phases. Equation 2.10, which is the equation of state for either of the phases, has been linearized in

the actual analytical derivation by Morioka and Matsui. Considering a disturbance of the form

$$p_k = p_0 (y) \exp [i (\chi z - \omega t)] \tag{2.11}$$

the above set of equations is solved to obtain the following dispersion relation.

$$\lambda \tanh (h\lambda) + (\lambda_* / \rho_*) \tanh [(1-h) \lambda_*] = 0 \tag{2.12}$$

where

$$\lambda^2 = \chi^2 - \omega^2 \; ; \; \lambda_*^2 = \chi^2 - \omega^2 / a_*^2 \tag{2.13}$$

Here, λ is the wave length, χ is the wave number and ω is the frequency and h is the liquid depth.

The pressure distributions along the upper and lower walls of the duct are expressed as follows

$$p_{g,y=h} = \sum_n \frac{2}{\pi} \int_0^\infty \frac{\sin (z\chi) \cos (t\omega_n)}{F (\nu, \lambda_*) \cos (h\nu)} \frac{d\chi}{\chi} \tag{2.14}$$

$$p_{l,y=(h-F)} = \sum_n \frac{2}{\pi} \int_0^\infty \frac{\sin (z\chi) \cos (t\omega_n)}{F (\nu, \lambda_*) \cosh [(1-h) \lambda_*]} \frac{d\chi}{\chi} \tag{2.15}$$

$$F(\nu, \lambda_*) = -\frac{\nu^2}{\nu^2 + a_*^2 \lambda_*^2}\left[1 + \frac{2(1-h)\lambda_*}{\sinh[2(1-h)\lambda_*]}\right] -$$

$$\frac{a_*^2 \lambda_*^2}{\nu^2 + a_*^2 \lambda_*^2}\left[1 + \frac{2h\nu}{\sin(2h\nu)}\right] \qquad (2.16)$$

where

$$\nu^2 = -\lambda^2 \qquad (2.17)$$

and ω_n is real function of χ provided from the dispersion Equation 2.12.

Morioka and Matsui (1975) have emphasized on the generation of solitons due to the wave propagation in a separated stratified system; however, Matsui (1975), working with the similar setup has not mentioned about the soliton in an air-water system. The experimental observations, such as high speed photography show that the changes in the interface is a very slow process as compared to the speed of propagation of the pressure wave. Also the magnitude of the overpressure measured experimentally in the gas and liquid phases are very close to each other and the variation is well within the experimental error. Though Matsui (1975) has worked experimentally on the similar system, he did not specify any difference in the overpressures of the phases. However, two separate expressions (Equations 2.14 and 2.15) are provided by Matsui for the theoretical analysis of the overpressures in the gas and liquid

phases based on the analytical technique of Morioka and Matsui (1975). The overpressures calculated by Matsui using this approach have shown agreement qualitatively with the experimental observations.

Stone (1983) and Duffey et al (1983) have also undertaken works similar to those of Morioka and Matsui (1975) and Matsui (1975) where the authors have accentuated on the theoretical investigation of the propagation of weak pressure waves in a stratified air-water system. Stone, in his review, stated that many of the assumptions leading to the theoretical work of Morioka and Matsui (1975) have not been observed to be valid. The vertical velocity in phase with the pressure, as assumed by Morioka and Matsui, has not been satisfied beneath the shock wave. According to Stone, the vertical component of the velocity can reach a high magnitude and this is in contrast to the assumptions made by Morioka and Matsui. Stone also tried to show, at least analytically, that five different classes of waves may be present in a two-phase stratified system through which a pressure wave is allowed to propagate. The propagation in water is concluded to be dominated by a Klein-Gordon type of equation. The second type of wave is the small amplitude pressure wave (more appropriately the pre-pulse) travelling along the liquid phase at a speed faster than the main pressure wave. An impulsive pressure applied on the water near a vertical wall may generate two types of wave travelling in the liquid phase. The last kind of wave is the shock wave propagating in the gas phase. The photographs of the experimental set-up of Stone (1983) give the impression that his long shock tube might not have been firmly secured on any permanent or heavy structure in order to reduce the effect of vibration

induced by the impingement of the pressure wave. Also the shock tube used in his experiment is a continuous one and this might transmit longitudinal waves along the walls of the tubes. These longitudinal waves will obviously influence the observed wave phenomena in the system. Stone adopted the linearized momentum equations together with the two-dimensional continuity equation steady with shock waves to find the solution of a finite amplitude pressure wave. The solution of these equations is obtained in terms of the density variation across a pressure wave as a function of shock speed, liquid depth , sound speed in liquid and the wave number. Stone has provided experimental data without sufficiently analysing these data. Like Morioka and Matsui (1975), he also tried to look for solitons, though theoretically, without undertaking any effort to visualize the interface using any high speed photographic technique. Though it is not clear whether a weak pressure wave will produce any solitary wave or not, however, the ranges of pressure waves selected by Stone, would not produce any solitary waves in an air-water system, as observed by the high speed photographic technique in this report. In other words, Stone has not paid any attention in order to look experimentally into the mechanisms present at the interface. Stone's work contains numerical analysis of the type of problem discussed in this work, however, the lack of proper analysis of the experimental data does not conclude the appropriateness of the theoretical analysis provided by Stone.

In the case of horizontal stratified gas-liquid system, the experimental observations done in rectangular tubes by Borisov et al (1965), Matsui (1975) and Sutradhar et al (1983) show that the slip in

velocity introduced between the phases by the propagation of the shock waves creates perturbations in the liquid surface which are then carried to the gas phase as small droplets. This phenomenon induces a flow regime transition from the stratified smooth to the wavy droplet flow condition.

2.3 Shock Wave Interaction with CANDU-Fuel Bundles

As a first approximation the fuel bundle assembly may be considered as an analogus system of a sudden contraction of the flow area. The work of Trengrouse and Soliman (1966) regarding the pressure wave in a sudden area change is worth mentioning here. The authors used the acoustic theory, the adiabatic theory and finally the isentropic theory to estimate the reflected and transmitted wave strengths for different area changes. However the predictions are very good for weak pressure waves in the subsonic range, but as the strengths of the shock waves increase, the difference between the theoretical and experimental values becomes more and more significant. This is shown in Figure 2.8 and Figure 2.9 for reflected and transmitted waves through a sudden area contraction. Also, for a small area and strong incident wave, the transmitted wave may suffer the condition of choking during its passage through the contracted area. The frictional effect, aggravating the choking in the case of subsonic range may also have to be taken into account in the system. In pure adiabatic or isentropic flow, the scope to include the frictional effect may not be adequate. The effect of choking has a non-linear characteristic on the flow phenomenon, hence when choking occurs in straight constrictions, the variation of the

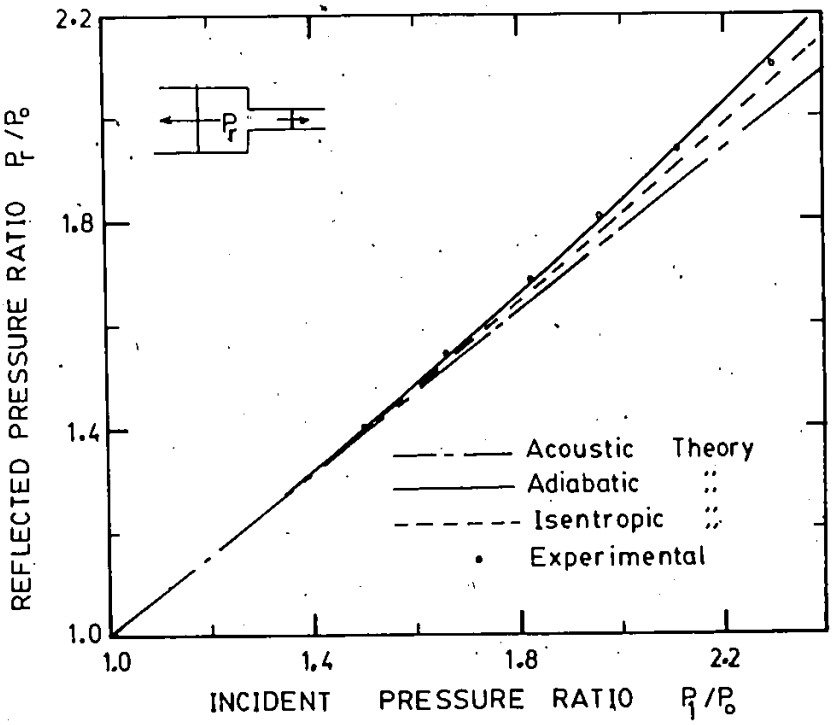

Fig.2.8: Reflected wave at sudden contraction [Trengrouse and Soliman (1966)].

pressure is no longer a linear one. Davies and Dwyer (1964) presented a theory for the pressure pulse in the exhaust systems of reciprocating engines based on the assumptions of one-dimensional, quasi-steady, isentropic flow. The experimental results for the expansion waves generated by a pressure pulse of 7.3 psi (gauge) have found to agree with the theoretical results.

On the other hand, the interaction of weak shock waves with the permeable materials in connection with the sound attenuation devices is gaining considerable attention in recent years. Compressible flow through porous material has been studied by Emanuel and Jones (1967) and Beavers and Sparrow (1971) where the authors aimed at the estimation of Mach numbers at different locations inside the porous materials. The reflection of the weak shock waves has been investigated by Beavers and Matta (1972) where the problem is formulated in connection with the shock speed upstream of the porous material to evaluate the strengths of the reflected shock waves. The flow through the fibrous porous materials with negligible inertia of the fluid has been extensively discussed by Collins (1961) and Schreagger (1957). Recently, Yoshida et al (1980) have formulated a theory in order to estimate the strengths of the waves through a porous material with single phase flow. The problem has been formulated by considering the fact that the porous medium has a certain resistance for the reflected and the transmitted waves generated by an incident shock wave. The relations for the physical quantities across the shock waves are considered using the laws of conservation of mass, momentum and energy based on the principle of Gas Dynamics for each of the incident, reflected and transmitted waves about the porous

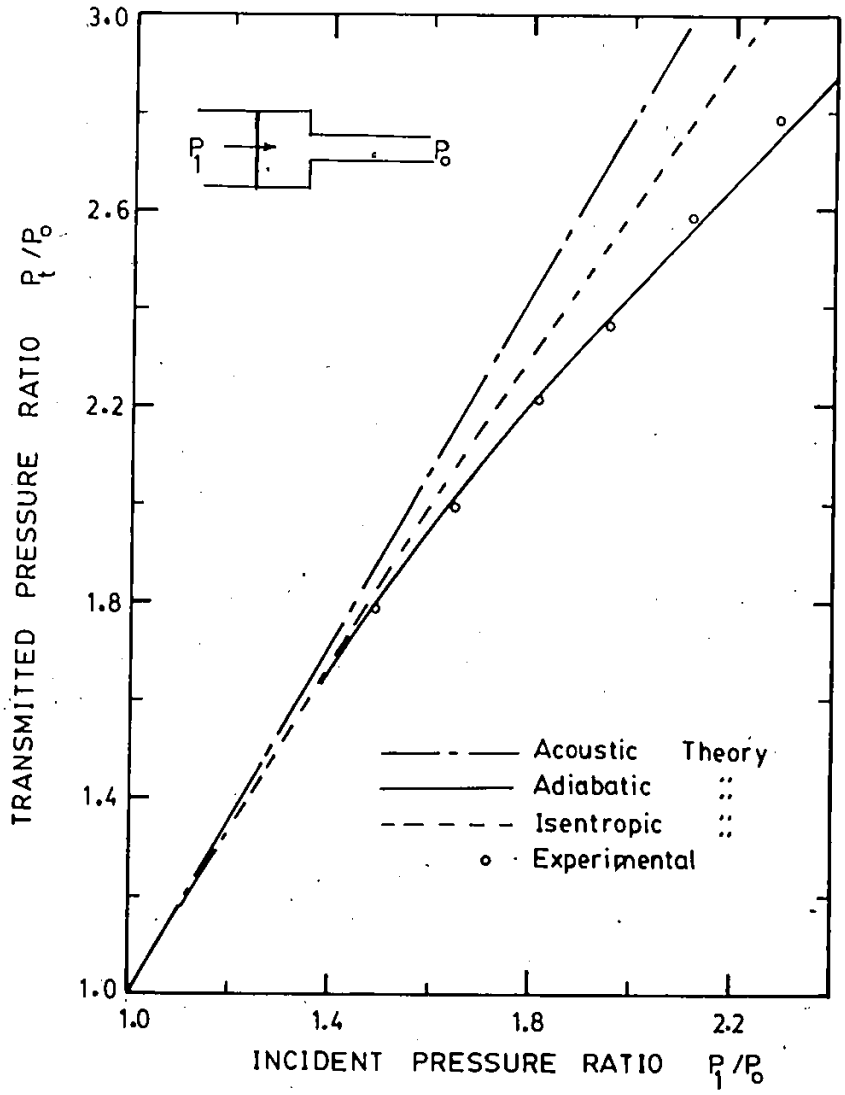

Fig.2.9: Transmitted wave at sudden contraction [Trengrouse and Soliman (1966)].

medium. The resistance term pertaining to each type of the porous materials has only been included in the momentum equation for the transmitted shock wave. For a very long porous material, where a transmitted wave may considerably attenuate during its course of propagation, in that case the reflected wave will not be influenced by the length of the porous medium. This statement may be realized because of the fact that the strength of a reflected wave will depend on the net solid area available to the incident shock wave. Also, the condition for choking, which might occur in a long constricted passage due to a strong shock wave, has not been mentioned in the work. The theoretical proposition forwarded by Yoshida et al (1980) has been found to be incomplete from the computational point of view. For eleven physical quantities, only ten equations are specified. However, a footnote at the beginning of the paper indicates the fact that the proposed theory agrees qualitatively with the experimental results and that further experiments are intended for the completeness of the theory.

In the presence of a two-phase stratified flow in a horizontal pipe, the shock wave interaction with the porous material presents a more difficult theoretical analysis. The extent of the information available in this connection from the literature review is very limited. Though the volume of liquid present in a stratified system in a duct may not change the strength of the shock wave very drastically, however, the expected moderate change in the wave strength needs to be carefully predicted for the durability of the fuel bundles used in a CANDU reactor.

CHAPTER 3

EXPERIMENTAL SET-UPS

3.1 Facility

3.1.1 Rectangular Lucite Duct

The aim of this set up is to investigate the interfacial behaviour of a two-phase stratified flow system during the passage of pressure waves over a smooth liquid surface. The pressure waves are set in the gas phase by bursting mylar diaphragms and these pressure waves are allowed to move through the two-phase stratified system. The basic structure of the lucite duct is shown in Figure 3.1. The liquid level could be varied to any suitable level (maximum up to 70.0 mm) and measured by using a steel ruler attached to the body of the duct. The duct is incorporated with the facility of replacing the liquid interface by suitably arranged plexiglass plates inside the duct so as to observe the effect of the area reduction of the gas phase on the wave propagation in single (gas) phase system.

The lucite duct is 140.0 mm X 163.0 mm and 1.50 meter long. The side walls are built using 19.0 mm thick plexiglass plates. The high pressure chamber which is separated from the low pressure chamber by a mylar diaphragm, is used to pressurize with air to a pressure of about

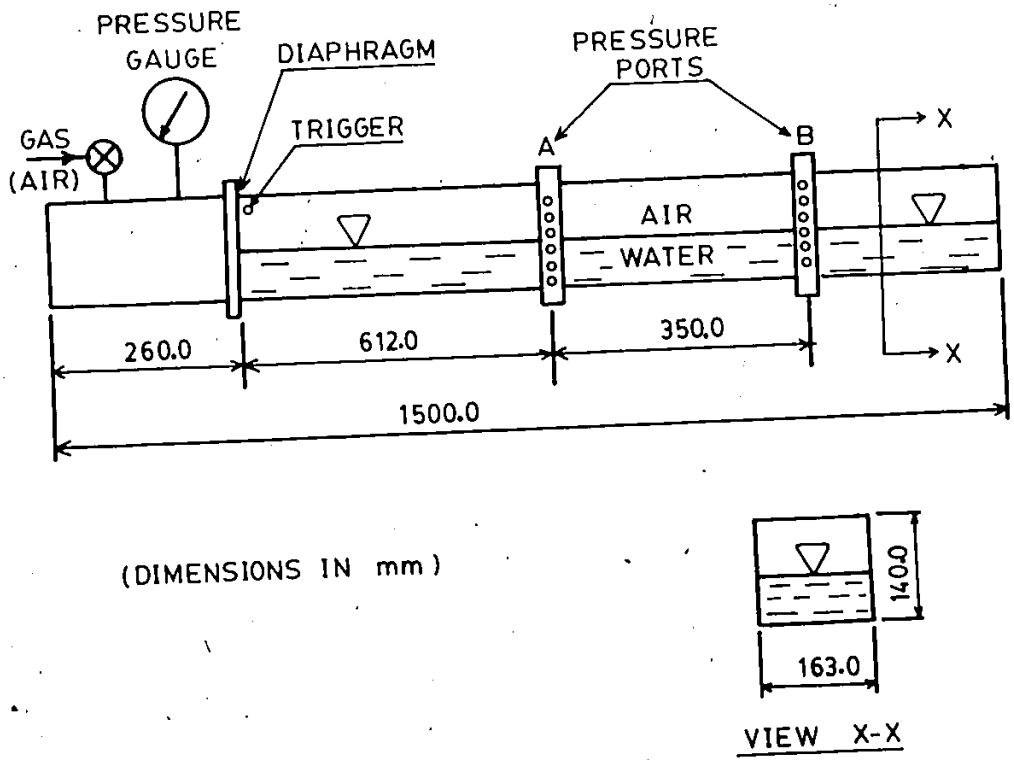

Fig.3.1: Rectangular lucite shock tube.

170.0 Kpa(abs) and the diaphragm is burst using a hypodermic needle placed inside the driven chamber. The pressure transducers can be placed at two locations A and B and the transverse pressure profiles are monitored by positioning the transducers at six vertical positions as shown in Figure 3.1. Also the block containing the transducers can be moved vertically up and down to adjust the transducer positions in transverse direction. The flow regime near the interface is recorded using a high speed movie camera with a frame speed of 1600 frames/sec. The enlarged prints of the selected exposures of the film are obtained for analysis and investigation of the surface waves produced due to the passage of the pressure waves through the phases.

3.1.2 Aluminum Pressure Tube

In order to study the CANDU pressure tube scenario in the event of loss of coolant accidents (LOCA), a 101.6 mm internal diameter, 6.35 mm thick aluminum pipe is used in designing a 1.5 meter long shock tube as shown in Figure 3.2. To eliminate the propagation of elastic waves through the wall of the tube, the shock tube is made up with two flange couplings interconnected using rubber gaskets. Also the mountings of the shock tube are provided with rubber paddings in order to alleviate the vibrational effects on the gas-liquid interface inside the tube.

A high pressure chamber of about 254.0 mm long and of the same cross-sectional area as of the pressure tube is attached at one end of the pressure tube so as to facilitate the loading and bursting of the mylar diaphragms for the generation of shock waves. The other end of

the shock tube may either be kept closed by an aluminum plate or be connected to network systems for the purpose of experimental investigation. The high pressure or driving chamber has a slide mounting with a screw drive in order to make the loading of the diaphragm more tractable each time of the operation. The pressure tube or the driven chamber is maintained under the atmospheric conditions in all the cases of the experiment and the driving chamber is pressurized by supplying compressed air at room temperature. The mylar diaphragms may be burst at desired pressures by pricking it with a suitable hypodermic needle located near the junction of the two chambers. To level the whole set up, the ultrasonic liquid level measuring technique, discussed later, is used. The liquid level is measured using two mechanical liquid meters one at the centre and other at the far end of the tube. The precise measurement of the liquid level is important for the accuracy in the measurements of the overpressures in the phases. The liquid level meter at the centre of the tube uses the principle of the U-tube manometer, and that connected at the far end of the tube utilizes the technique of direct viewing. The pressure waves in the gas and liquid phases are intercepted using piezotype pressure transducers (discussed later) at different locations C and D of the pressure tube, shown in Figure 3.2. Also to construct the transverse pressure profiles, attachments are provided to arrange the pressure transducers radially in a semicircular fashion from top to bottom at a definite angular position.

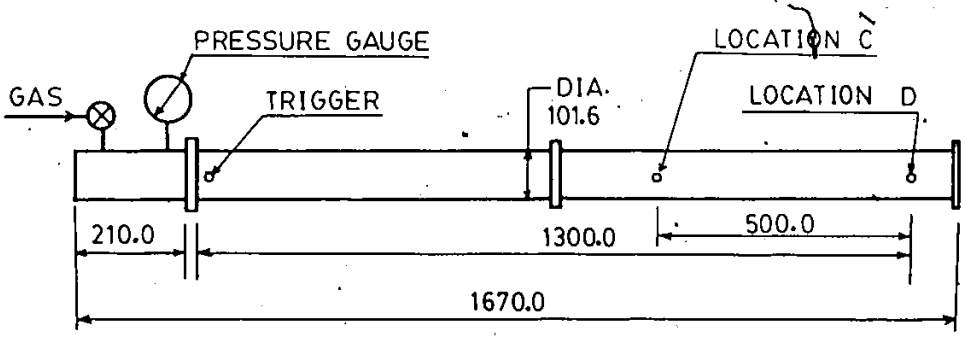

Fig.3.2: Aluminum pressure tube.

3.1.3 Branched Pipes

A welded 'TEE' section as shown in Figure 3.3 made out of the same size of aluminum pipe can be connected at the far end of the pressure tube through a flange coupling and rubber gaskets. Similar to the case of the straight tube, the levelling of the branched pipe is done using the ultrasonic technique. In order to ascertain the liquid level inside each leg of the branched pipe, two direct viewing type liquid level meters are attached to either side of the branched pipe. The 'TEE' section is used to investigate the pressure wave behaviour upstream and downstream of the 'TEE' junction with different liquid levels inside the whole system. The pressure wave propagation for at least two cases, symmetric 'TEE' and asymmetric 'TEE' may be studied with re-orientations of the branched pipe connections to the pressure tube. The branched pipe has the facility of recording the pressures at different locations downstream of the point of initiation of the pressure wave and these locations are marked as E, F, G and H for symmetric 'TEE' branch and K, L, M, N, P and Q for the asymmetric 'TEE' branch system. Each location has adapters arranged radially for the purpose of the investigation of the transverse pressure profiles at each location of the pressure tube assembly.

3.1.4 Pressure Tube with Fuel Bundle

Different CANDU fuel bundles may be inserted inside the pressure tube and the incident pressure waves of different strengths may be allowed to interact with the fuel bundles in order to detect the

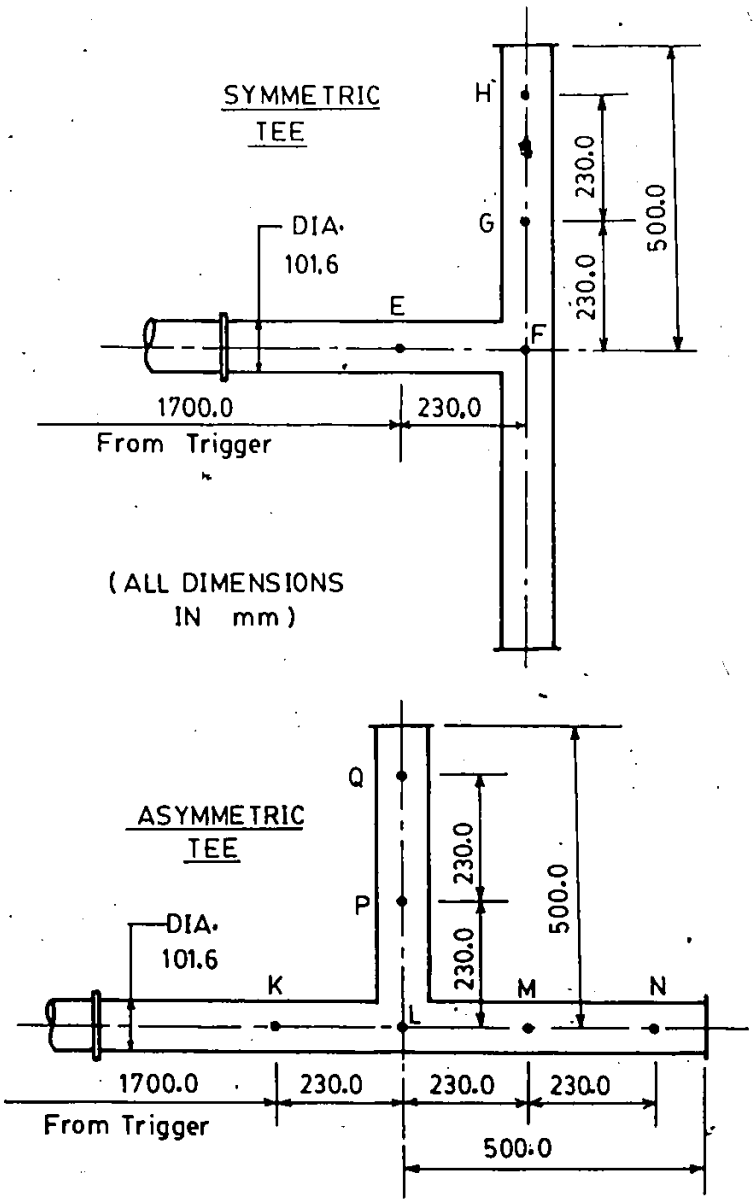

Fig.3.3: Symmetric and Asymmetric branched pipes.

strengths of the reflected and transmitted waves under single and two phase conditions. Three fuel bundles, 18-element, 28-element and 37-element may be positioned near the far end of the straight shock tube. Two small screws each about 3.2 mm in diameter are used to fix the bundle inside the pressure tube. The pressure transducers are positioned upstream and downstream of the bundles as shown in Figure 3.4. Also the pressures midway of the fuel bundles may be measured in a similar way. The high pressure chamber is supplied with pressure ranging from 190 Kpa to 300 Kpa(abs) in order to obtain different strengths of the incident pressure waves while the liquid level is varied from 0.0 to 50.0 mm.

3.1.5 Check For Tube Distensibility

Due to the bursting of a mylar diaphragm, which separates the high pressure driving chamber from the low pressure chamber, a sudden pressure energy is released near the entrance of the low pressure chamber. If the magnitude of the impulsive pressure is comparable to the Hoop stress developed in the tube wall, then the effect of the tube distensibility will be felt on the propagation of the pressure wave. Obviously, the effect will be predominant in a thin walled tube than in a tube with thicker wall.

If d is the inner diameter of a thin walled tube with wall thickness s, the force per unit axial length acting inside the tube due to the overpressure (pressure behind a shock wave), p_1 is the product of p_1 and d and this in turn generates a Hoop's stress along the

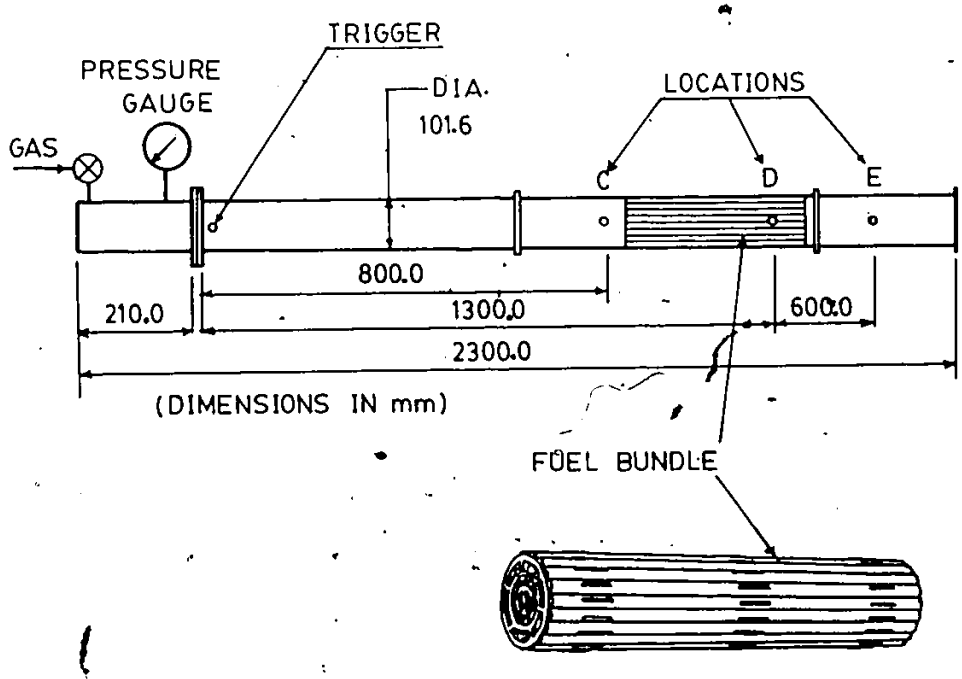

Fig.3.4: Fuel bundle and pressure ports on the pressure tube.

circumference of the tube having the following magnitude.

Stress in the tube wall is

$$\frac{p_1 d}{2s} \tag{3.1}$$

Using the bulk modulus of elasticity E for the tube material (here commercial Aluminum), the wall strain is calculated as follows.

Strain in the wall is equal to

$$\frac{p_1 d}{2sE} \tag{3.2}$$

As for the circular tube, the total elongation of the circumference is equal to

$$\frac{\pi p_1 d^2}{2sE} \tag{3.3}$$

The maximum pressure used for the experimental purposes is about 180.0 KPa(gauge) and this produces a shock wave of incident pressure of approximately 90.0 KPa(gauge); the diameter of the tube is 0.1016 meter, thickness s is equal to 0.00635 meter and the value of E is 71.0 Giga-Pascal for the commercial Aluminum, then the maximum wall elongation of 6.0 micro-meter is produced by a pressure of 180.0 KPa(gauge).

To understand the effect of the tube distensibility on the propagation of pressure waves, the continuity and momentum equations are considered here. Following the work of Lighthill (1978), the equations are written as

$$\partial(\rho A)/\partial t + \partial(\rho A u)/\partial z = 0 \tag{3.4}$$

$$\rho(\partial u/\partial t + u\,\partial u/\partial z) = -\partial p_1/\partial z \tag{3.5}$$

Considering a negligible entropy change across the pressure waves considered here, the above equations may be linearized as follows

$$\partial(\rho A)/\partial t + \rho_0 A_0\,\partial u/\partial z = 0 \tag{3.6}$$

$$\rho_0\,\partial u/\partial t = -\partial p_1/\partial z \tag{3.7}$$

Evaluating the second order partial derivatives with respect to time and space from the above equations and equating them, the equation of the wave propagation is obtained as

$$\partial^2 p_1/\partial z^2 = \frac{1}{A_0}\,\partial^2(\rho A)/\partial t^2 \tag{3.8}$$

Here ρ_0 and A_0 are estimated from

$$\rho = \rho(p_1) \tag{3.9}$$

$$A = A(p_l) \tag{3.10}$$

for $p_l = 0$ and Equation 3.8 is transformed as

$$\frac{\partial^2 p_l}{\partial z^2} = \frac{1}{a^2} \frac{\partial^2 p_l}{\partial t^2} \tag{3.11}$$

where the velocity a is defined as

$$\frac{1}{a^2} = \frac{1}{A_0} \left[\frac{d(\rho A)}{dp_l}\right] p_l = 0 \tag{3.12}$$

The value of the wave speed a will be affected by the tube distensibility, the above equation may be written as

$$\frac{1}{\rho_0 a^2} = \left[\frac{1}{\rho} \frac{d\rho}{dp_l} + \frac{1}{A} \frac{dA}{dp_l}\right] p_l = 0 = K + D \tag{3.13}$$

where K is the compressibility of the fluid and D is the distensibility of the tube.

The compressibility effect is attributed mainly due to the presence of the gas phase in a two-phase system, and the value of the compressibility is

$$\left(\frac{1}{\rho a^2}\right)_{gas} \tag{3.14}$$

but for the presence of the liquid-phase, a mean density of 1000.0 Kg/cu.m. may be used in estimating the compressibility value K. So with a=340.0 m/sec in air and a mean density of 1000.0 Kg/cu.m., the compressibility is obtained as K = 8.65 nano-sq.m/N. If the tube is filled completely with water, then for a=1450 m/sec, the compressibility K=0.51 nano-sq.m/N is obtained.

The diametrial strain is calculated as

$$\frac{p_1 d}{2sE} \tag{3.15}$$

and the relative increase in the area of the tube

$$\frac{A-A_0}{A_0} = \left[1 + \frac{p_1 d}{2sE}\right]^2 - 1 \approx \frac{p_1 d}{sE} \tag{3.16}$$

The distensibility D is calculated as

$$D = \frac{A-A_0}{A_0}\left(\frac{1}{p_1}\right) = \frac{d}{sE} \tag{3.17}$$

For the aluminum pressure tube considered here, the value of the distensibility D is 0.224 nano-sq.m/N.

The compressibility value for the tube completely filled with liquid is comparable to the distensibility value calculated above. But

in a stratified system, the presence of the gas-phase increases the compressibility effect more compared to the distensibility effect of the tube. Hence the distensibility effect of the tube may safely be discarded in the analysis of the propagation of the pressure waves considered in this work.

3.2 Instrumentation

3.2.1 Pressure Transducers

Piezoelectric pressure transducers (Figure 3.5) of Sundstrand Data Corporation, Model 211B5 are used in the experimental measurements of the strengths of the shock waves. The quartz pressure transducers work on the principle that when certain crystals are stressed they produce a surface potential difference in appropriate direction. In Sundstrand transducers, the stack of quartz plates are arranged interleaving by gold electrodes and when the crystals are subjected to dynamic pressure loading, the charges produced by the individual quartz plate are summed up to produce an appropriate charge output. A predetermined pre-load is applied to the quartz plates so as to enable the transducers to be used in detecting the pressures below atmospheric condition. The signal output from the transducer has a high impedance electrostatic charge which may be fed to an oscilloscope or a transient memory to register the signal in the desired form. An integral converter is mounted within the transducer which cancels the effect of acceleration of the quartz plates for a very rapid pressure jump. The transducers produce a linear voltage output with an impedance of less

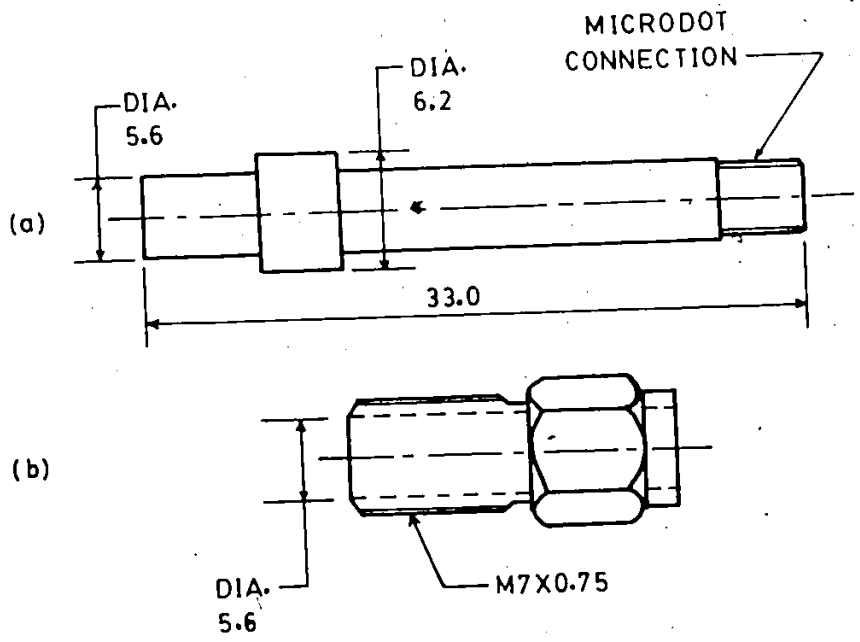

Fig.3.5: Sketch of (a) Transducer and (b) Floating nut.

than 100 Ohms. The transducer characteristics are summarized in Table 3.1. The transducer includes a stainless steel casing with a co-axial electrical connector at one end, and at the other end, a stainless steel diaphragm covers the cavity containing the sensing element. The body of the transducer contains necessary construction features so as to mount the transducer flushed with the wall of the duct. When any load is applied, it produces a proportionate charge output which is negative with respect to a positive pressure applied at the diaphragm of the transducer. Signal modulation due to the resonances is electrically attenuated by a standard filter (3 db at 150 KHz) connected to the pressure transducer. Three transducers are used for the purpose of the experiment. All the three are tested for the reproducibility and found to have similar characteristics in general. The calibration chart supplied by the manufacturer for the individual transducer is used in transforming the output voltage of the transducer to the recorded pressure of the transducer. To mount the transducers on the shock tube, special adapters as per the instructions of the manufacturer are used taking into consideration the concentricity of the holes made in the adapters. For the lucite tube, a sliding adapter is made which allows one to record the pressures at 6(six) transverse positions. Also the adapters are separated from the main testing structure using rubber gaskets and silicon grease. Extreme care is exercised while flush mounting the transducers so that the edge of the transducer diaphragm is provided with the specified clearance for the purpose of reproducibility.

Table 3.1 Transducer Characteristics

PARAMETERS	VALUE
a) Performance	
Pressure Range	100 psi (689.47 Kpa)
Over Pressure	150 psi (1.03 Mpa)
Maximum Pressure without damage	500 psi (3.45 Mpa)
Sensitivity (+2%)	59 mv/psi
Resolution	0.001 psi(rms)
Linearity (best fit straight line)	±1%
Resonant Frequency	250 KHz
Rise Time (10-90%)	2 micro-second
Low Frequency Response (-5% point)	0.005 Hz
High Frequency Response (+5% point)	50 KHz
b) Electrical	
Minimum Output Current	2 mA
Polarity Pressure increase	Negative
Bias Voltage	11 ± 3 Volts
Output Impedance	100 Ohms
c) Mechanical	
Weight	7.0 gms
Case Diaphragm	Stainless Steel
d) Power Supply	
Constant Current Source	4 ± 1mA
Supply Voltage, (No Load)	20-30 V(D.C)
Source Impedance	250 Kilo-Ohms

3.2.2 Ultrasonic Technique

Ultrasonic technique is used for the measurement of the liquid depth inside the circular pressure tube with the two-phase system and subsequent levelling of the pressure tube. Pulse echo technique, similar to the principle of sonar is used where the sound pulse is sent through the gas-liquid or wall-liquid interface and the pulse is received by the same transducer as it travels back from the interface. The transit time of the pulse gives a measure of the distance of the interface from the transducer face. A sound (usually in the MHz range) emitting transducer is used in contact with the tube wall and one part of the sound pulse discharged from the transducer is reflected at the tube wall-liquid surface and recieved by the transducer. The remaining part of the pulse is transmitted through the liquid in the tube and this sound is reflected from the liquid-gas interface as a result of the mismatch of the impedances at the interface and this part of the sound is also received by the transducer. The transit time of the pulse is converted to the distance between the interfaces once the sound speeds in the material of the tube wall, the liquid and gas are known. The ultrasonic pulse is generated by a Panametrics Ultrasonic Analyzer (Model 50524 UA) and discharged from a 1.0 MHz, 1.0 inch diameter Panametrics Contact Transducer (Part number V102). The signal generated and received by the transducer is stored in a Kawasaki MR-50E transient memory @ 50 nano-second sampling rate equiped with a Kawasaki TMC-300 high speed averager.

In order to level the pressure tube, the tube is filled with water approximately to a height of 30.0 mm. This liquid level is checked at five different places along the tube by placing the transducer in contact with the wall at the bottom of the tube. The tube is levelled accordingly if there is any discrepancy among the readings at those five places and also the 'TEE' section is levelled using the same technique. Moreover, the levelling is checked periodically to ensure the correct liquid depth all along the tube length. he data are then compared displaying on a TEKTRONIX-468 digital oscilloscope. This provides with an accuracy in the measurement of the liquid level up to one percentage (plus-minus) of the actual liquid level inside the duct.

3.2.3 High-Speed Photography

A HYCAM-II 16 mm high speed rotating prism camera (Redlake Corporation, CA, U.S.A.) is used to monitor the events occurring at the gas-liquid interface when a pressure wave is allowed to traverse through the phases. The camera employs the continuous film flow principle of operation with its operating range from 20 to 11,000 full format (16 mm) frames per second. The rotation of the prism assembly actuates a speed sensor to provide the necessary speed regulation input to the electronic speed control device. The electronic speed control having solid state circuitry provides a speed control within 1% accuracy over the HYCAM-II operating range. The number of meters of the film available since the start of the camera is counted electronically to match the settings of the direct reading digital switch. The servo brake of the camera is

used to maintain the correct film tension during the entire operation of the camera. The lens used for this photography is a TELE-XENAR 1:2.8/75 (Schneider, Germany) lens. The type of lens used is suitable to achieve the close up study of the interface phenomena. The intensity of the light required for the particular type of film, its speed, frame speed, exposure time and diaphragm opening is assured using an X-L meter (Photographic Analysis Ltd.). Usually a black and white Eastman 4-X negative (DIN 27,7224) 30.5 meter long film is used. In order to visualize the surface perturbations, a film speed of 1600 frames per second is used with the optimum combination of the available facilities. Once the film is completely exposed, it is developed by the manufacturer of the film and the enlarged prints for few selected exposures are obtained for the purpose of analysis.

3.3 Methodology

3.3.1 Data Acquisition and Analysis

The output from the piezo-type pressure transducers are stored in Transient Memories (Kawasaki Electronic, Japan, TM 1410; specifications provided in Table 3.2) at suitable sampling rate in order to obtain the optimum resolution of the pressure profiles. The usual sampling rate adopted is 5 micro-second per sample totalling 5 milli-second duration for intercepting a pressure profile having 1024 data points. The sensitivity gauge of the transient memory allows one to control the output amplitude of the transducers- this is in turn is

useful in monitoring the pressure profiles in an oscilloscope. A trigger transducer (Columbia Research Laboratories, Model P-200-1) with an appropriate charge amplifier (Columbia Research Laboratories, Model 4103) connected in series with the trigger transducer is used to trigger the transient memory. When using a charge amplifier for the trigger transducer, the magnitude of the parameter being measured is calculated by dividing the transducer sensitivity (33.2 pcmb/psi) expressed in pico-coloumbs into the output voltage expressed in millivolts for an amplifier gain of 1. Also for the selection of delayed or advanced trigger system, the trigger timing can be adjusted as a percentage of total traverse time. The schematic of the data acquisition system is depicted in Figure 3.6.

The data stored in the transient memory can be visualized in an oscilloscope, or recorded using a chart recorder, or stored in computer disc. For the majority of the acquired data,computer storage is preferred for the ease of subsequent analysis of the recorded data. The computer program (BASIC) for acquiring and storing the data on the discs is provided in Appendix A. An APPLE-IIe micro-computer is used for the storage of the data. The pressure at two different points along the pressure tube can be monitored simultaneously. The data are transferred from the transient memories through a home made electronic interface which can handle two channels at a time. Once the data acquisition is complete for one particular type of experiment, the data are printed using an appropriate program (Appendix A) and a printer. The printed data are checked and the start of the incident and reflected wave

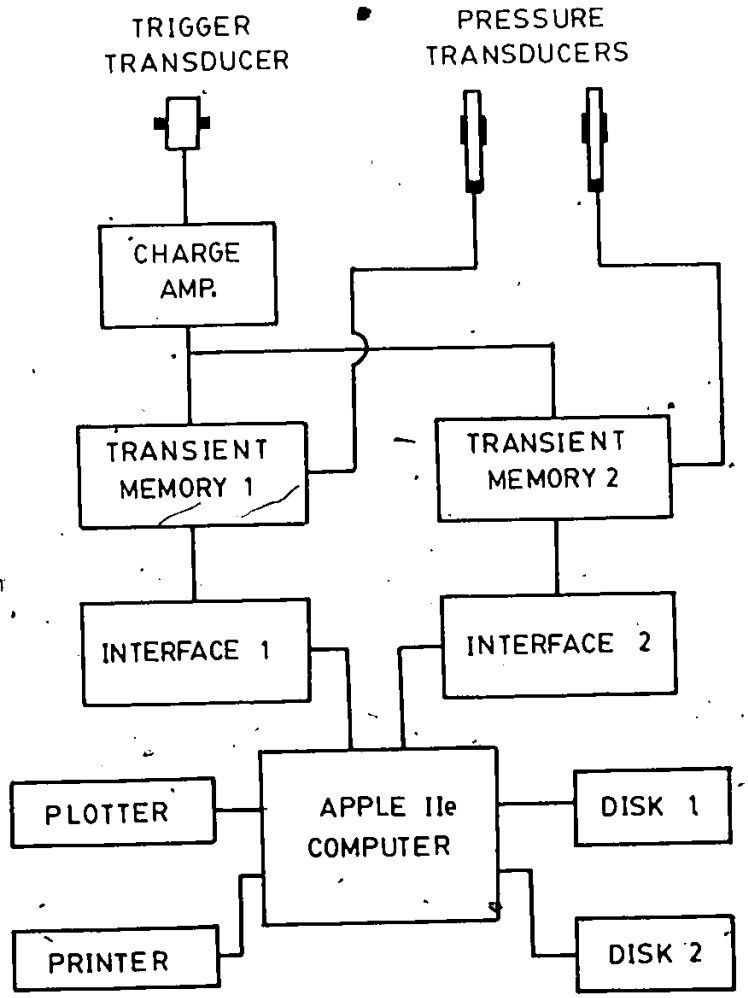

Fig.3.6: Schematic of data acquisition system.

timings are marked on the printed data plot as a percentage of the total time of the wave propagation. The data are analyzed for the maximum pressure, average pressure in both gas and liquid phases, using BASIC computer programs as presented in Appendix A.

Table 3.2 Specifications for Transient Memory, TM 1410

Parameter	Value
a) Storage	
Memory Capacity	8 bits × 1024 words
Maximum Sampling Speed	1 micro-second/word
Storage Elements	MOS IC Cells
(b) Voltage Axis	
Inut Channel	Single
Maximum Input Voltage	100 V (rms)
Maximum Linearity Error	±1% Full Scale
(c) Time Axis	
Internal Clock	1 micro-second/word to 100 milli-second/word
Frequency Characteristics	dc to 300 KHz 3 db
(d) Writing	
Trigger Mode	Internal, Exteſnal
Coupling	Ac, DC
(e) Reading	
Analog Output	±5 V of full scale 100 Ohms single ended
External Clock	Up to 1 MHz
Digital output	8 bits binary code

CHAPTER 4

EVALUATION OF PHASIC OVERPRESSURE

4.1 Introduction

This chapter contains the theoretical and experimental evaluation of the magnitudes of the overpressures developed in both the gas and liquid phases during the passage of a shock wave through a two-phase stratified system in the aluminum pressure tube. The liquid phase, with its higher propagation speed of sound than that in the gas phase, promotes the generation and subsequent propagation of small amplitude pulses moving ahead of the main shock wave. The roughness of the interface due to these pre-pulses is estimated both theoretically and experimentally (high speed photography) to find the roughness parameter to be used in the calculation of the interfacial friction factor. A separated flow model, after suitable assumption, is used to compute the strengths of the incident shock waves for various diaphragm pressure ratios with negligible effect of the liquid phase. The presence of the liquid phase reduces the compressible area of the system, which in effect enhances the strengths of the shock waves for the same diaphragm pressure ratio. Once the strengths of the shock waves in the gas (single) phase are known, a quasi-steady analysis is adopted to balance the energy expenses in the phases as well as that in the interface to estimate the magnitude

of the overpressure in the phases. The theoretical predictions are then compared with the experimental results obtained for the various strengths of the shock waves in conjunction with different liquid inventories in the pressure tube.

4.2 Interfacial Phenomena (Lucite Duct)

4.2.1 Theoretical Background

In order to analyze the perturbations at the interface in the case of the lucite tube, a short pulse of finite duration of about 0.7 m-seconds is used. The pulse or the shock wave, after impinging on the liquid phase produces a group of small pre-pulses, which, due to the larger sonic speed in the liquid, travels ahead of the main shock wave. The main shock wave, in the case of the stratified two-phase system travels at the speed of sound in the gas phase. The pre-pulses here, may be classified as the wave moving under a free surface. Stone (1982) has extensively studied the generation and the subsequent propagation of these pre-pulses under a free surface, however, Stone has not mentioned any experimental observation of the interfacial phenomenon using any kind of sophisticated high speed action. The theoretical approach for the analysis of the interface is similar to that of Stone, except that the interface behaviour is given more practical attention than compared to the work of Stone.

Fourier analysis of the finite short pulse shows that the frequency spectrum of the pulse may be presented as [Redwood (1960)]

$$\omega = 4n\pi/T_p \qquad (4.1)$$

where T_p is the duration of the pulse, ω is the frequency and n = 1, 2, 3,..... for different mode of propagation. In the present experimental set up, the length of the driving chamber is set to be about 24.0 to 25.0 cm. long and using the velocity of sound in air at the normal temperature, the duration, T_p equal to 0.7 m-seconds, is calculated. The time period τ and the wave length λ of any wave may be specified respectively by

$$\tau = 2\pi/\omega \text{ and } \lambda = a_0\tau \qquad (4.2)$$

Here, a_0 may be assumed to be the velocity of sound of air at atmospheric conditions. The values of the different parameters for n=1, 2, 3 and 4 are presented in Table 4.1.

Table 4.1 Wave Characteristics

n	Frequency (rad/sec)	Period (m-sec)	Wave-length (mm)
1	1. 80E+04	0.35	120.0
2	3. 60E+04	0.18	62.0
3	5. 40E+04	0.12	41.0
4	7. 20E+04	0.09	31.5

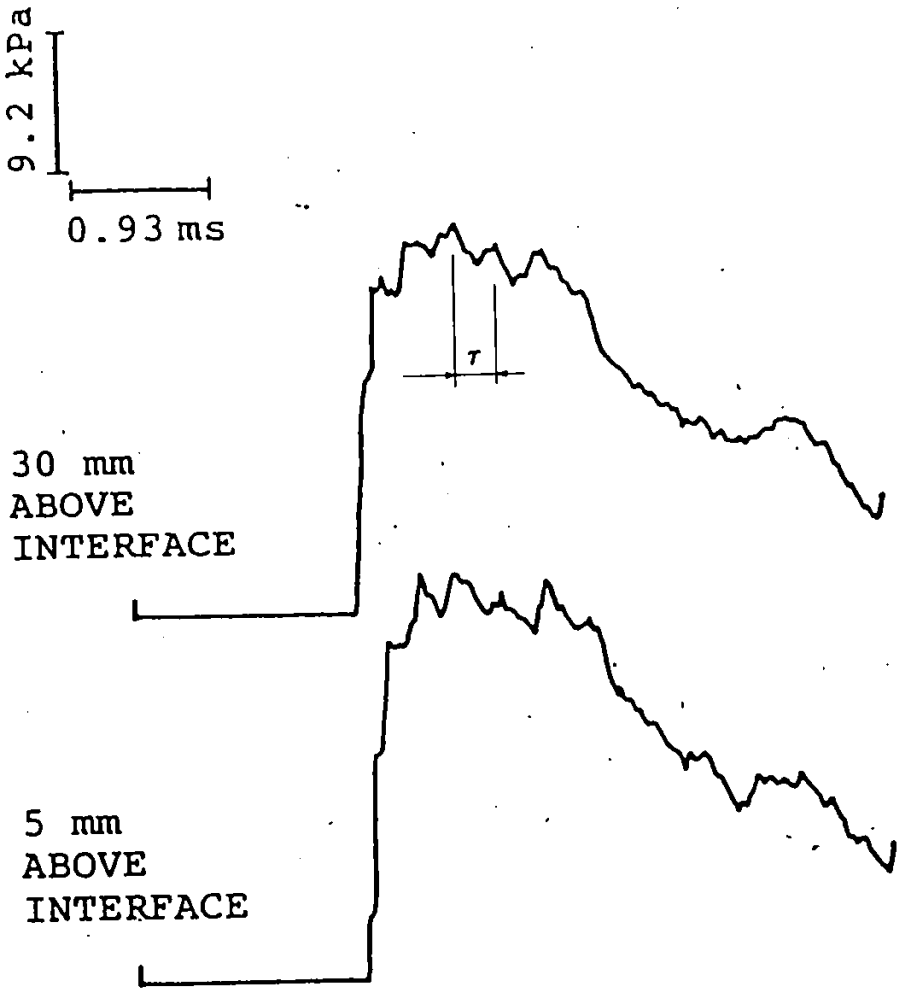

Fig. 4.1: Typical pressure waveforms at location A of lucite tube.

From Table 4.1 it is observed that the period of the wave propagating through the two-phase system should not be greater than 0.35 m-seconds and the corresponding wave length be less than 120.0 mm. From the pressure pulse obtained in the experiment (Figure 4.1), it is noticed that the time period is well below the 0.35 m-seconds limit. Moreover, as the pulse in the gas phase moves over the liquid phase, the pulse spectrum is modified due to the pre-pulses moving through the liquid phase. The interface at the time of the passage of a shock wave is thus believed to be under the combined influences of the pulse moving through the liquid phase and reflecting from the free surface.

The wave generation and its subsequent propagation in fluid bounded by a solid and a free surface are analyzed using the potential function. For a two-dimensional system (Figure 4.2) the wave equation may be written as

$$\frac{\partial^2\phi}{\partial y^2} + \frac{\partial^2\phi}{\partial z^2} = \frac{1}{a^2}\frac{\partial^2\phi}{\partial t^2} \qquad (4.3)$$

Referring Tolstoy and Clay (1966), the above equation may be solved with suitable boundary and initial conditions to obtain the following solution

$$\phi = A \cos[(n + \tfrac{1}{2})\tfrac{\pi}{h} y] \exp [i(\omega t - \chi z)] \qquad (4.4)$$

where χ is the wave number and the other parameters are shown in Figure 4.2. During the process of the evaluation of above equation, the

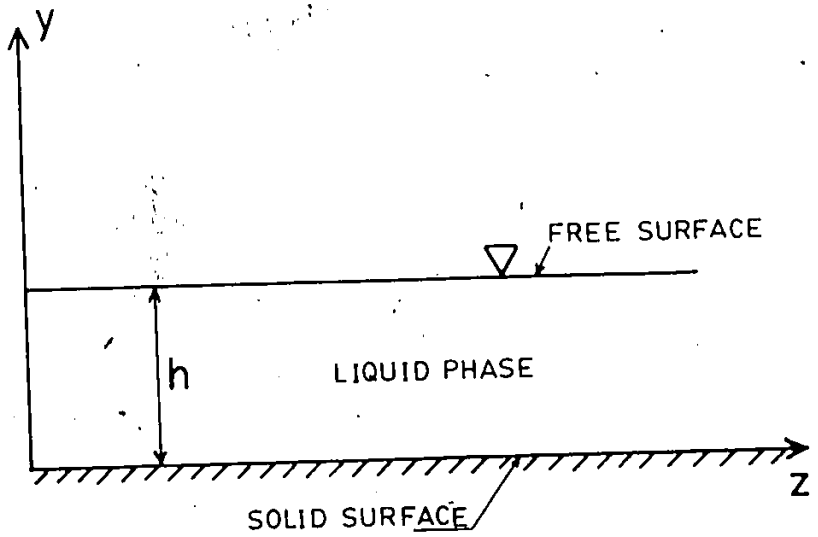

Fig. 4.2: Liquid phase bounded by a free and a solid surface.

sine terms are discarded, as at y=0.0, the sine terms automatically vanish. The value of χ in Equation 4.4 is expressed as

$$\chi^2 = (\omega/a)^2 - [(n+\tfrac{1}{2})\ \pi/h]^2 \qquad (4.5)$$

and the frequency ω is

$$\omega = \pm\, a\ [\chi^2 + (n+\tfrac{1}{2})^2\ (\tfrac{\pi}{h})^2\ ]^{1/2} \qquad (4.6)$$

Following the work of Redwood (1960), the group velocity is calculated as

$$c_g = \frac{d\omega}{d\chi} = \pm\, a\chi/[\chi^2 + (n+\tfrac{1}{2})^2\ (\tfrac{\pi}{h})^2\ ]^{1/2} \qquad (4.7)$$

Hence in order to have the group velocity real,

$$\omega > a\ (n+\tfrac{1}{2})\ \pi/h \qquad (4.8)$$

then for n=0,

$$f > a/(4h) \qquad (4.9)$$

or, the time period $\tau < 4h/a$ (4.10)

In case of the lucite duct, the experiments are conducted with a liquid level, h=60.0 mm and for water, the speed of sound, a=1440.0

m/sec; then for n=0, the time period τ is found to be less than 0.17 m-second and the frequency, f > 6.0E+03 cycles/second. Equation 4.4 represents the wave travelling along the Z-direction, however, the speed of propagation is not the speed of sound in the liquid. This is also clear from the dispersion relation of Equation 4.5. If the term under the square root is negative, then the value of the wave number χ attains an imaginary magnitude and the strength of the mode varies exponentially with the distance along the tube. The plane wave mode is always believed to travel for (n+1/2)=0, however, for the propagation of higher modes, the frequency must be greater than the minimum of 6.0E+03 cycles/second. Usually, when the wave length is greater than twice the height of the liquid depth, only the plane waves propagate, all other modes can not propagate - this is the "Cut-Off" frequency.

The pulse analyzed by Fourier method also observed to have ω equal to 3.6E+04 rad/second for n=2. As the wave in the liquid is being generated by the pulse impinging on the liquid surface, the frequency ω of the gas phase pulse tends to disperse towards the higher modes of propagation. With the increase of the liquid depth h, the mode frequency decreases and approaches the normal mode of propagation.

As the gas moves over the liquid surface at high speed, the liquid in contact with the gas phase attains certain velocity (less than the gas phase velocity) in the direction of the gas flow. The pulse in the gas phase contains disturbances having frequency calculated by Fourier analysis. Considering the 2nd order mode of the gas phase pulse,

the frequency, ω of 3.6E+04 rad/second and the time period, τ of 0.18 m-second are obtained.

If in the limit, the liquid surface has the same velocity as of the induced gas phase velocity i.e. 60.0 m/second (approximately) generated by a shock wave of strength 65.0 KPa(g), then the wave length of the ripples should be equal to velocity times the time period i.e. 10.8 mm. Also for the normal mode of the gas phase velocity, τ is equal to 0.35 m-second and in that case, the liquid surface may have velocity lower than that of the gas phase. For higher mode of wave propagation, the wave length of the ripples at the interface should be smaller in magnitude. The experimental value of the wave length of the ripples is observed to be 8.0 mm to 11.0 mm.

The turbulent gas flow behind a shock wave that is moving through a two-phase system generates a vortex sheet near the interface separating the phases. The induced motion in the phases makes the situation analogus to the classical case of Kelvin-Helmholtz problem that deals with the stability of a vortex sheet separating the two fluids of different densities moving in the same direction. A surface initially plane is disturbed by the propagation of pre-pulses along the liquid phase which is below the wavy surface. This liquid phase has the density ρ_1 and moves at a mean speed of u_1 where as the gas phase, which is on top of the heavier liquid, has density ρ_g and moving at a mean speed of u_g.

A plane disturbance with real wave number χ can be specified with the following equation

$$\eta = \exp [i\chi (z-Ct)] \tag{4.11}$$

where η is the surface displacement and C is the propagation velocity. If C is real, the wave will travel along the Z-direction with velocity C, but if C is imaginary, then the surface will be unstable. Referring Chandrashekar (1961), the Kelvin-Helmholtz instability problem may be solved to obtain the value of C as follows

$$C = \left[\frac{\rho_g u_g + \rho_l u_l}{\rho_g + \rho_l}\right] \pm \left[\frac{(\rho_l - \rho_g)}{\rho_g + \rho_l} \frac{g}{\chi} - \frac{\rho_g \rho_l}{(\rho_g + \rho_l)^2} (u_g - u_l)^2\right]^{1/2} \tag{4.12}$$

For the typical values of u_g = 60.0 m/second, u_l = 1.0 m/second (obtained using the linear wave equations for the liquid phase) and λ = 120.0 mm (from Table 4.1, corresponding to the normal mode), the value of C is found to contain a real and an imaginary parts. This indicates that the waves at the interface will grow exponentially with time.

4.2.2 Interfacial Roughness

When a gas flows over a liquid containing waves or small ripples at the surface, in that case the resistance to the gas flow is larger than the case where the interface is maintained smooth. In calculating

the friction factor and the associated drag, it is convenient to estimate the surface roughness due to the presence of the ripples on the liquid surface. The works of Ursell (1956), Ellison (1957), Ellis and Gay (1959), Lilleleht and Hanratty (1961), and Cohen and Hanratty (1968) show the fact that the resistance to the gas flow over a liquid is increased due to the presence of the surface roughness at the interface. For the case of shock wave propagating in a two-phase stratified system, the induced gas flow behind the shock wave encounters a stronger resistance due to the presence of the interfacial roughness. The interface roughness is considered to be generated by the pre-pulses moving, and undergoing multiple reflections from the solid and free surface, ahead of the principal shock wave.

For the case of aluminum pressure tube, the pre-pulses are observed to be very prominent and the magnitude of the overpressure generated by these pre-pulses is obtained from the experimental observation. The particle velocity u is calculated using Equation 1.14 of Chapter 1. Hence the liquid is induced by a velocity of magnitude u in all direction from the point of impingement of the shock wave. Now as discussed earlier, if only plane waves propagate, then the appropriate group velocity may be calculated from the equations supplied earlier in this chapter. The difference in the velocities of the pre-pulse and the main shock wave provides the value of the lead velocity of the pre-pulse at a point before a shock wave interacts with the perturbation at the interface generated by the pre-pulse. From the experimental data, the time for the shock to the first pre-pulse is estimated. The distance covered by the pre-pulses before the arrival of the main shock wave is

calculated using the values of the time period and the velocity of the pre-pulses in the liquid phase. After that, the time for the main shock wave to reach that point is calculated using the strength of the particular shock wave under consideration. During this time gap the rise of the liquid interface is calculated. In this way a typical value of the surface roughness of about 0.0024 mm is estimated. Then Colebrook's equation [Murdock (1978)] for turbulent flows is used to find the interfacial friction factor.

$$\frac{1}{\sqrt{f_i}} = -2 \log_{10} \left[\frac{\varepsilon/D_h}{3.7} + \frac{2.51}{Re\sqrt{f_i}} \right] \qquad (4.13)$$

Reynolds number, Re obtained for the range of shock waves considered here, is found to be 4.0E+05 to 7.0E+05. The variation is due to the fact that the hydraulic diameter of the gas phase varies with the liquid level in a circular pipe as well as the gas phase velocity is a function of the incident shock wave.

4.2.3 Experimental Results

(a) Basic Waveforms

In this section, the propagation of pressure waves in a two-phase system with 60.0 mm of water in the lucite duct is considered. The waveforms observed in the liquid phase, generated by a shock wave are shown in Figure 4.3. The results are very reproducible, as shown by superimposing the pressure traces from two separate experiments in this

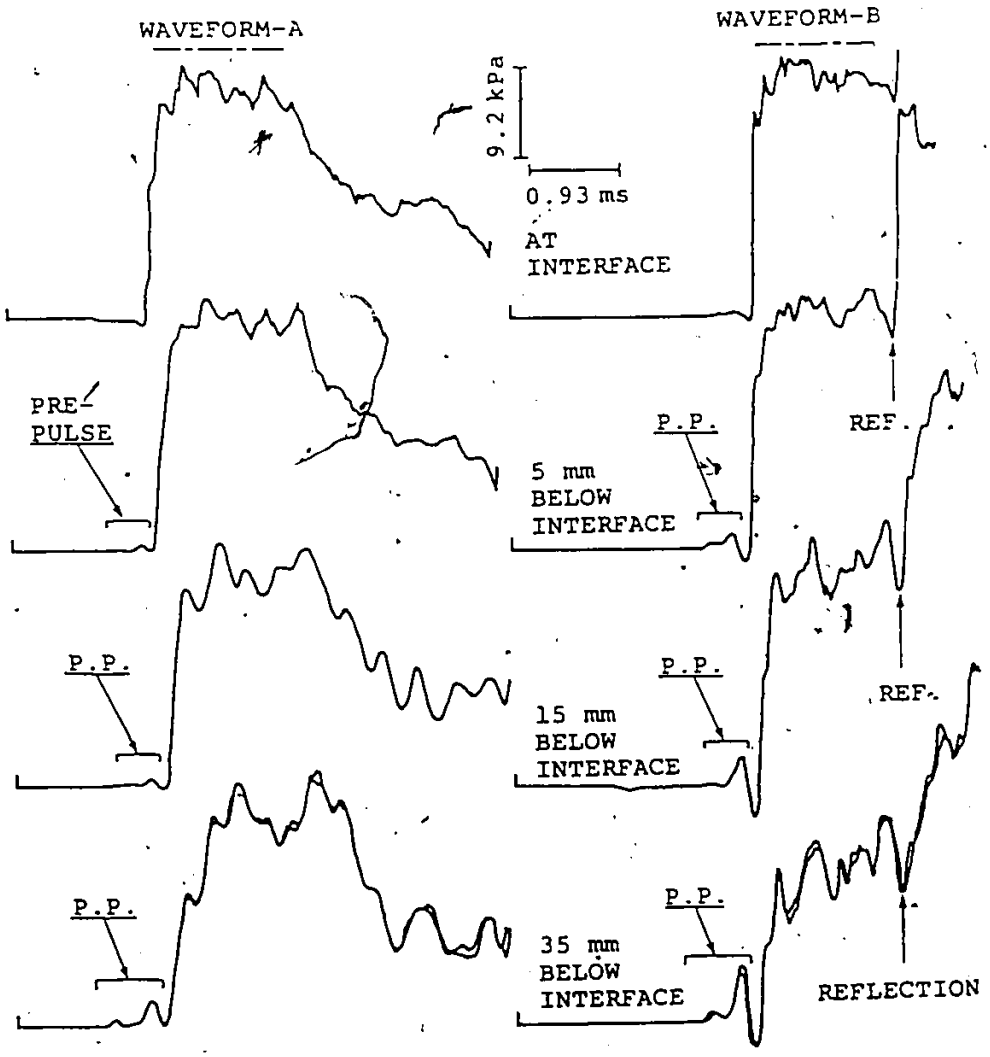

Fig. 4.3: Pressure waveforms at various depths in liquid phase; Two-phase system with 60 mm liquid level.

figure (top and bottom traces). From other experimental data, it is observed that, in the gas phase, general trend of the propagation of pressure waves in the single (gas) and two-phase cases is quite similar to each other. As will be shown later in this section, however, there appear some differences in the magnitude of the overpressure between these cases. On the other hand, for the waves propagating in the liquid phase, several interesting features can be noticed (Figure 4.3). In a certain range of depth (15 to 35 mm) downward from the interface, the waveforms seem to be somewhat rounded off or relatively smooth compared with those observed in the gas phase. In other words, a small-amplitude high frequency perturbation, which is superimposed on the waves in the gas phase, is considered to attenuate appreciably in the liquid phase. The most interesting feature of the waves in the liquid phase is the formation of the pre-pulse. Although the results are not shown, the reflected waves in the liquid phase from the end wall, placed far from the diaphragm, are found to have negligible influence on the pre-pulse structure. The reflected waves in the liquid phase are considered to return from the far end wall much faster than the waves in the gas phase. This effect was checked by using some blocks to change the end wall position in the liquid phase. As can be seen in Figure 4.3, the pre-pulse has the following features:

(1) pre-pulse amplitude is enhanced during the propagation between locations A and B;

(2) pre-pulse appears more remarkably near the rigid bottom surface than near the gas-liquid interface;

(3) most pre-pulses observed to have a crest (or compression front) and

a trough (or expansion front). The trough always precedes the main shock wave;

(4) at a far distance from the interface, pre-pulse exhibits somewhat perturbed structure as compared to that near the interface.

Also as the wave propagates, its transverse shape is also observed to be changing in time. The transverse distribution is plotted at each time step. In Figure 4.5, the distribution of the transverse overpressure at various time steps, as shown in Figure 4.4 is presented. As shown in Figure 4.5, in the air phase, the distribution of overpressure scarcely change its shape over the time steps considered, while, in the liquid phase the distribution fluctuates considerably at almost every time step compared with that in the gas phase. This fact suggests that, the various waves which travel repeatedly across the liquid phase (waves reflected from the interface and bottom surface) may play an important role in constructing the basic wave structure. For the purpose of comparison, the results of the single phase (air only) case are superimposed in Figure 4.5. As shown in this figure, the distribution of the overpressure in the single phase case hardly changes its shape. This trend is quite similar to that of the two-phase case. However, the magnitude of the overpressure shows some differences between the single (gas) and two-phase cases.

(b) Flow Regime Transition

High speed photography of the lucite duct demonstrates the change of the flow regime from the smooth stratified to the wavy

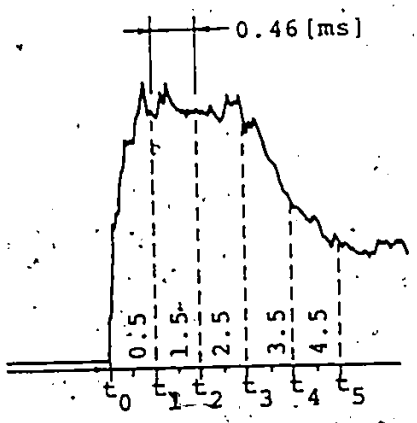

Fig. 4.4: Definition of time steps;
t_0 is incident shock wave time.

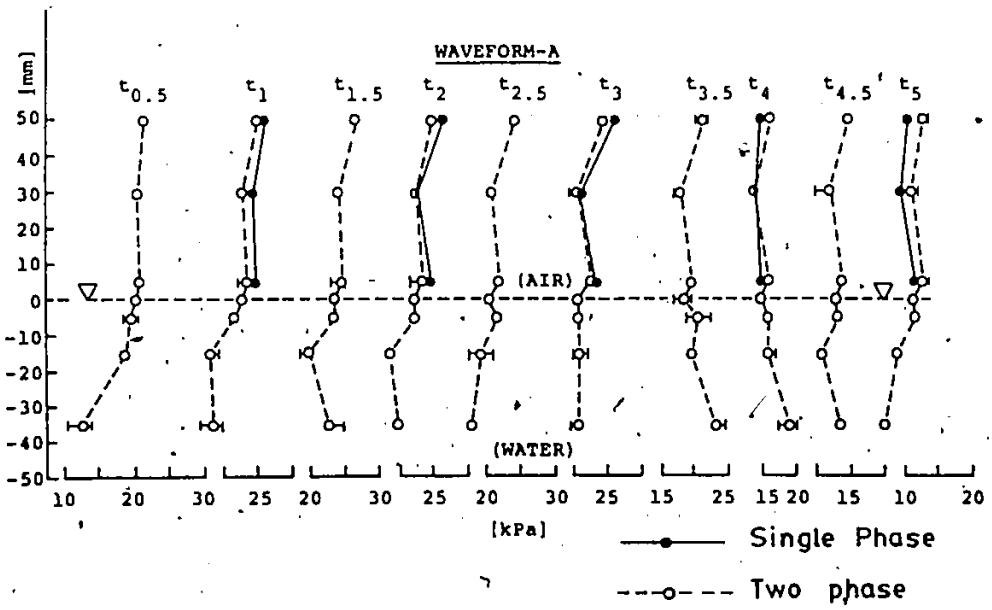

Fig. 4.5: Transverse distribution of overpressures at location A of lucite tube for various time steps.

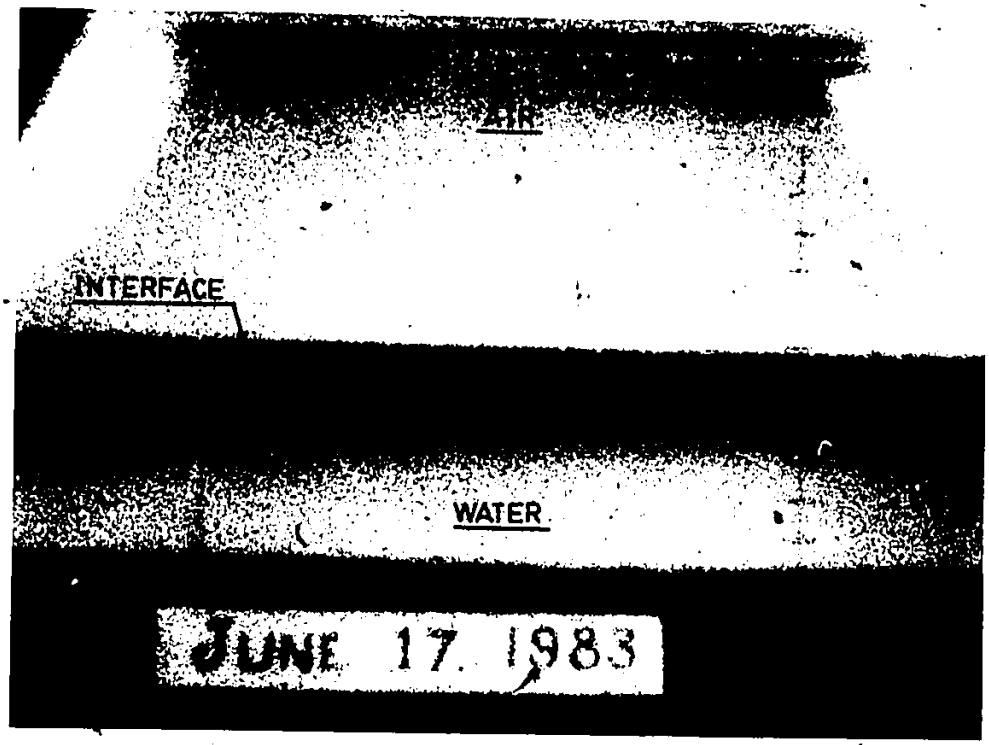

Photoplate 4(a)

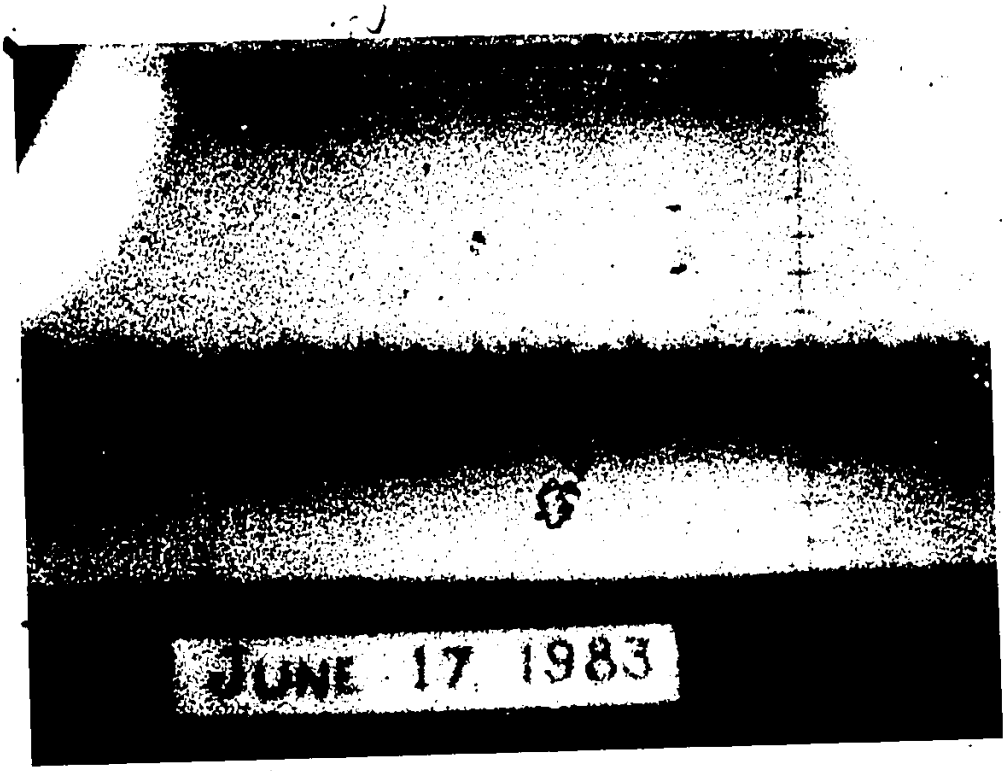

Photoplate 4(b)

stratified flow due to the passage of the shock wave of strength 62.0 to 63.0 KPa (gauge) through the phases. The photography is done using a HYCAM-II (mentioned earlier in Chapter 3) high speed movie camera @ 1600 frames pet second. Few selected shots are enlarged after the whole film is processed and developed. The photoplate 4(a) shows the stratified smooth interface just at the start of the shock wave. In photoplate 4(b) the interface is observed to become roughened approximately after 10 to 20 m-seconds from the time of the start of the shock wave. A ruler is placed inside the lucite duct to facilitate the measurement of the wave length of the ripples directly from the photo-plates. The wave length of the ripples as estimated from the photographs is found to be in the range of 8.0 to 10.0 mm. The analysis of the high speed photography reveals two distinct mechanisms, qualitatively may be discussed in the lights of Kelvin-Helmholtz instability where the vortex sheet generated by the turbulent gas flow over the low amplitude ripples makes the surface highly unstable. For the situation as in this experiment, a critical speed of 60.0 cm/second of the gas relative to the liquid is sufficient to make the surface unstable. The photoplates 4(c) and 4(d) show the gradual changes occurring at the interface. The second mechanism is related to the generation of surface waves of longer wave lengths at the interface. The high speed gas induces a mass motion of the liquid layer adjacent to the interface in the direction of the propagation of the shock wave. The gradient of the velocity at the interface sustained by the densities of the fluids play an important role in this type of problems (Figure 4.6). But the presence of the end wall at the downstream end of the shock tube, makes the shock wave as well as the liquid strip to reflect in the opposite direction. The

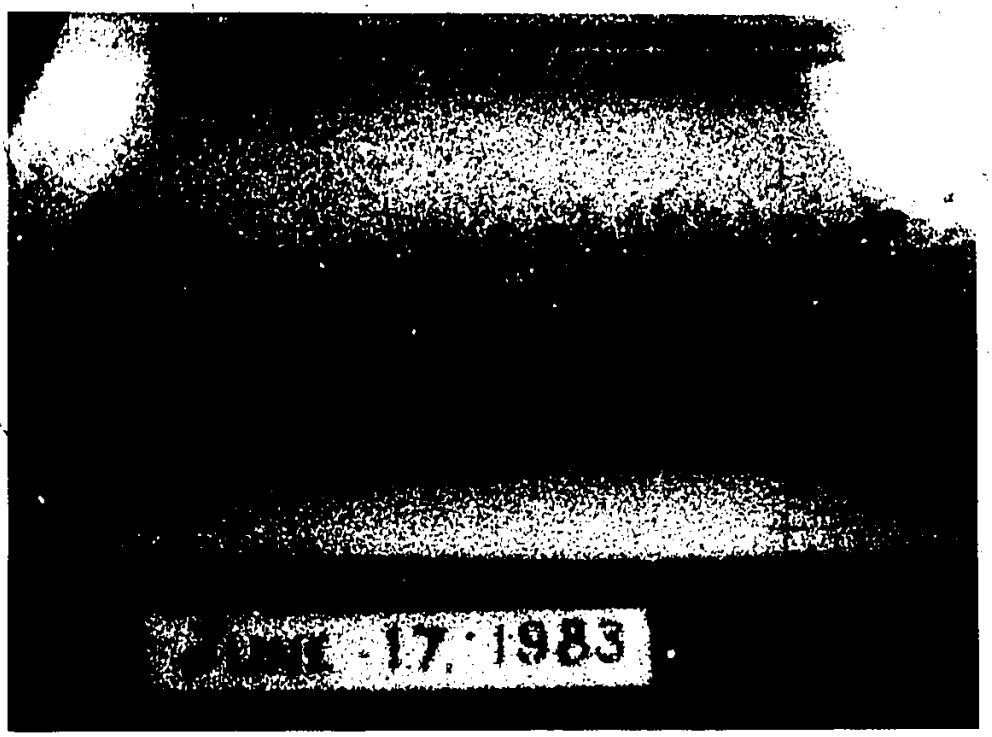

Photoplate 4(c)

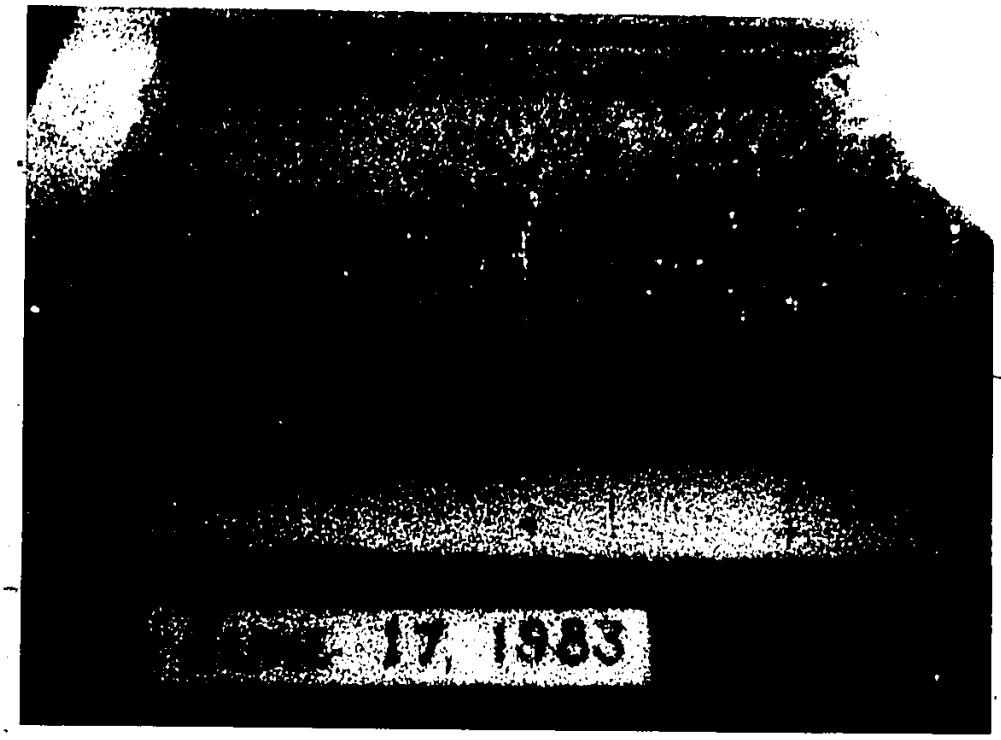

Photoplate 4(d)

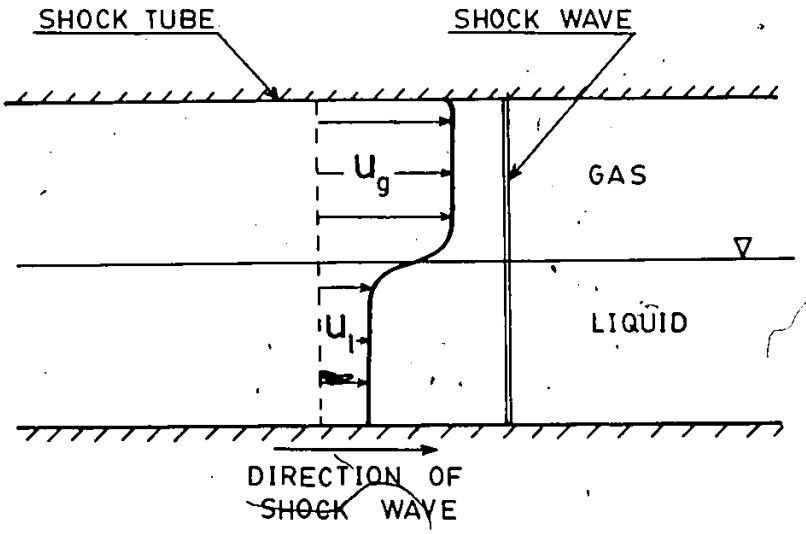

Fig. 4.6: Shock-induced velocities in gas and liquid phases in a two-phase horizontal stratified system.

Photoplate 4(e)

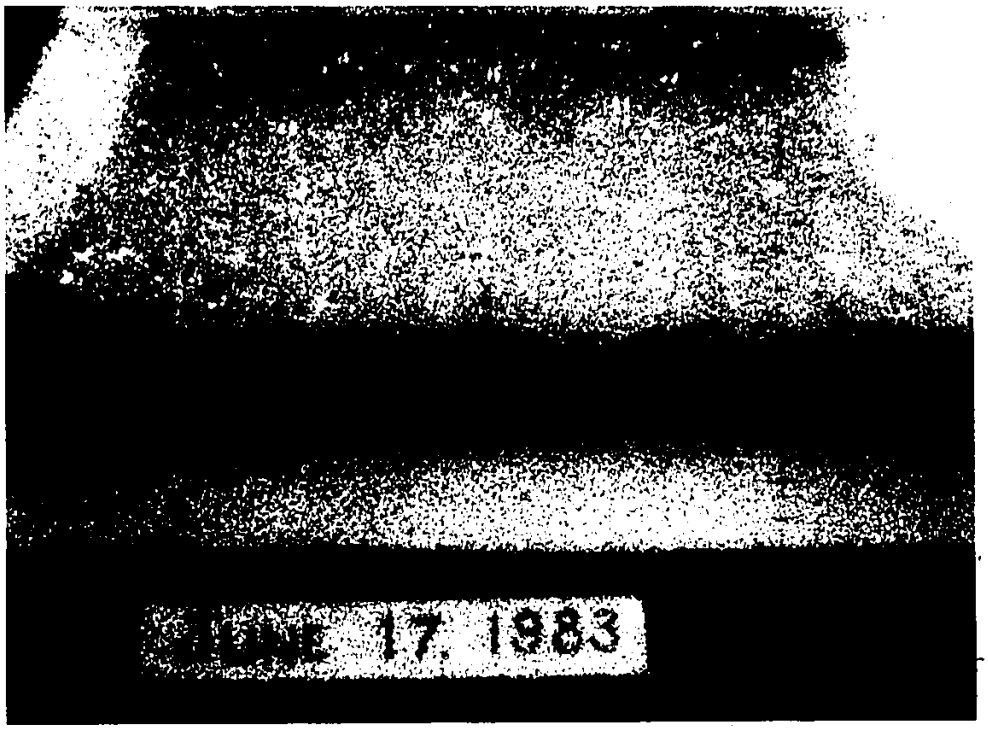

Photoplate 4(f)

collision of two wave trains moving in the opposite directions near the interface is pressumed to generate waves of longer wave length. This phenomenon is shown in photoplates 4(e) and 4(f). The time of occurrence of this phenomenon is very much delayed compared to the duration of the shock wave propagation through the phases; this is of the order of 60.0 m-seconds and up. The sequence of the mechanisms at the interface is summarized in Figure 4.7.

4.3 Estimation of Overpressure In Phases

4.3.1. Two-Fluid Modelling for Stratified Flow

If $\bar{J}$ and ψ are the efflux and source of any quantity Φ respectively, then the total accumulation of Φ in time dt is the sum of the net efflux $\bar{J}$ through a small area ds and the generation within the control volume element dv. Using the definition of Reynolds transport theorem and Gauss theorem, the generalized local instantaneous conservation equation for any phase k can be written as

$$\frac{\partial}{\partial t}(\rho_k \Phi_k) + \nabla\cdot(\rho_k \Phi_k \bar{v}_k) = -\nabla\cdot\bar{J}_k + \rho_k \psi_k \qquad (4.14)$$

Here $\bar{v}_k$ and ρ_k are the velocity vector and the density of the phase k. The use of Liebnitz rule and Gauss theorem provides the generalized volume averaged one-dimensional conservation equation in the following form

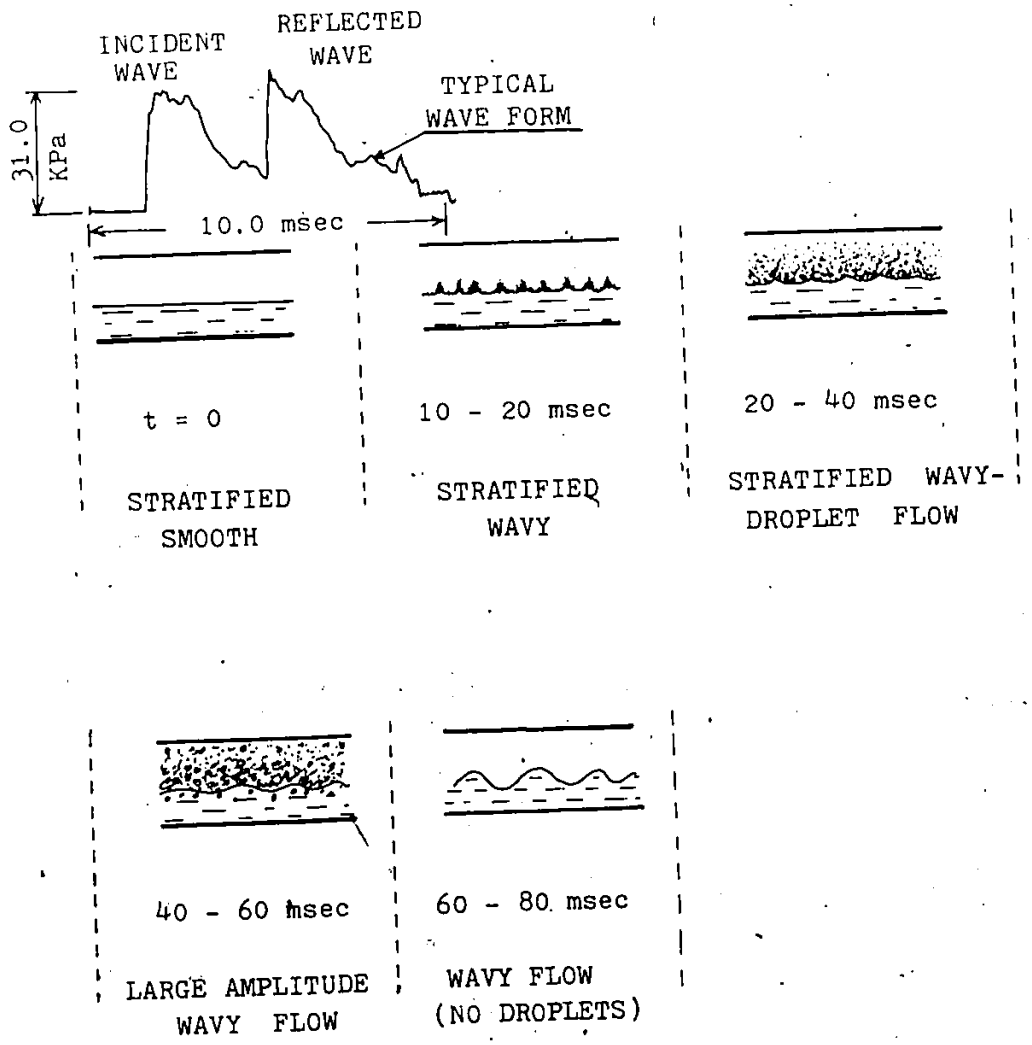

Fig. 4.7: Pressure waveform and observed flow regime transition in lucite shock tube.

$$\frac{\partial}{\partial t}\alpha_k < \rho_k \Phi_k > + \frac{\partial}{\partial z}\alpha_k < n_z \cdot (\rho_k \Phi_k \bar{v}_k + \bar{J}_k) > -$$

$$\alpha_k < \rho_k \psi_k > = -\frac{1}{V}\int_{A_i} (\dot{m}_k \Phi_k + n_k \cdot \bar{J}_k)\, dA - \frac{1}{V}\int_{A_k} n_k \cdot \bar{J}_k\, dA \quad (4.15)$$

where A is the surface area and

$$V = \Sigma V_k \;\; ; \;\; \alpha_k = \frac{V_k}{V} \text{ and } u_k = n_z \cdot \bar{v}_k$$

Following the work of Ishii (1976) and Banerjee and Chan (1980) the terms in the above equation may be replaced with suitable variables such as stress tensor, external force vector, internal energy, body heating, heat flux etc. to obtain the conservation equations of mass, momentum and energy as follows

$$\frac{\partial}{\partial t}\alpha_k < \rho_k > + \frac{\partial}{\partial z}\alpha_k < \rho_k u_k > = - < \dot{m}_k >_i \quad (4.16)$$

$$\frac{\partial}{\partial t}\alpha_k < \rho_k u_k > + \frac{\partial}{\partial z}\alpha_z < \rho_k u_k^2 > + \alpha_k \frac{\partial}{\partial z} < p_k >$$

$$- \frac{\partial}{\partial z}\alpha_k < n_z \cdot \bar{T}_z > - \Delta p'_{ki} \frac{\partial}{\partial z}(\alpha_k)$$

$$= \alpha_k < \rho_k \dot{F}_k > - < \dot{m}_k u_k >_i - < \Delta p'_{ki} >_i + < (n_z \cdot \bar{T}_z) >_i +$$

$$< (n_{kw} \cdot \bar{T}_z) >_w \quad (4.17)$$

$$\frac{\partial}{\partial t}\alpha_k \langle (\rho_k E_k) \rangle + \frac{\partial}{\partial z}\alpha_k \langle \rho_k E_k u_k \rangle +$$

$$\frac{\partial}{\partial z}\alpha_k \langle q_{z,k} \rangle + \frac{\partial}{\partial z}\alpha_k \langle p_k u_k \rangle$$

$$-\frac{\partial}{\partial z}\alpha_k \langle n_z (\bar{T}_k \cdot \bar{v}_k) \rangle = \alpha_k \langle \rho_k (u_k \dot{F}_k + Q_k) \rangle$$

$$-\frac{1}{V}\int_{A_i} [\dot{m}_k E_k + n_k \cdot (q_k + p_k \bar{v}_k - \bar{T}_k \cdot \bar{v}_k)]\, dA$$

$$-\frac{1}{V}\int_{A_{kw}} n_k \cdot q_k \, dA \qquad (4.18)$$

In the above equations, the subscripts i and w respectively refer the conditions pertaining to the interface and wall of the system.

The equations derived here have the volume averaged form for the local, instantaneous properties. The equations have the volume averaged products of the fluid properties such as density, pressure, temperature, velocity etc. For the purpose of the computation, these products of the averages have to be made products of the averages of the fluids. A fluid property may be written as a sum of the low frequency component and a high frequency component. Following the work of Sha et al (1983), it can be assumed that depending on the noise level acquired in the system, the high frequency term may be neglected or retained. The procedure of the time averaging after the volume averaging leads to the complete set of equations of the mass, momentum and energy for a system. If there is no

fluctuation of the variables with the time, the area or volume averaged products become the simple products of the averages of the properties. As shown by Sha et al (1983), for low frequency components which are usually associated with the blow down or wave propagation cases, the time-volume averages do not reduce any generality of the equations and the forms of the equations remain same after the time-volume averaging. Though for general solution we have to solve the differential integral equations, these can be simplified to the partial differential equations with the suitable constitutive equations for mass, momentum and energy flows across the interfaces and the boundary walls. The averaging operators are cumulative in nature. The averages of the products in the conservative equations are separated as the products of the averages of the dependent variables.

Once the complete set of the equations for a general multi-phase flow system has been developed, these equations can now be modified in order to make them suitable for the situations under consideration here. In the perspective of studying the shock wave propagation in a horizontal stratified system, the mathematical equations describing the system can be made more simple and thus easing the process of computation and making the analytical treatment a tractable proposition. It is useful to derive the complete two-fluid model and reduce it to simplified form with suitable assumptions pertaining to the physical situation of the system. The intuitive ideas about the physical process may call for the elimination of several secondary parameters without diverging too much from the reality. For example, in the problem considered here, the system is an adiabatic one, hence the terms related

to heat transfer and enthalpy have to be dropped from the energy equation. In general, the following assumptions can be enforced on the system under consideration.

(a) No interfacial mass transfer;

(b) no heat transfer from or to the system;

(c) void fraction does not change with time or space during the wave motion;

(d) only interfacial friction, f_i and gas side wall friction, f_w are considered;

(e) hydrostatic pressures induced by the volume of the gas and the liquid are negligible; and

(f) no gravity or body force on the system.

With these assumptions, the volume averaged system of equations for any phase can be presented as follows

$$\frac{\partial}{\partial t} < \rho > + \frac{\partial}{\partial z} < (\rho u) > = 0 \qquad (4.19)$$

$$\frac{\partial}{\partial t} < (\rho u) > + \frac{\partial}{\partial z} < \rho u^2 > + \frac{\partial}{\partial z} < p > = - < (T)> \qquad (4.20)$$

$$\frac{\partial}{\partial t} < (\rho E) > + \frac{\partial}{\partial z} < (\rho u\ E) > + \frac{\partial}{\partial z} < (pu) > = 0 \qquad (4.21)$$

Substituting the continuity equation (Equation 4.19) in the momentum equation, the momentum equation for any phase in general, is simplified as

$$\langle \rho \rangle \left[\frac{\partial \langle u \rangle}{\partial t} + \langle u \rangle \frac{\partial \langle u \rangle}{\partial z}\right] = - \frac{\partial \langle p \rangle}{\partial z} - \langle (T) \rangle \quad (4.22)$$

To form the energy equation in a more pliable condition, the following thermodynamic relation for the energy is used

$$E = e + u^2/2 \quad (4.23)$$

Now using Maxwell's relations from the thermodynamic properties [Zemansky (1968)] and the velocity of sound, the energy equation can be written as

$$\frac{d}{dt} \langle p \rangle + a^2 \langle \rho \rangle \frac{\partial \langle u \rangle}{\partial z} = - a^2 \left(\frac{\partial \rho}{\partial h}\right)_p \langle uT \rangle \quad (4.24)$$

Again, the derivative of the density with respect to the enthalpy can be used to reduce the energy equation to be used for the estimation of the shock wave propagation in a system. The final form of the equations of mass, momentum and energy are reduced to the following forms

$$\frac{\partial \rho}{\partial t} + \frac{\partial}{\partial z} (\rho u) = 0 \quad (4.25)$$

$$\frac{\partial u}{\partial t} + u \frac{\partial u}{\partial z} + \frac{1}{\rho} \frac{\partial p}{\partial z} = - T/\rho \quad (4.26)$$

$$\frac{\partial p}{\partial t} + u \frac{\partial p}{\partial z} + \gamma p \frac{\partial u}{\partial z} = - uT \quad (4.27)$$

where γ is the ratio of the specific heats of the medium under consideration.

4.3.2 Theoretical Estimation of Phasic Overpressure

The wave propagation in an incompressible liquid does not produce a substantial compressibility effect, and hence in particular to water used in this work, this effect may be neglected for all practical purposes. The above equations are only applied to the gas phase keeping in mind that the values obtained here will be coupled in the numerical evaluation of the overpressure in the phases. During the passage of the shock wave through the phases, the energy is spent in both the phases as well as at the interface. The interfacial energy may be approximated by the evaluation and proper use of the interfacial frictional energy dissipation. However, the frictional force in the above equations mainly has two components: (1) one due to the interface and (2) the other due to the wall friction on the gas phase. The interface friction has predominant effect due to the perturbations on the interface caused by the pre-pulses present in the system. The interfacial friction term per unit volume is assumed as

$$F_i = 0.5\, f_i\, \rho_g\, u_g\, |\, u_g - u_l\, |/D_h \qquad (4.28)$$

In the above equation f_i is the interfacial friction factor, ρ_g is the gas phase density, u_g is the gas phase flow velocity and

u_l is the liquid phase induced velocity. For the case of weak shock waves, $u_g >> u_l$ and hence in many cases, the liquid velocity may safely be neglected. The interfacial friction factor, f_i is calculated from the knowledge of the pre-pulses and discussed in the previous section.

The gas phase wall frictional loss is accommodated by using an appropriate friction formula for high speed flows inside a smooth pipe. Referring the work of Rudinger (1955), the friction factor, f_w can be estimated from the following equation

$$\frac{1}{\sqrt{f_w}} = 2.0 \log_{10} (Re \sqrt{f_w}) - 0.8 \qquad (4.29)$$

The Reynolds number, Re usually is very high for the problems associated with the compressible flows, and hence the effect of the frictional losses for many practical applications may be ignored in the analysis of the compressible flow phenomena. The computational values show very negligible change in the pressure drop due to the wall friction. The frictional losses are inserted into the conservation equations, presented above, with a suitable friction force expression similar to Equation 4.28. This assumption may be justified because the shock wave propagation through a smooth stratified system, the propagation of shock wave can be analyzed by using a single phase conservation equations and then modified by a quasi-steady energy balance between the phases. Either in single (gas) phase or in two-phase situations, the shock waves are produced using the same diaphragm pressure ratio; hence

the energy input remains constant for a certain condition of the high pressure chamber. At first, it is assumed that the shock wave is propagating in the gas phase only without any friction. The shock wave strength under this condition is estimated after solving the set of conservation equations (Equations 4.25 to 4.27). The estimated shock strengths obtained with different diaphragm pressure ratios are used in the quasi-steady analysis for the overpressure with different liquid levels.

For a single phase shock tube experiment (Figure 4.8), the rate of work done is the product of the overpressure and the particle velocity. Hence, the total rate of work done on the gas behind the shock wave is

$$= p_1 \, u \, A \qquad (4.30)$$

Here p_1 is the pressure rise due to the shock wave, u is the particle velocity induced by the shock wave and A is the cross sectional area of the pipe. The gas in front of the shock wave has no induced motion, hence the work done on the stationary gas is zero. Once the liquid is introduced inside the pipe, the gas phase area is reduced. Due to this reduction in the gas phase area, the pressure as well as the particle velocity of that phase will increase so as to re-distribute the total energy imposed on the gas phase. In the presence of the two-phase system, the total energy is shared by the phases as well as by the interface. The shock wave propagation in a two-phase system is shown in Figure 4.9. If subscripts g and l denote the conditions pertaining to

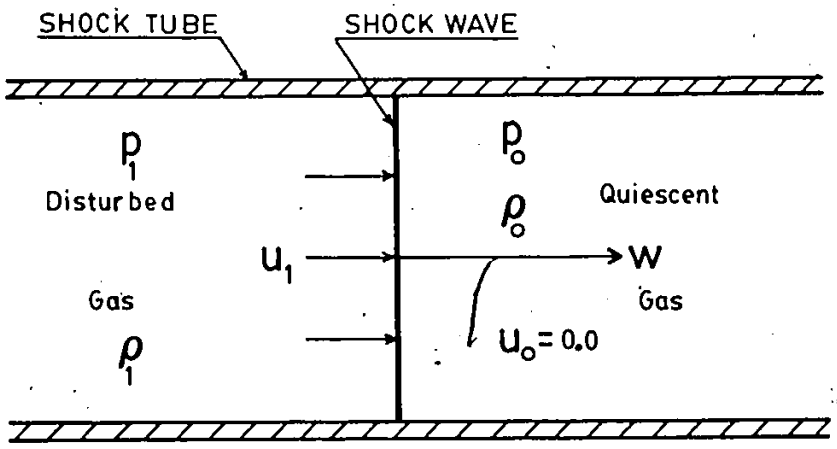

Fig. 4.8: Shock wave propagation in a quiescent gas.

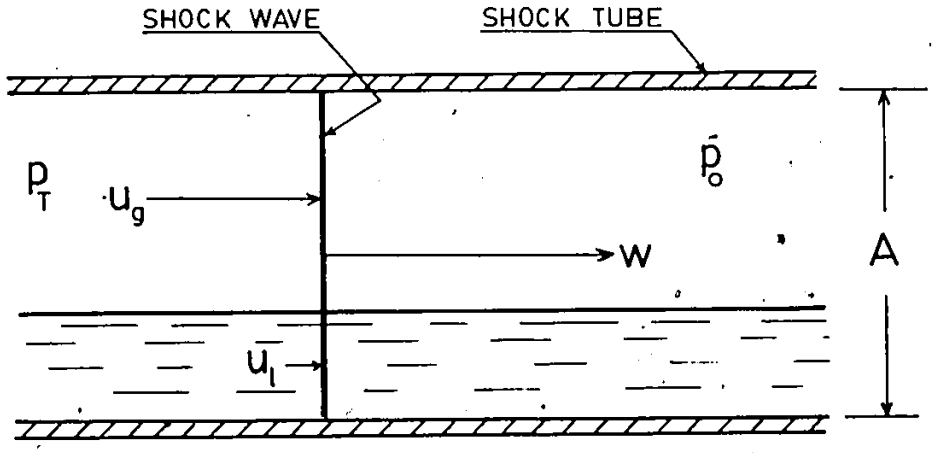

Fig. 4.9: Shock wave propagation through a horizontal two-phase stratified system.

the gas and liquid phases, then the total rate of work done on the gas phase is

$$= p_g u_g A_g \tag{4.31}$$

Similarly, the total rate of work done on the liquid phase is

$$= p_l u_l A_l \tag{4.32}$$

The total input energy or rate of work done is the same either in the presence or absence of the liquid phase, it can then be written that

$$p_g u_g A_g + p_l u_l A_l = p_l u A \tag{4.33}$$

In the above equation, the frictional effect either due to the wall or due to the interface is not included. The interface, which exhibits the phenomenon of the flow regime change, generates sufficient roughness so as to weaken the strength of the shock wave during its course of propagation through the phases. For a circular pipe, the width of the interface increases with the increase of the liquid level inside the pipe up to a maximum value equal to the diameter of the pipe for 50% void fraction. Denoting the diameter of the pipe by d and the liquid level by h, the interface width C_i may be obtained from the standard relation of geometrical configuration [Franklin (1978)] as follows

$$C_i = 2\sqrt{[h\ (d-h)]} \tag{4.34}$$

From Figure 4.10, the value of the perimeter in contact with the liquid phase may be obtained as

$$S_l = d\ [(\pi/180) * \{\text{Arc cos}\ (1-2h/d)\}] \tag{4.35}$$

Once C_i, h,d, and the liquid phase parameters are known, then again from the geometrical considerations, the gas phase cross sectional area is obtained as a function of the above parameters. Here, the hydraulic diameter is defined as

$$D_h = 4\ A_g/\xi_g \tag{4.36}$$

where ξ_g is the gas phase perimeter. The plot of C_i and D_h versus the liquid level, h/d is presented in Figure 4.11. The contribution of the interfacial friction varies directly with the increase in the liquid level (up to the 50% void fraction, for circular pipes). Now defining a parameter for this proportionality as

$$\beta = C_i/D_h \tag{4.37}$$

the total friction force up to a distance L from the commencement of the shock wave can be written as

$$F = \beta\ f_i\ [0.5\ \rho_g\ u_g|\ u_g - u_l|/D_h]\ AL \tag{4.38}$$

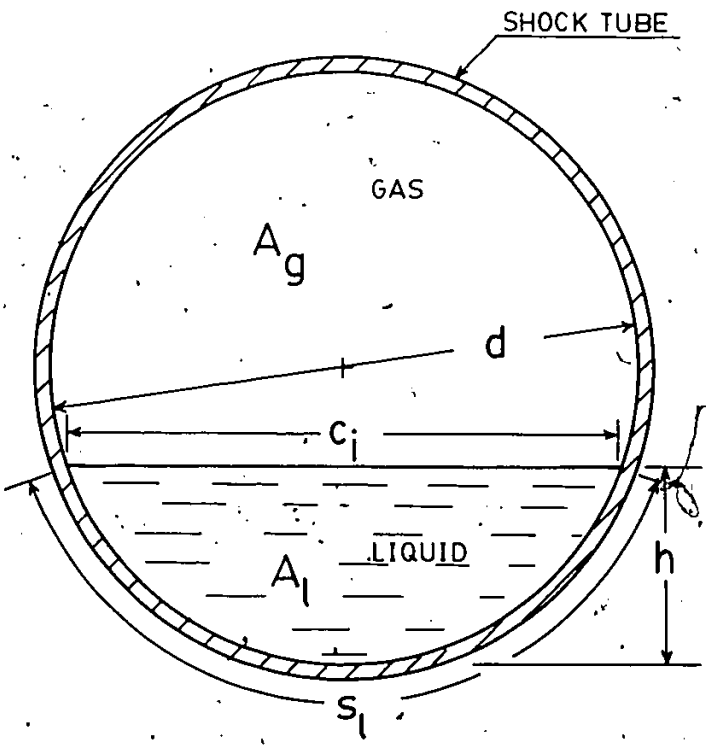

Fig. 4.10: Parameters describing two-phase gas-liquid system in circular pipes.

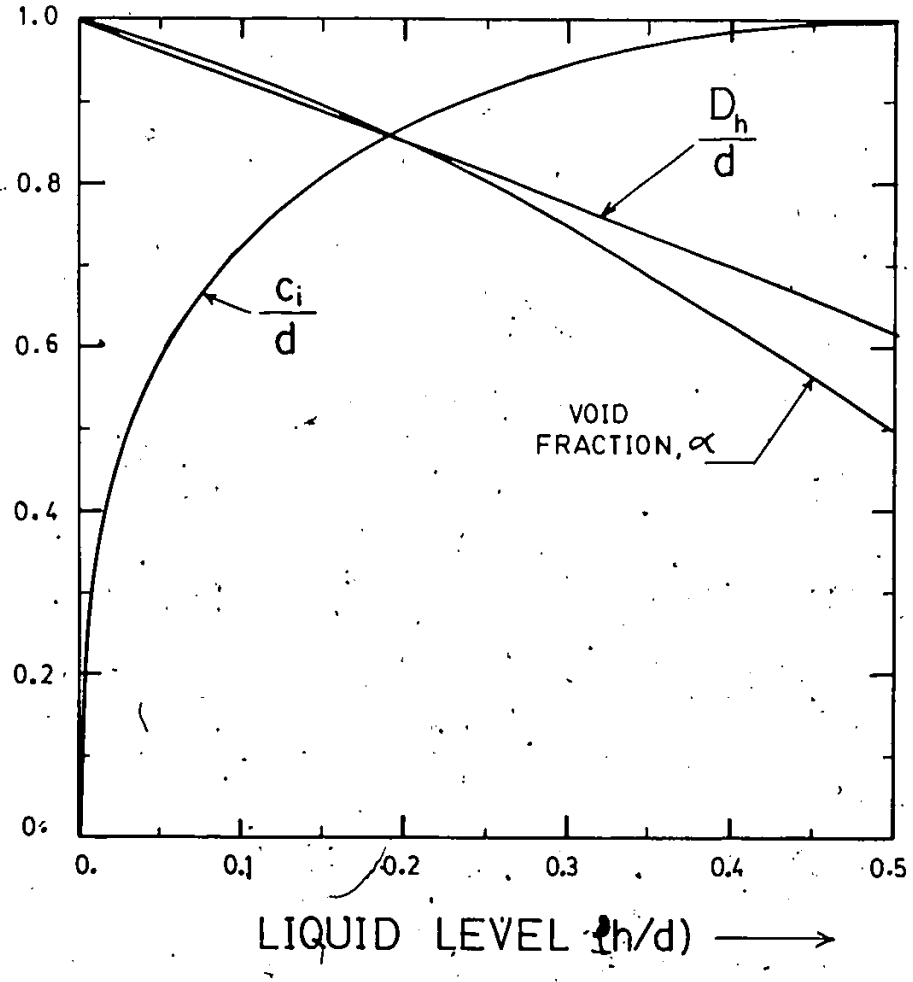

Fig. 4.11: Interfacial Width, Hydraulic Diameter and Void Fraction as a function of liquid level.

The two-phase energy balance is written as

$$p_g u_g A_g + \rho_l u_l A_l + F u_g = \hat{p_l} u A \qquad (4.39)$$

and assuming that the magnitudes of the overpressure in the gas and liquid phases are same and is equal to p_T; the final equation for the phasic overpressure can be forwarded [Sutradhar and Chang (1985a)] as

$$p_T [\alpha u_g + (1-\alpha) u_l] + F u_g = p_l u \qquad (4.40)$$

The pressure p_l for the single phase is obtained using the mass, momentum and energy Equations 4.25 to 4.27. Once p_l is known, the single phase particle velocity u is calculated from Equation 1.9 (in Chapter 1). The gas phase particle velocity u_g is estimated from the assumed value of p_T. The value of u_l is obtained from Equation 1.14 of Chapter 1 for the liquid phase particle velocity.

4.3.3 Computation

To solve the equations involving the phenomenon of unsteady wave propagation, the computation needs special care from the points of view of cost and memory limitations. The non-linear hyperbolic system of equations 4.25 to 4.27 is solved using the FORSIM-VI simulation package [Carver et al (1979)] based on the principle of the Method of Lines. The pressure, velocity, density etc at different locations along the shock tube as well as at different time steps can be obained using this program. The hyperbolic system of equations when solved numerically may

generate spurious oscillations which may dominate the solutions. The error introduced by the solution of the system of equations may be damped by introducing an artificial dissipation term in to the main equations. The numerical value chosen for the artificial dissipation term is imprecise, and as per Carver et al (1979), the solution as well as the error wave has to dissipate to some extent. Though the hyperbolic system of equations may be solved using the Method of Characteristics, but the method is difficult to use when the equations contain many independent variables. Moreover, the propagation of absolute error is higher when using the Method of Characteristics than that found in the use of the Method of Lines. The results obtained using the FORSIM-VI Simulation Package are shown in Figures 4.12 to 4.14 for the overpressure due to the shock wave propagation in a single phase system. In Figure 4.12, the pressure at a grid point for all the time steps are drawn using the computational method with time interval of 0.01 m-seconds. The oscillation in the output curve of pressure plots is controlled by the artificial dissipation parameter, but the reduced oscillations will provide dispersed shock wave which is not again desirable for the case under consideration. In Figure 4.13, the same pressure plot is obtained for a certain instant of time, say for 1.0 m-second at all the non- dimensional coordinate points along the shock tube. From the point of view of the computer time, a 71-point grid is chosen for the optimum combination of time and cost. Figure 4.14 is same as Figure 4.12, except that it provides the average values of the overpressures due to the shock wave propagation through the system. The wall friction f_w is estimated after iteration of Equation 4.31 using the method of functional iteration technique. The induced flow velocity

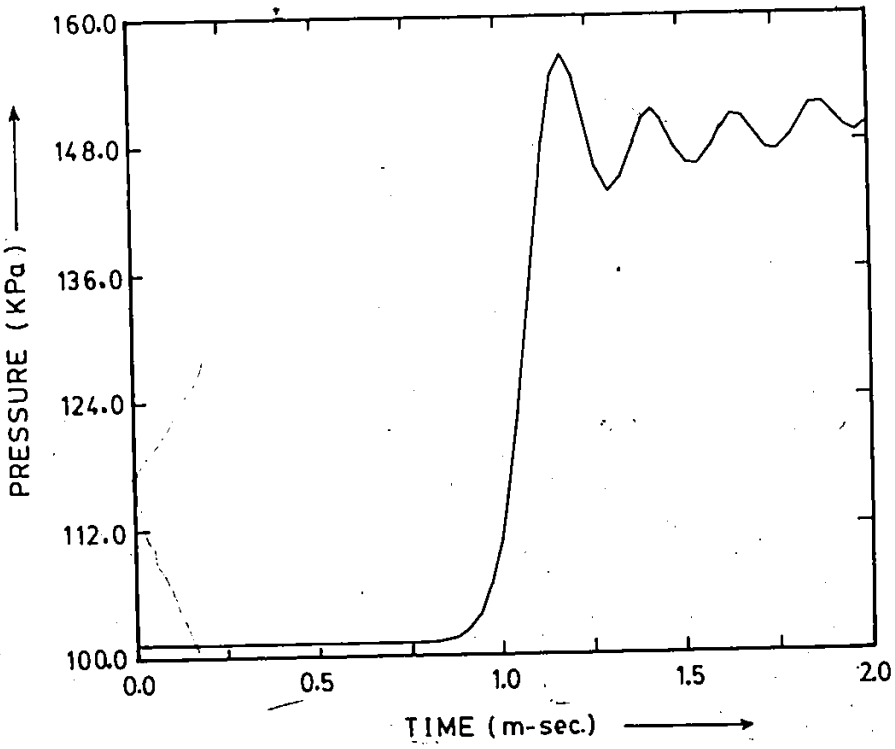

Fig. 4.12: Computer solution of a shock wave for different time steps at a point inside Aluminum shock tube.

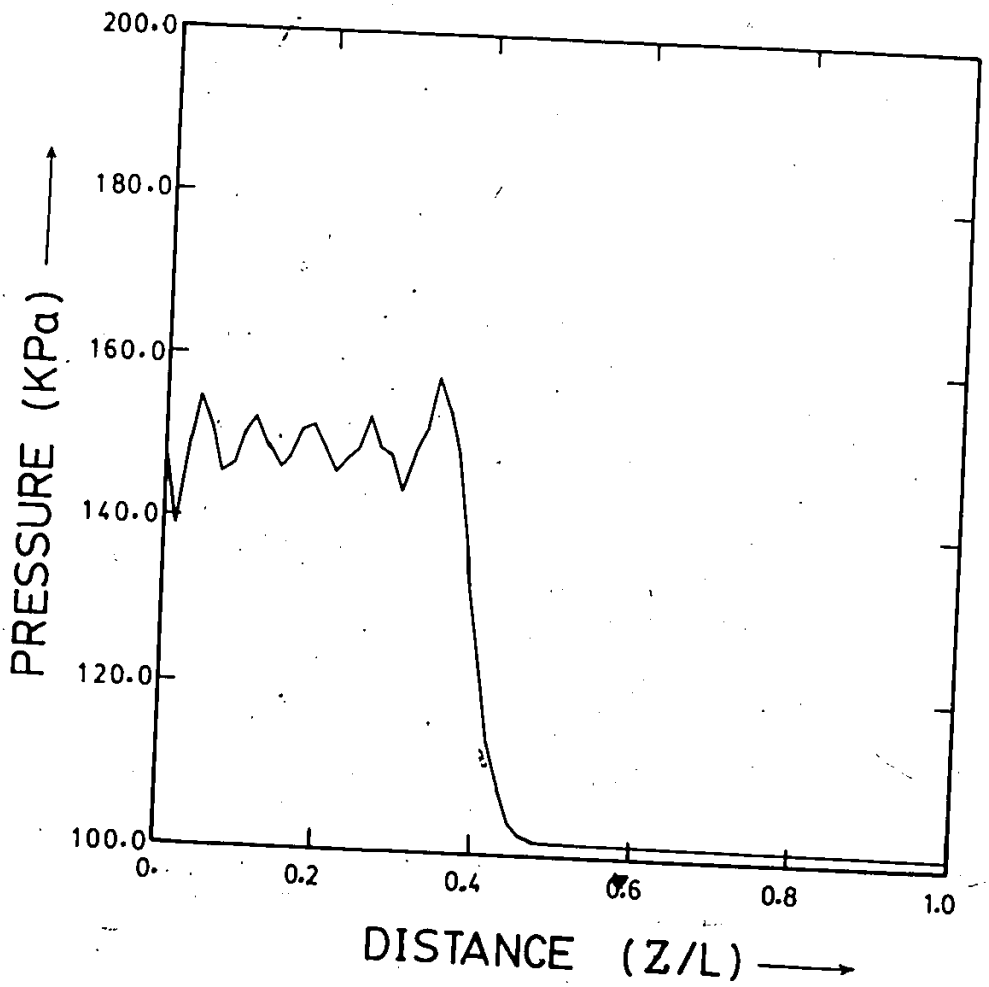

Fig. 4.13: Computer results of the overpressure at different locations, 1 m-sec. after diaphragm burst.

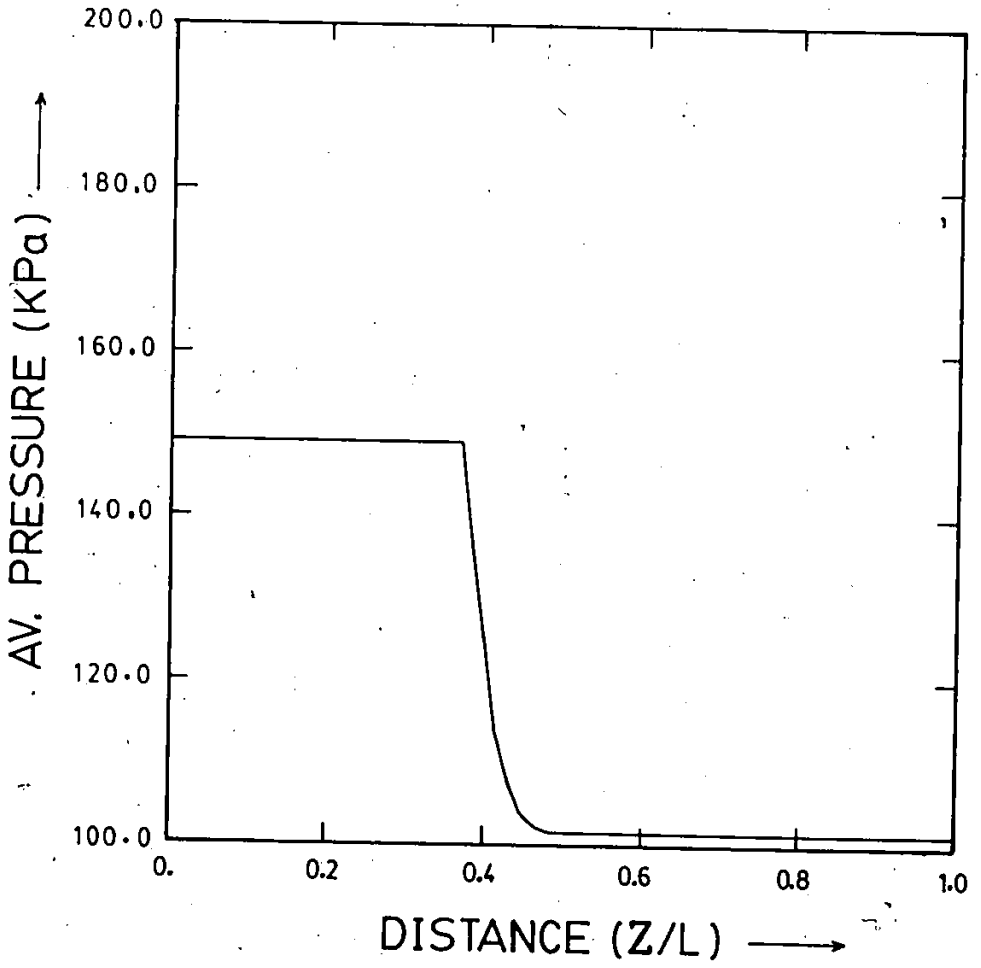

Fig. 4.14: Time averaged value of the overpressure, 1 m-sec. after diaphragm burst.

is used in estimating Reynolds number of the flow of the gas behind the shock wave. The time-average value of the overpressure due to the shock wave propagation with different diaphragm pressure ratios are obtained using this computational technique and the results for the diaphragm pressure ratios of 1.9, 2.2, 2.5 and 2.75 are respectively plotted in Figure 4.15. Equation 4.40 is solved using Newton-Raphson iteration technique to find the values of the overpressures in the phases. A functional iteration procedure is adopted to evaluate the values of the interface friction factor using Equation 4.13.

4.4 Experimental Results and Discussions

The experimental data explicitly indicate the fact that the speed of propagation of a shock wave in a two phase stratified flow system is identical to the speed of propagation in the gas phase alone. This is concluded by actually measuring the time taken by a shock wave of known strength to travel a certain distance along the shock tube. Also in Chapter 6, the experimental results for the propagation speed for the weak shock waves around 'TEE' junctions are presented. Under these circumstances, the shock wave phenomenon in a single (gas) phase system is taken as a reference point to calculate the effect in a two-phase stratified flow problems. Though the effect of the wall friction on the strengths of the incident shock waves is found to be very small and this effect is clearly shown in Figure 4.16. The slope of the curve of the friction factor is very flat for the ranges (0 to 0.02) of the friction factors of all practical purposes. With higher frictional losses, the strengths of the shock waves become very much reduced. In

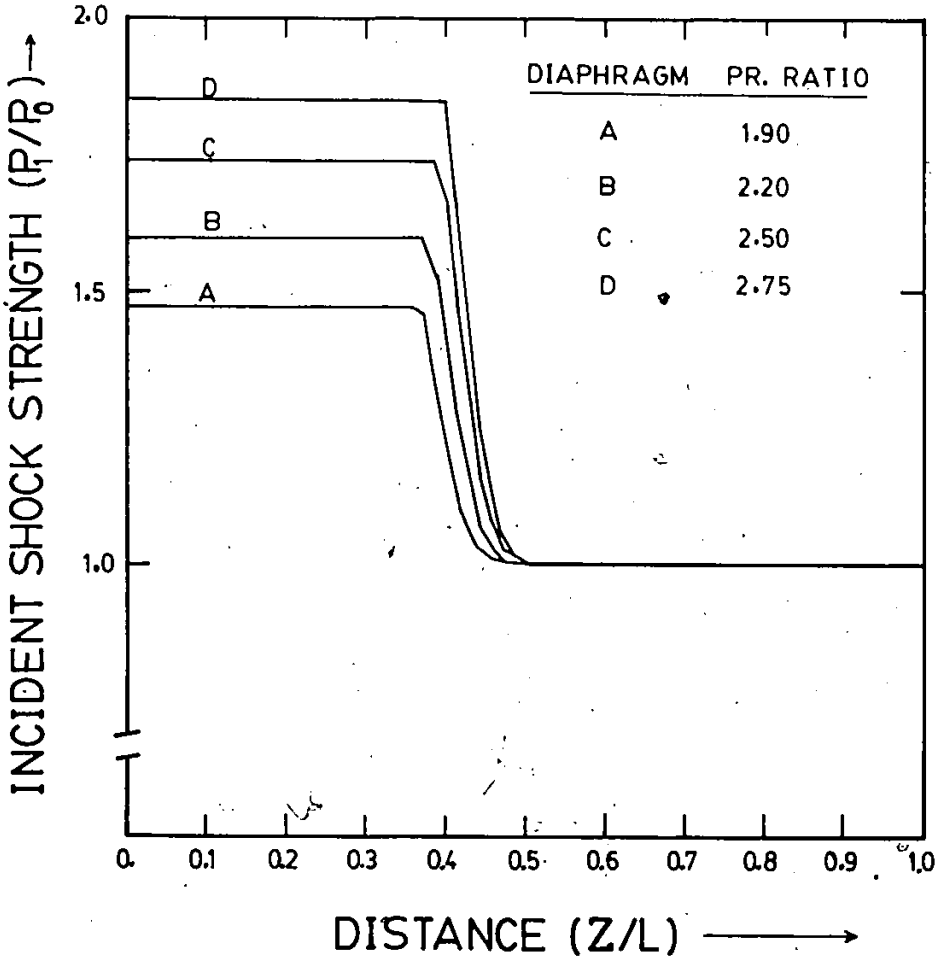

Fig. 4.15: Incident shock strengths calculated using FORSIM-VI as a function of diaphragm pressure ratio.

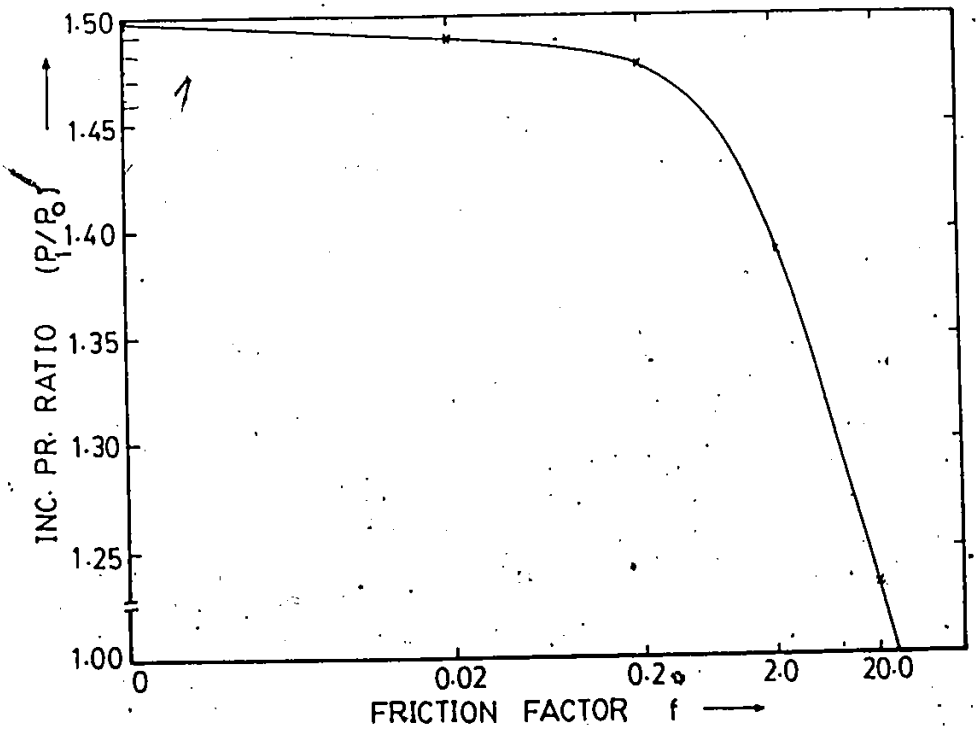

Fig. 4.16: Effect of wall friction on the strengths of incident shock waves in single (gas) phase system.

calculating the strengths of the incident shock waves, Equations 4.25 to 4.27 are used with friction factor of 0.01 to 0.015 and these values are obtained after iterating Equation 4.29 for the wall friction factor. For different diaphragm pressure ratios, the magnitudes of the overpressure due to the incident shock waves are obtained numerically and these values are plotted in Figure 4.17 against the experimental results for different diaphragm pressure ratios. The experimental values are plotted along with the error bars for the range of the values of the incident shock wave strengths. The pressure profiles at location D which is about 13-diameter downstream of the point of initiation of the shock waves, for the diaphragm pressure ratios of 1.8, 2.6 and 2.8 are presented in Figure 4.18 for the purpose of comparison. Once the data for the single phase flow system are obtained, then the attention is focussed in obtaining the data relating the case of two-phase flow situation. Liquid (here water) is poured into the shock tube to different heights of the tube and the shock waves are intercepted in the gas and the liquid phases at location D. The liquid heights of 15.0, 30.0 and 45.0 mm are used for the purpose of the experiment. In few cases, the liquid heights of 20.0 mm and 40.0 mm are used in the experiment to check the continuation of the theoretical predictions. In evaluating the magnitudes of the overpressures, a flat topped shock wave is considered in every case by averaging the data for a certain duration of time. For few cases, high oscillations are observed in the recorded data, particularly in the liquid phase of the system. The pressure profiles recorded in the liquid phase exhibit higher degree of dispersion than those observed in the gas phase. The rise in pressure in the liquid phase is slower than the rise in overpressure in the gas phase.

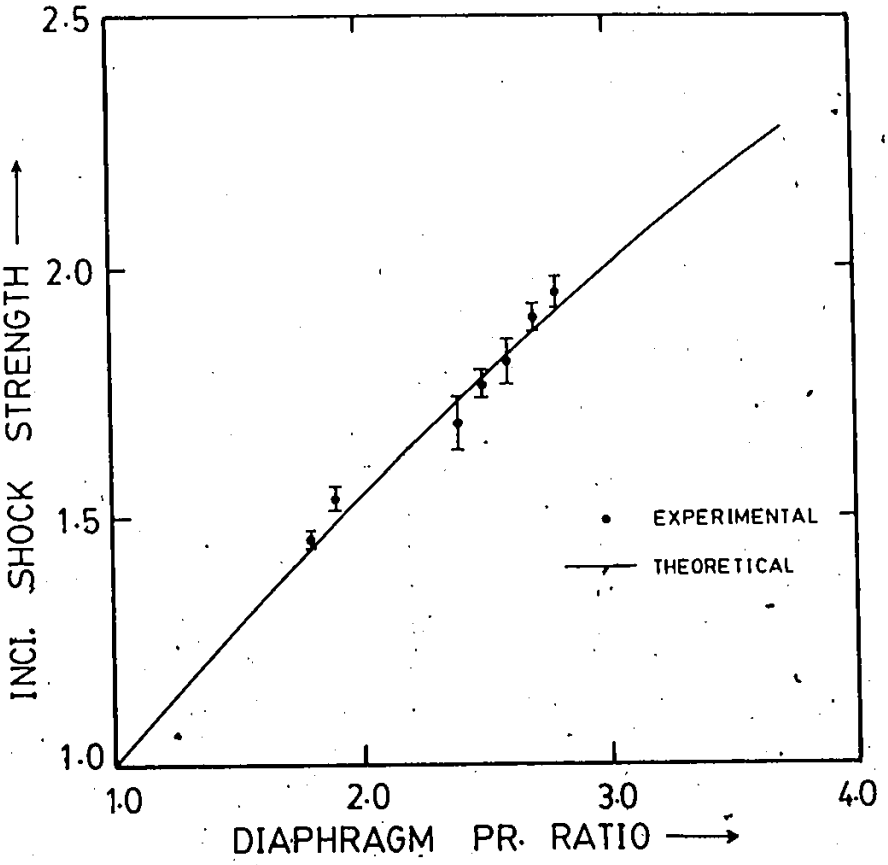

Fig. 4.17: Comparison of theoretical and experimental results of incident shock strengths as a function of diaphragm pressure ratio.

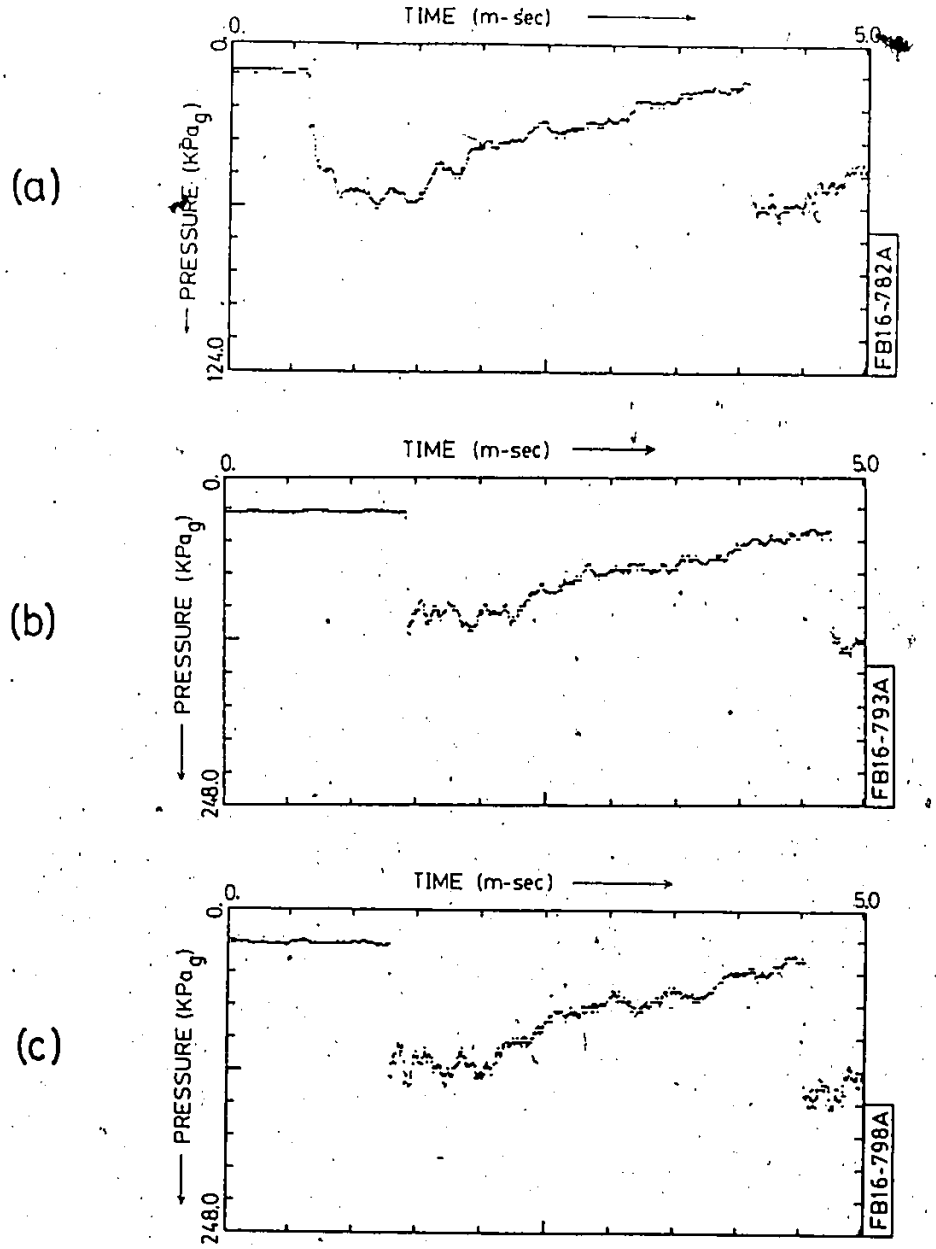

Fig. 4.18: Pressure waveforms in single (gas) phase system for diaphragm pressure ratios of a) 1.8, b) 2.6 and c) 2.8.

Gas phase maintains a sharp rise of overpressure and the shock waves are very distinct in the gas phase. Strengths of the shock waves are found to be gradually increasing with the increase in the liquid height while the diaphragm pressure ratio is maintained at a constant level. Similar trend is observed in both the phases and these results are shown in Figure 4.19 with the theoretical values obtained using Equation 4.40. With the higher liquid level, the predicted pressure is higher than the one observed experimentally; the experimental results show a linear increase of the pressure with the liquid level whereas the predicted values follow a non-linear trend. At higher liquid level, the formation of the shock waves may be slower because of the depth of the liquid present in the system. The discrepancies at deeper liquid layer may be attributed to the higher order of dispersion that is associated with the shock waves propagating in a highly incompressible fluid.

The actual pressure profiles recorded under various physical conditions are depicted in Figures 4.20 to 4.23 for the purpose of comparison. The experiments are conducted with closed end of the shock tube for fixed end condition. As expected, the reflected shock waves are stronger than the incident shock waves; however, when compared to the case of reflections in a single phase system, the strengths of reflected shock waves in the two-phase case are found to be very weak. The energy dissipation mechanisms in the case of reflections on two-phase stratified system may be studied in future. One possibility is that during the process of reflection, the interface becomes highly turbulent; also the gas phase in front of the reflected waves is highly infected by the water droplets or mists raised from the vortex sheet

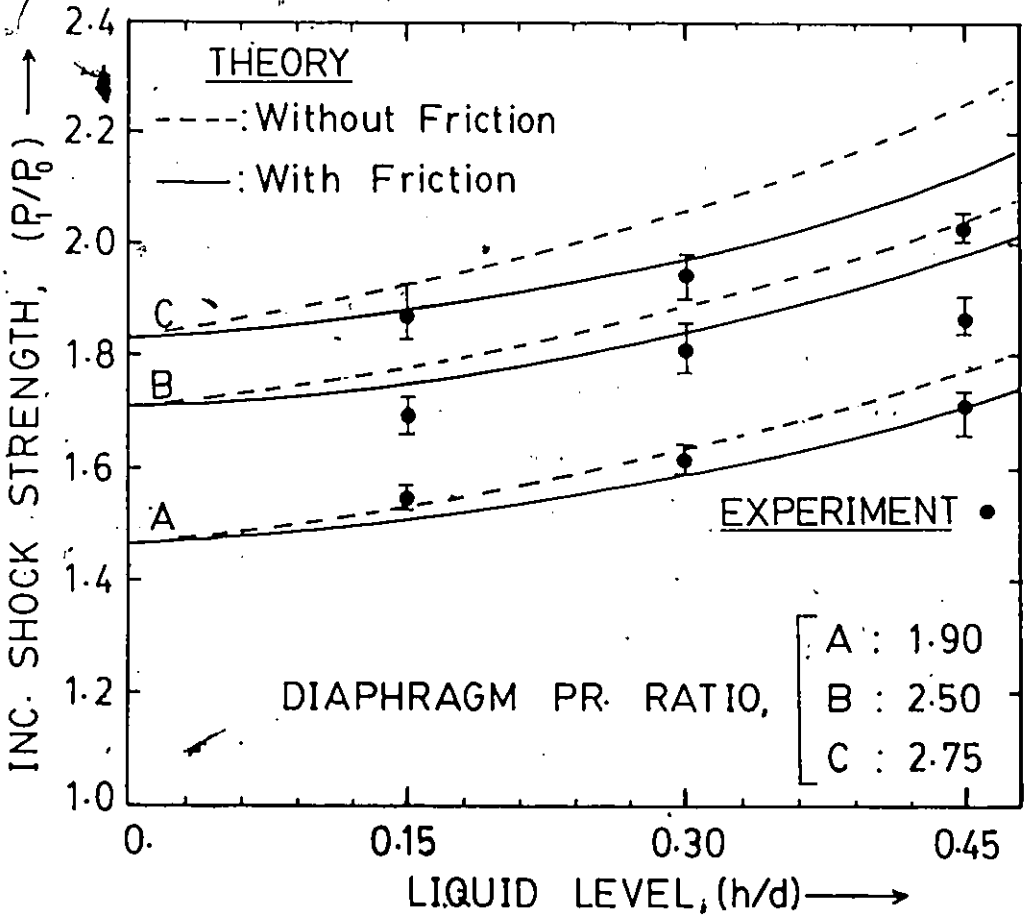

Fig. 4.19: Theoretical and experimental results of the effect of liquid level on the strengths of incident shock waves.

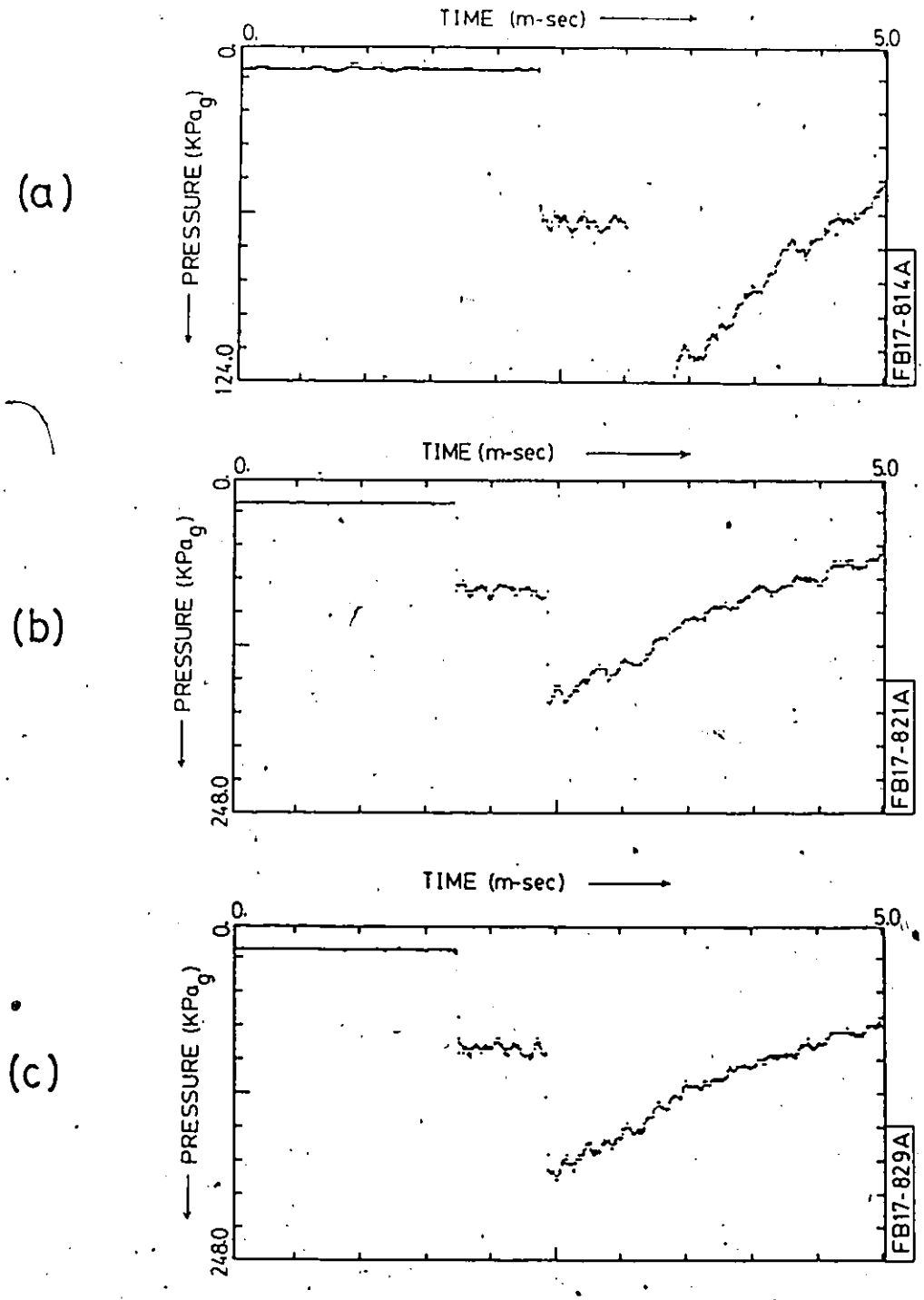

Fig. 4.20: Pressure waveforms in gas-phase for different liquid levels; a) 15, b) 30 and c) 45 mm for a diaphragm pressure ratio of 1.90.

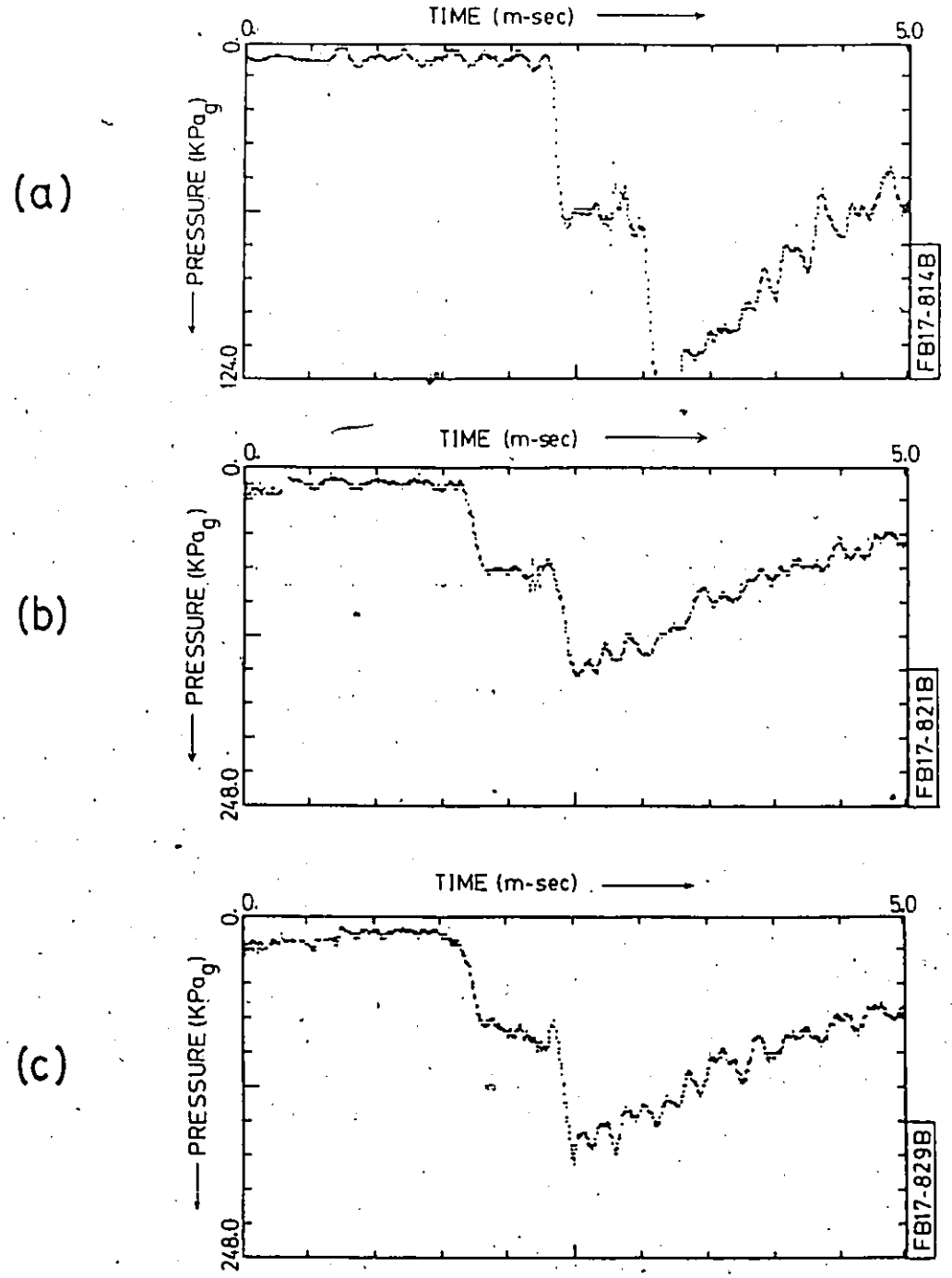

Fig. 4.21: Pressure waveforms in liquid-phase for different liquid levels; a) 15, b) 30 and c) 45 mm for a diaphragm pressure ratio of 1:90.

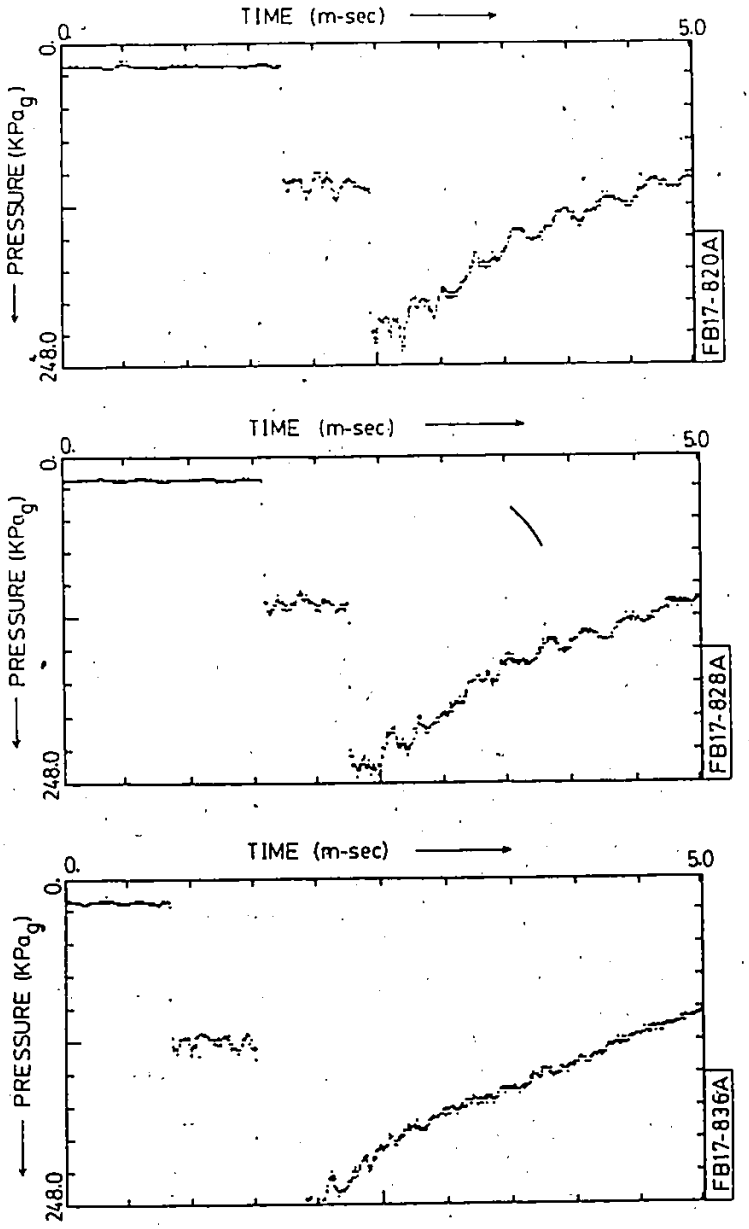

Fig. 4.22: Pressure waveforms in gas-phase for different liquid levels; a) 15, b) 30 and c) 45 mm for a diaphragm pressure ratio of 2.75.

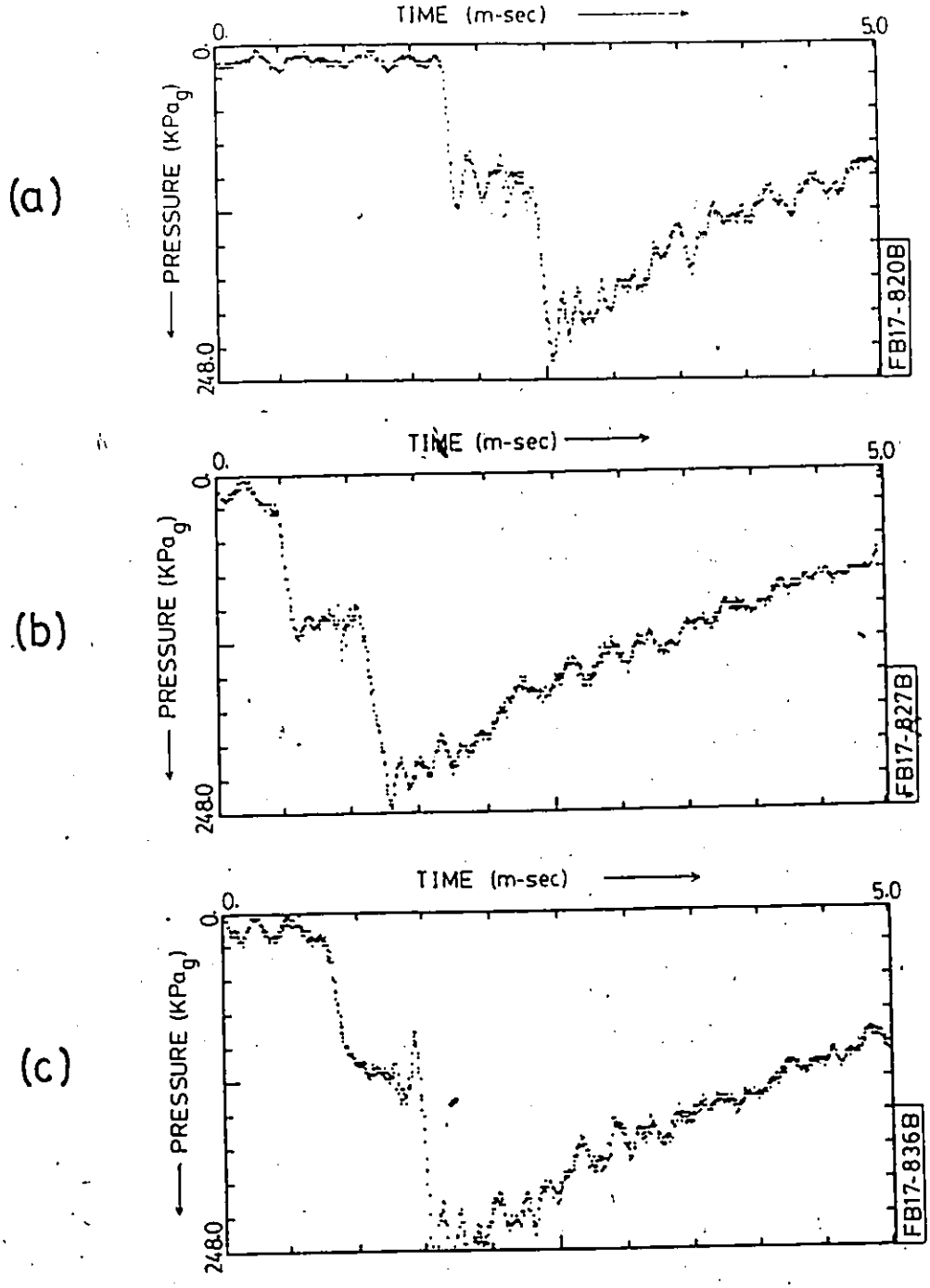

Fig. 4.23: Pressure waveforms in liquid-phase for different liquid levels; a) 15, b) 30 and c) 45 mm for a diaphragm pressure ratio of 2.75.

generated behind the incident shock wave. The high speed photography exhibits a high degree of interaction of the gas phase by the mist or the water droplets raised from the liquid interface. The situation is analogous to the case of shock wave propagating through a mixture of gas and liquid droplets. The calculation of the amount of moisture present in the gas phase needs further observations and study and the modelling for the overpressure in the phases may be based on the amount of the dispersed water droplets present in the gas phase.

CHAPTER 5

SHOCK WAVE INTERACTION WITH FUEL BUNDLES

5.1 Introduction

The pressure tubes of a CANDU-type nuclear reactor contain the fuel bundles arranged in tandem to allow the coolant to flow and carry the nuclear heat from the fuel elements. In the event of a LOCA (Loss Of Coolant Accident) or a blow-down accident, the weak shock waves generated in the Primary Heat Transport (PHT) system will interact with the fuel bundles. The flow stratification which is an aftermath of the LOCA, complicates the shock wave phenomenon due to the presence of the gaseous compressible fluids. In a stratified system, the shock wave phenomenon is highly influenced by the properties of the compressible phase rather than the incompressible phase of the system. The velocity of the wave propagation is dictated mainly by the sonic speed and other properties of the compressible phase. The presence of the liquid phase enhances the shock wave strength by reducing the effective cross sectional area of the compressible phase. The reflected and transmitted waves are also influenced in a similar way by the liquid level. Another important phenomenon, which is effective in reducing the strength of transmitted shock wave, is the occurrence of the choking inside the fuel bundles. The available flow area through a fuel bundle may be specified by the parameter called the porosity, e for each individual fuel bundle.

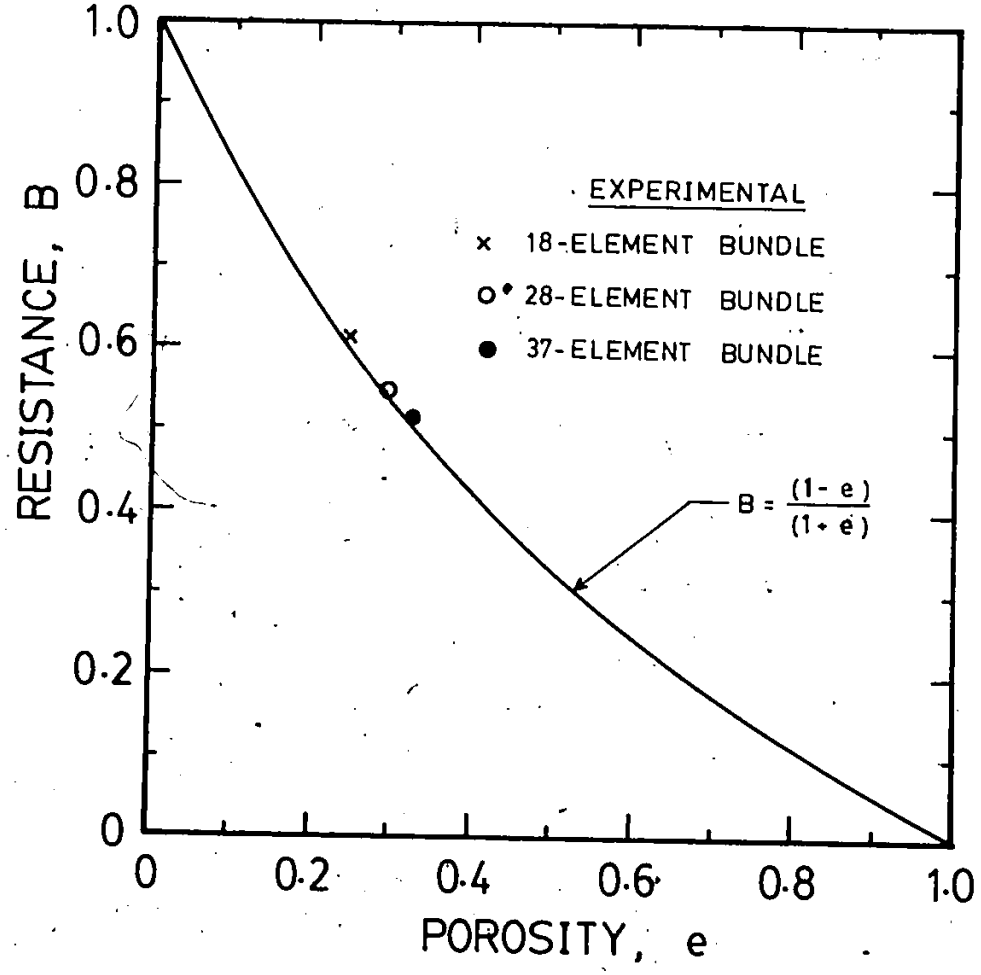

Fig. 5.1: Porosity vs. Resistance for different CANDU-fuel bundle.

In order to estimate the porosity, the fuel element, end covers, spacers etc of each fuel bundle are measured carefully and the porosity is estimated from the actual flow area perpendicular to the flow direction through the fuel bundle. After evaluating the porosity of each fuel bundle, a resistance parameter, B is defined as follows [Yoshida et al (1980)]

$$B = (1-e)/(1+e) \tag{5.1}$$

The plot of the resistance parameter, B as a function of e is shown in Figure 5.1.

5.2 Problem Formulation

5.2.1 Single-Phase Interaction

The schematic of the wave interaction is shown in Figure 5.2. The analysis is approached with the single phase shock dynamics where the contribution of the gas phase has the dominating influence on the interaction with the fuel bundles. As shown in Figure 5.2, a shock wave of initial strength p_1 is approaching towards a fuel bundle positioned in quiescent gas at some reference condition, p_0. The velocity of the incident shock wave is w_1 and the corresponding values of the density and the particle velocity behind the incident shock wave are shown in Figure 5.2(a). After the interaction, a reflected wave moves in the upstream direction and another part travels through the fuel bundle and emerges on the far end of the bundle. The conditions behind the reflected and the transmitted shock waves are denoted by the subscripts

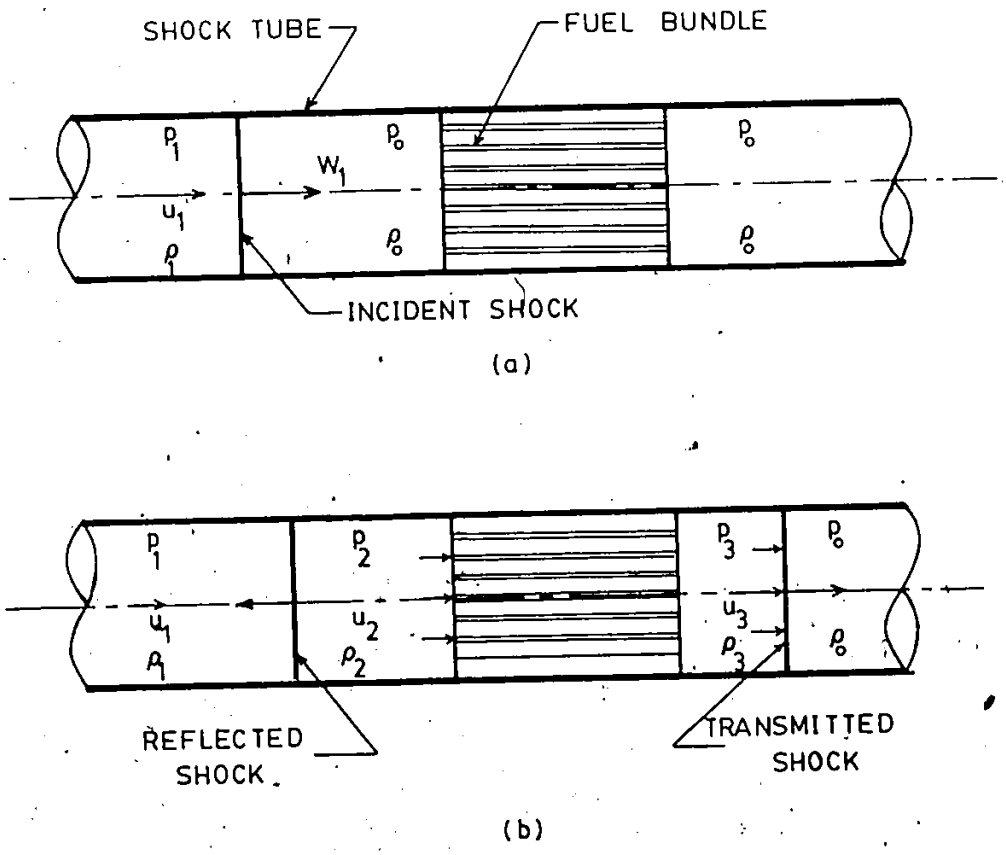

Fig. 5.2: Sketch of shock wave interaction with fuel bundle inside a pressure tube.

2 and 3 respectively. For the range of the strength of the shock waves considered here, the generation of the enthalpy due to the shock waves is negligible and hence, only the conservation of mass and momentum under a quasi-steady flow condition is considered.

For the reflected wave, the mass and momentum equations are

$$\rho_1 (u_1+w_2) = \rho_2 (u_2+w_2) \tag{5.2}$$

$$p_1 + \rho_1 (u_1+ w_2)^2 = p_2 + \rho_2 (u_2 + w_2)^2 + B (p_c - p_2) \tag{5.3}$$

The value of p_c which represents the strength of the completely reflected wave from an impermeable substance for a known strength of the incident shock wave is obtained using the principle of superposition of two shock waves moving in the opposite directions [Wade (1985)] as follows

$$p_c/p_0 = [2 (p_1/p_0)^{(\gamma-1)/2\gamma} - 1]^{2\gamma/(\gamma-1)} \tag{5.4}$$

The values of the particle velocity, density behind a shock wave and the speed of the shock wave may be obtained from the standard shock wave relations presented in Chapter 1. Combining Equations 5.2 and 5.3 and eliminating u_2, the implicit equation for the strength of the reflected wave is obtained as follows [Sutradhar and Chang (1985b)]

$$\frac{p_2}{p_0} = \frac{p_1}{p_0} + \frac{\rho_1}{p_0} (u_1+w_2)^2 \left(1 - \frac{\rho_1}{\rho_2}\right) - B \left(\frac{p_2}{p_0}\right) \left(\frac{p_c}{p_2} - 1\right) \qquad (5.5)$$

Following a similar argument, the conservation of mass and momentum for the transmitted shock wave may be written as

$$\rho_2 u_2 = \rho_3 u_3 \qquad (5.6)$$

$$p_2 + \rho_2 u_2^2 = p_3 + \rho_3 u_3^2 + B (p_2-p_0) \qquad (5.7)$$

In the calculation of the strength of a transmitted shock wave, the factor concerning the choking inside the fuel bundle for flow velocities greater than the sonic velocity will be considered in appropriate place at a later stage of the development. Now, combining Equations 5.6 and 5.7, the strength of the transmitted shock waves can be stated as follows [Sutradhar and Chang (1985b)]

$$\frac{p_3}{p_0} = \frac{p_2}{p_0} + \frac{\rho_2}{p_0} \left(1 - \frac{u_3}{u_2}\right) u_2^2 - B \left(\frac{p_2}{p_0} - 1\right) \qquad (5.8)$$

For complete blockage, Equations 5.2 and 5.3 are modified with assumptions that for B=1, $p_c = p_2$ and the resultant particle velocity u_2 after the reflection is zero. To evaluate the pressure, the solution of the momentum Equation 5.3 will provide the values of the pressure of the reflected shock waves under this condition.

5.2.2 Frictional Effect inside Fuel Bundles

The fuel bundles offer frictional resistances due to the high speed flow of gas over the fuel elements and keeping this in mind, the critical Mach number inside the fuel bundle is calculated using Fanno flow phenomenon [Shapiro (1953)]. For the transmitted part of the shock wave, the bundle is treated as a simple convergent-straight nozzle. The initial velocity into the bundle is calculated just at the nozzle inlet and that at the bundle outlet is based on the exit section of the bundle geometry. The appropriate area reduction proportional to the porosity of each bundle, also calculated in the process of the model development. The equivalent friction factor is estimated using the formula forwarded by Rudinger (1969) (Equation 4.29 of Chapter 4).

Depending on the inlet Mach number to the bundle, the transmitted shock wave strength is modified by the amount of frictional loss using the following equation [Shapiro (1953)]

$$f \frac{L_{max}}{D_h} = \int_M^1 \frac{2(1-M^2)}{[1+(\gamma-1)M^2/2]M^3} dM \qquad (5.9)$$

where the maximum length corresponds to the point where the Mach number inside the fuel bundle attains a value equal to unity, f is the friction factor obtained for the frictional loss inside the bundle, D_h is the hydraulic diameter of the equivalent convergent-straight nozzle and M is the Mach number at the entrance to the bundle system.

The theoretical plot of Equation 5.9 is presented in Figure 5.3. This plot shows the effect of the wall shear stress on the Mach number at the entrance to the constant area duct. In calculating the losses due to the friction in a convergent-straight nozzle, the maximum inlet Mach number may be restricted to unity. The solution of Equation 5.9 in terms of the inlet Mach number for air can be obtained (integrating by method of partial fraction) as follows

$$f\frac{L_{max}}{D_h} = \frac{2}{\gamma}\left[\frac{1+\alpha}{2}\ln(1+\alpha M^2) - \frac{1}{2}\left(\frac{1}{M^2}\right) - (1+\alpha)\ln M\right]_M^1 \quad (5.10)$$

here $\alpha = (\gamma-1)/2$

For certain values of f and D_h, the maximum length of the duct, L_{max} to the point of choking for a certain inlet Mach number can be evaluated with this equation. Once choking occurred inside the bundle, the Mach number at the exit of the duct is assumed unity. If p^* denotes the pressure corresponding to the point of choking, then the following identity may be used to find the pressure drop inside the bundle due to the frictional loss [Shapiro (1953)].

$$\int_p^{p^*}\frac{dp}{p} = -\int_M^1 \frac{1}{M}\left[\frac{1+(\gamma-1)M^2}{1+(\gamma-1)M^2/2}\right]dM \quad (5.11)$$

Similar to Equation 5.9, the solution of this equation for air is obtained as follows

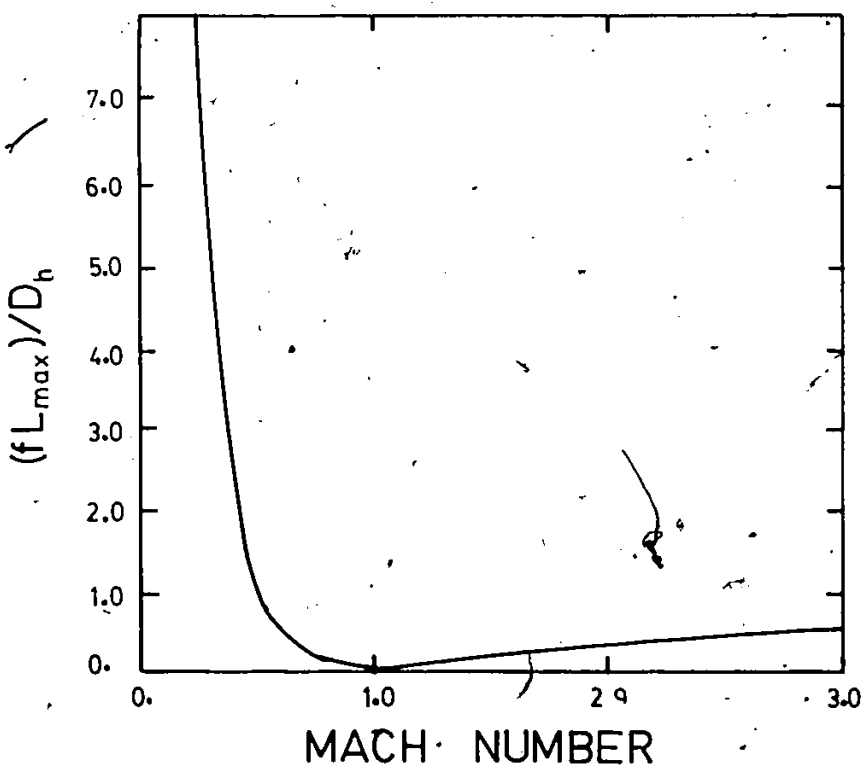

Fig. 5.3: Frictional effect as a function of Mach number under Fanno flow condition.

$$p = p^{*} \exp[0.09\ 1 - \ln \{M[1+0.2\ M^2]^{1/2}\}] \qquad (5.12)$$

The expression presented above has the limitation for its application to flows with inlet Mach number less than unity. For higher inlet Mach number condition, further modification is intended for future work.

In the CANDU system, the length of the pressure tube is about 4.0 metres i.e. 8 fuel bundles each of 0.5 metre long can be put end-to-end. If the concept of choking is applied, then for most of the pressure ranges of the practical application the choking seems to be inevitable. Though the reflected waves will be maintaining their strengths unchanged, the strengths of the transmitted shock waves will be significantly reduced due to the presence of the choking and as a consequence, these waves will have diminishing strengths at the exit of the tube array. However, in the process of the transmission, the shock waves may induce high vibrational effect on the fuel elements which may reduce the life of the fuel bundles.

5.2.3 Bundles in Two-Phase System

To estimate the pressure behind a reflected wave in the presence of a two-phase system, the problem is analyzed in a fashion similar to the case of two-phase flow in straight pressure tube of Section 4.2. The principle of conservation of energy under a quasi-steady shock wave phenomenon is applied in finding the strength of the reflected wave under a two-phase situation. The reflected shock waves in single- and

two-phase situation are dealt as independent shock waves similar to the incident waves. To evaluate the strength of the reflected wave, the following steps are followed. At first, the incident wave strength for a particular diaphragm pressure ratio is obtained for different liquid depths. The strength of the reflected wave for a particular liquid level is obtained using the theory developed earlier in this section. While considering the reflected wave, it is treated as an independent shock wave generated by the bundle itself. The reflected shock strength is then modified using the principle of conservation of energy under a quasi-steady wave flow condition using Equation 4.40.

For the transmitted shock waves, the choking becomes very severe in almost all the cases under consideration. The strengths of the transmitted waves should either decrease or remain same for the range of the liquid levels considered here. The shock waves, while propagating through the fuel bundle, will try to increase the pressure inside it and this trend may have detrimental effect on the life and durability of the fuel bundles. The oscillations of the fuel elements induced by the shock waves greatly enhance the perturbations at the interface of the two-phase systems.

5.2.4. Computation

In order to evaluate the implicit Equation 5.5 and 5.8 for the strengths of the reflected and the transmitted shock waves for different porosities, Newton-Raphson iteration technique is used. The value of the resistance parameter, B for a particular porosity is obtained from

Equation 5.1 and then the strengths of the completely reflected shock waves are evaluated using Equation 5.4. Other shock wave parameters such as propagation speed, density, temperature, particle velocity pertaining to each type of flow situation are estimated from the standard shock wave relations as specified in Chapter 1. The estimation of the strengths of the reflected shock waves for different porosities of the fuel bundle is obtained using Equation 5.5. To obtain the strengths of the transmitted waves, Equation 5.8, as mentioned earlier is solved using Newton-Raphson iteration technique. However, for the transmitted waves, three different hypotheses are examined. At first, the values of the transmitted shock wave pressure ratios are obtained without any frictional effect. Then in the second step, the frictional effect with pure incompressible flow through the fuel bundle assembly is assumed and the values obtained in the first step is modified by the frictional loss through the bundles. In the third step the choking is introduced up to the point of subsonic flow range. The non-linear plot obtained in this case, show the presence of the choking for all the pressure ranges considered here. Choking in the fuel bundles is calculated on the basis of the Fanno flow effect inside a constant area duct in the presence of the friction.

5.3 Experimental Results and Discussions

5.3.1 Single-Phase System

Three fuel bundles, viz. 18-element, 28-element and 37-element are used for the purpose of the experiment. The porosity of each bundle is determined by accurately measuring the fuel element diameter and

other related physical parameters. The diameters of fuel elements of 18-, 28- and 37-element fuel bundles are respectively 19.9 mm, 15.4 mm and 13.1 mm. The blockage due to the end cover, bearings, spacers and studs is approximated to be 15% of the blockage area of all the fuel elements of each type of the bundle. The porosity is defined as the percentage of the net flow area available to the fluid for flowing through the fuel bundles. The overall diameter of the bundle (bearing to bearing) is about 101.0 mm. With all the physical dimensions of the fuel bundles, the porosities for 18-, 28- and 37-element fuel bundles are found to be respectively 0.24, 0.29 and 0.32. These values are plotted in Figure 5.1 against the resistance as per Equation 5.1. The end conditions are such that when the porosity is zero, the resistance is one hundred percent and when the porosity is unity, the resistance due to the fuel bundle assembly is absent.

The experimental and the theoretical results for the reflected shock waves for different fuel bundles are shown in Figure 5.4 along with the results obtained with complete blockage. The porosities of three types of fuel bundles considered here are very close and as a result, the theoretical curves drawn using Equation 5.5 are also observed to be very close to each other. The present facilities can be used to find the strengths of the shock waves for the diaphragm pressure ratio up to 2.8 which corresponds to the incident shock wave strength of about 1.75. The experimental data are averaged over a certain time period to obtain the smooth flat-topped waveforms for all the pressure profiles. Also the theoretical results for the incident shock wave strengths of 1.0 to 3.0 for different porosities are plotted in Figure

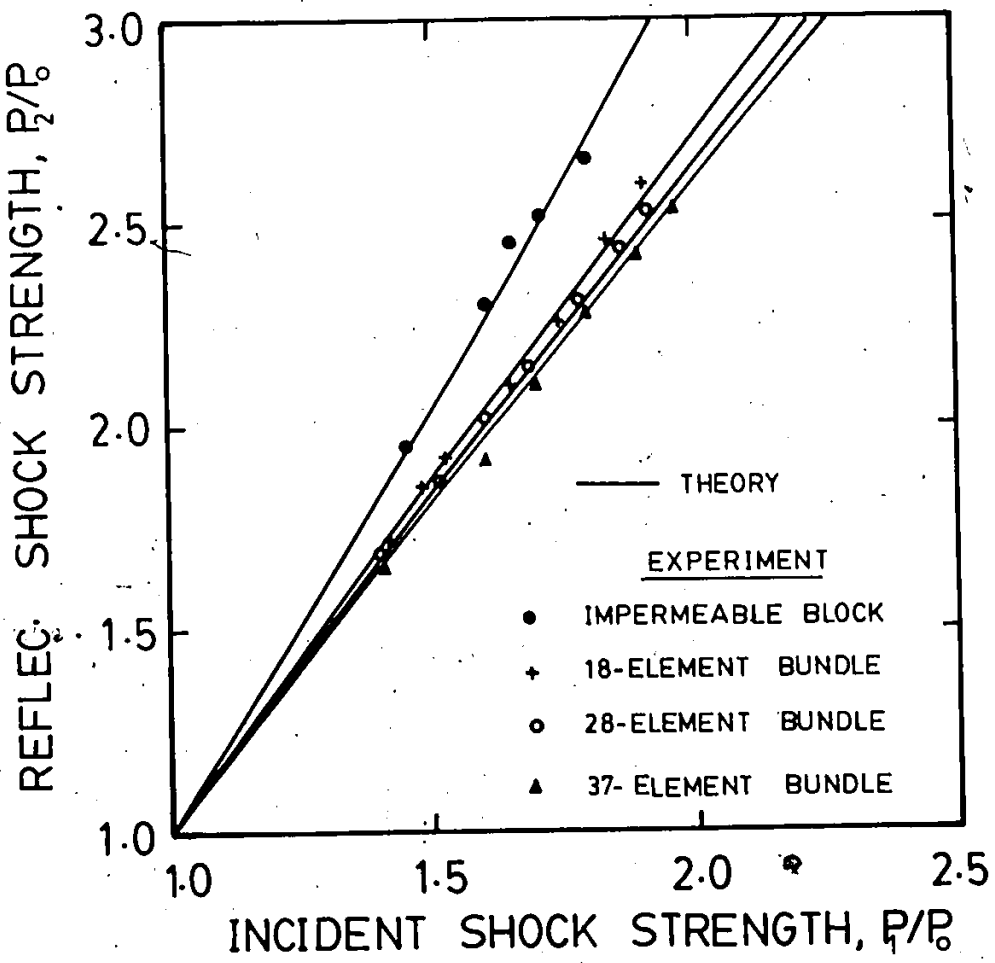

Fig. 5.4: Reflected vs. incident shock strengths for different fuel bundles in single (gas) phase.

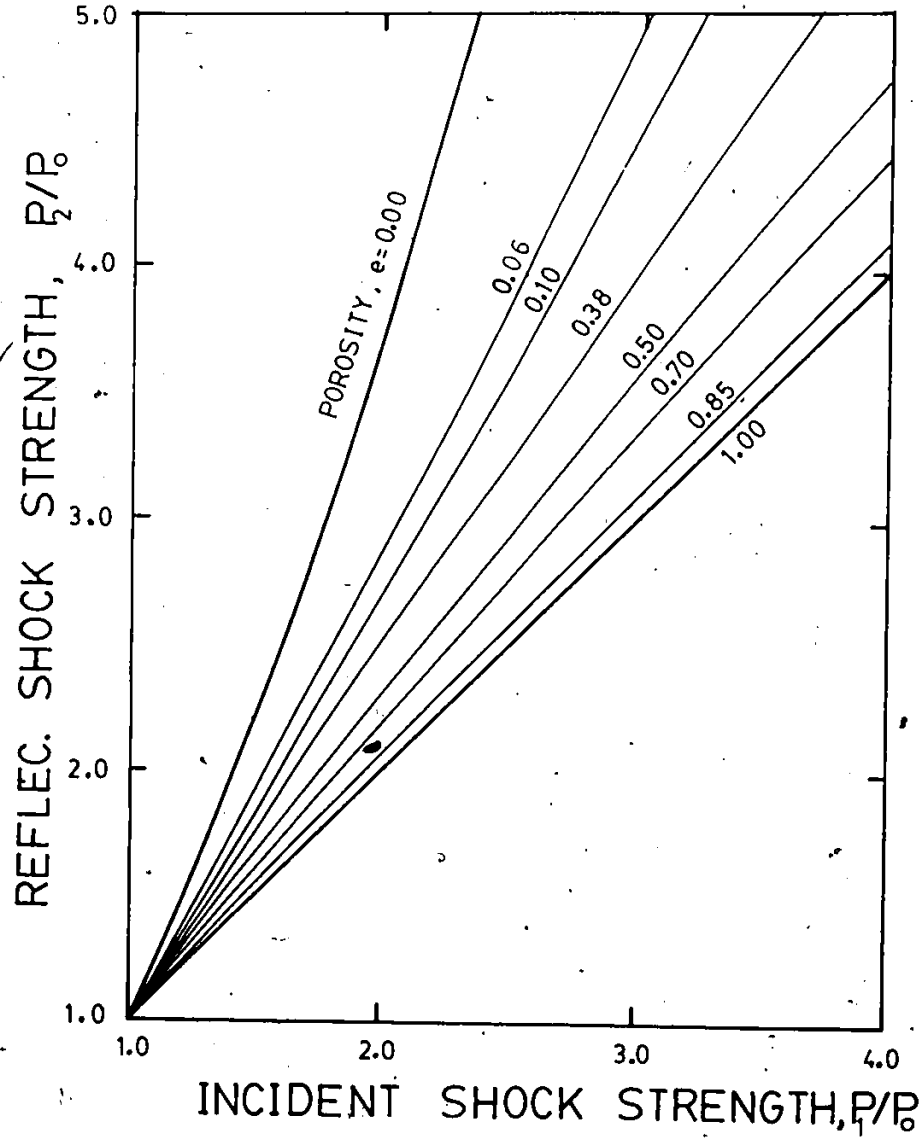

Fig. 5.5: Reflected vs. incident shock strengths for different porosities in a single (gas) phase.

5.5. The theoretical results along with the experimental values of the strengths of the transmitted waves for three different fuel bundles are shown in Figure 5.6. The non-linear portion of each curve is the theoretical evaluation of the choking effect that may be present in the case of individual fuel bundle. The Mach number at the entrance of the fuel bundle is considered from subsonic to sonic condition only. For straight channel, the supersonic velocities inside the fuel bundle are not considered. Near the choking zone, the present experimental data do not show clearly any choking effect, but theoretically, if the entrance Mach number attains more than the unity, there should be choking in the system. If instead of considering the choking, only ordinary frictional loss through the passage is considered, then the theoretical plot will look like the one presented in Figure 5.7. In this case, the theoretical values are a little higher than those obtained in the experiment. The theoretical estimation of the Mach number distributions at the inlet and exit of the 37-element fuel bundle is shown in Figure 5.8. The solid line in that figure shows the Mach number at the inlet and the dotted line for Mach number at the exit of the bundle assembly. The frictional effect due to the fuel elements increases the Mach number in the downstream direction. Theoretically, for the incident shock strengths more than 2.0, the bundle assembly exhibits the effect of choking.

5.3.2 Two-Phase System

The passage of a shock wave through a fuel bundle placed inside the pressure tube having a two-phase gas liquid system in stratified condition, shows a different waveform in the gas and the liquid phases.

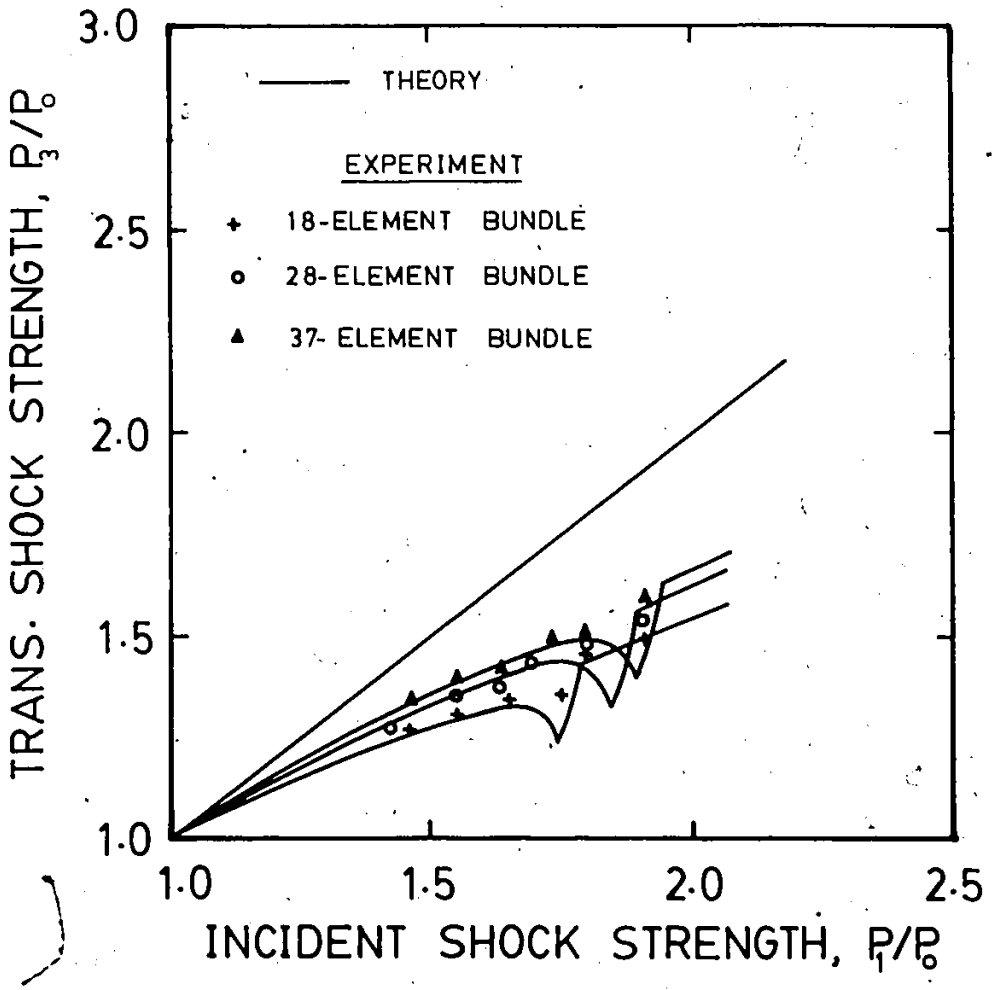

Fig. 5.6: Transmitted vs. incident shock strengths for different fuel bundles in single (gas) phase.

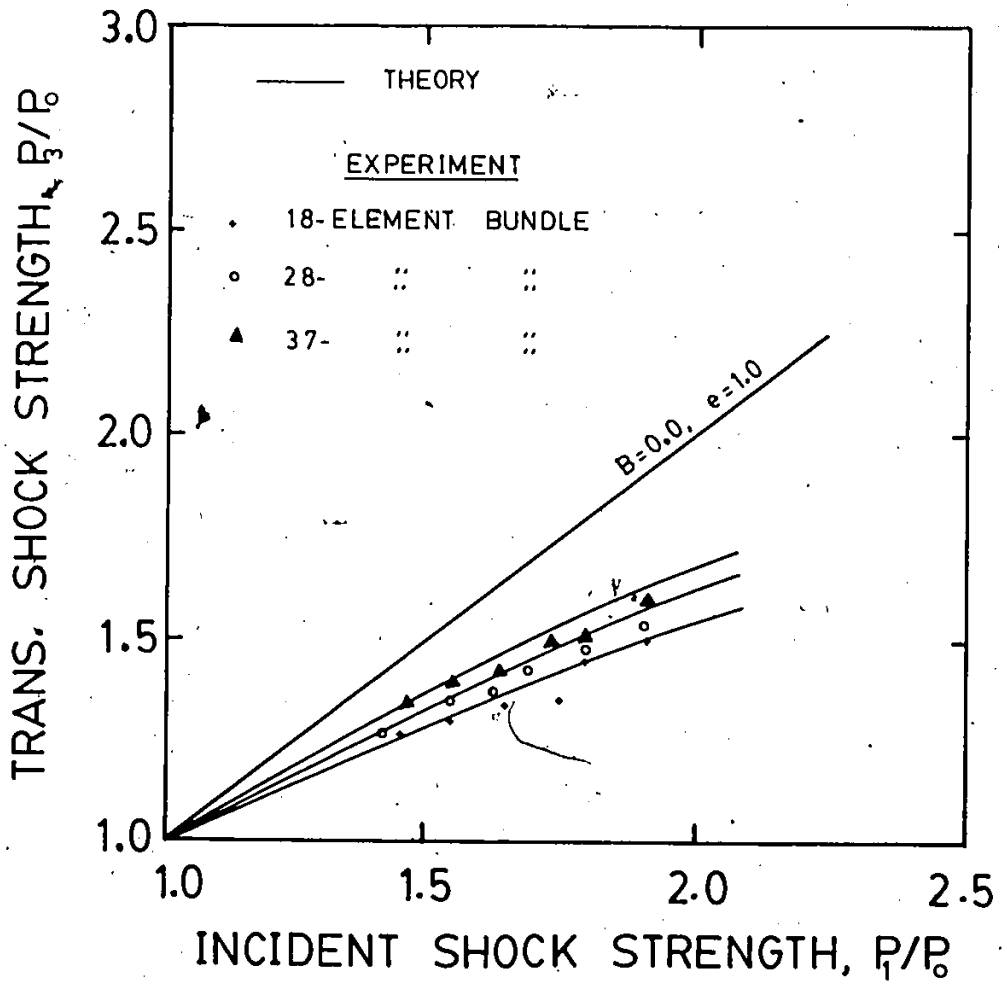

Fig. 5.7: Transmitted vs. incident shock strengths for different fuel bundles obtained using incompressible hydraulic loss under single (gas) phase condition.

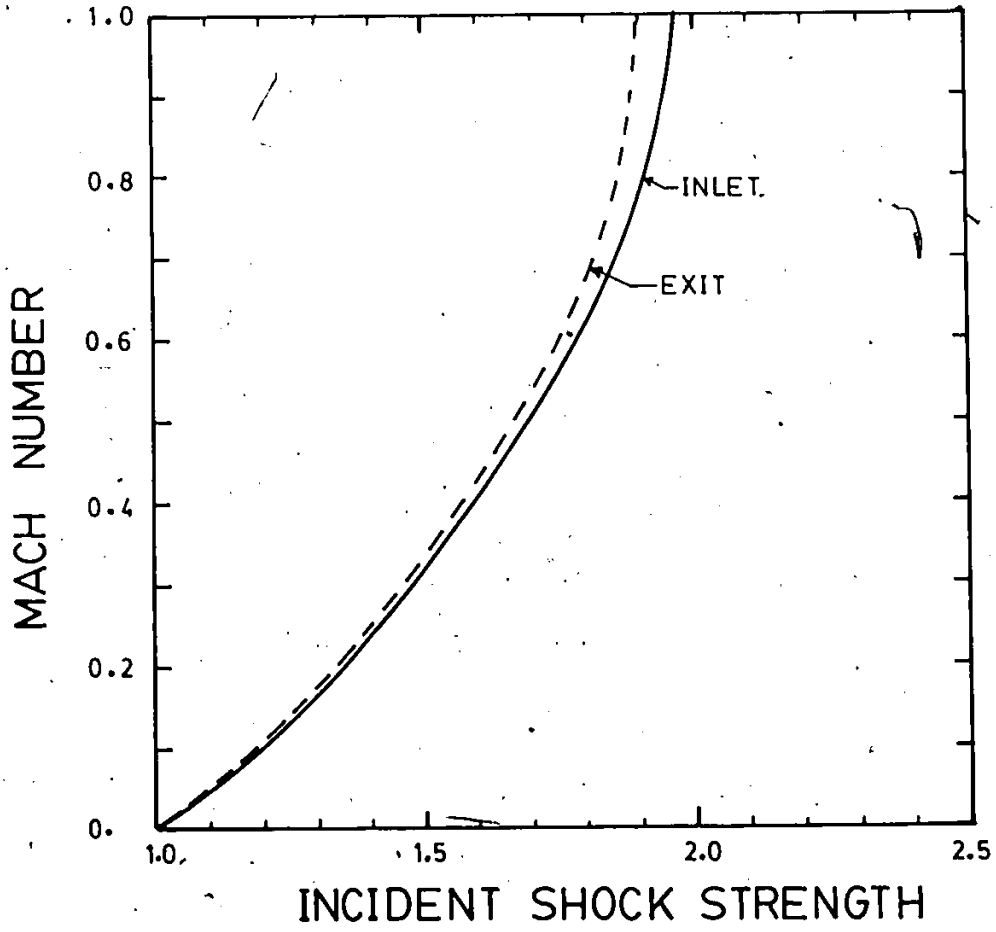

Fig. 5.8: Mach numbers at inlet and exit of 37-element fuel bundle as a function of incident shock strength, calculated using compressibility effect.

For the case of 37-element fuel bundle, the experimental results of this effect is shown in Figure 5.9. In the gas (single) phase (Figure 5.9(i)), the waveform almost has a flat-topped characteristic whereas that in the liquid phase (Figure 5.9(ii)) has a sharp peak with sufficient oscillations. The experimental results for the strengths of the pressure waves propagating through the fuel bundles are shown in Figures 5.10 and 5.11 for the gas and the liquid phases respectively. Both the maximum and the average pressures are plotted for the different diaphragm pressure ratios. In the gas phase, the average pressure shows a moderate increase with the increase in the liquid level, but in the liquid phase, the increase is prominent in magnitude. The high oscillations in the pressue distribution make the system very unstable and these characteristics may induce high flow-induced vibrations in the fuel bundle elements. The severe vibrational effects may, in many cases dislodge some fuel elements from the bundle assembly.

In contrast to the experimental evidences inside the fuel bundles, those observed upstream and downstream of the fuel bundles show moderate behaviour in the magnitude of the overpressures. The fluctuations observed inside the fuel bundles do not seem to be present outside the fuel bundles. In Figure 5.12 the experimental waveforms for the reflected shock waves in the gas and the liquid phases demonstrate the gradual changes in the overpressure. Some arguments seems to be true for the strengths of the transmitted waves in the gas and the liquid phases in the presence of the fuel bundles, as shown in Figure 5.13. For the two-phase stratified system, the shock wave interaction with the fuel bundles has revealed the condition of enhanced strengths of the

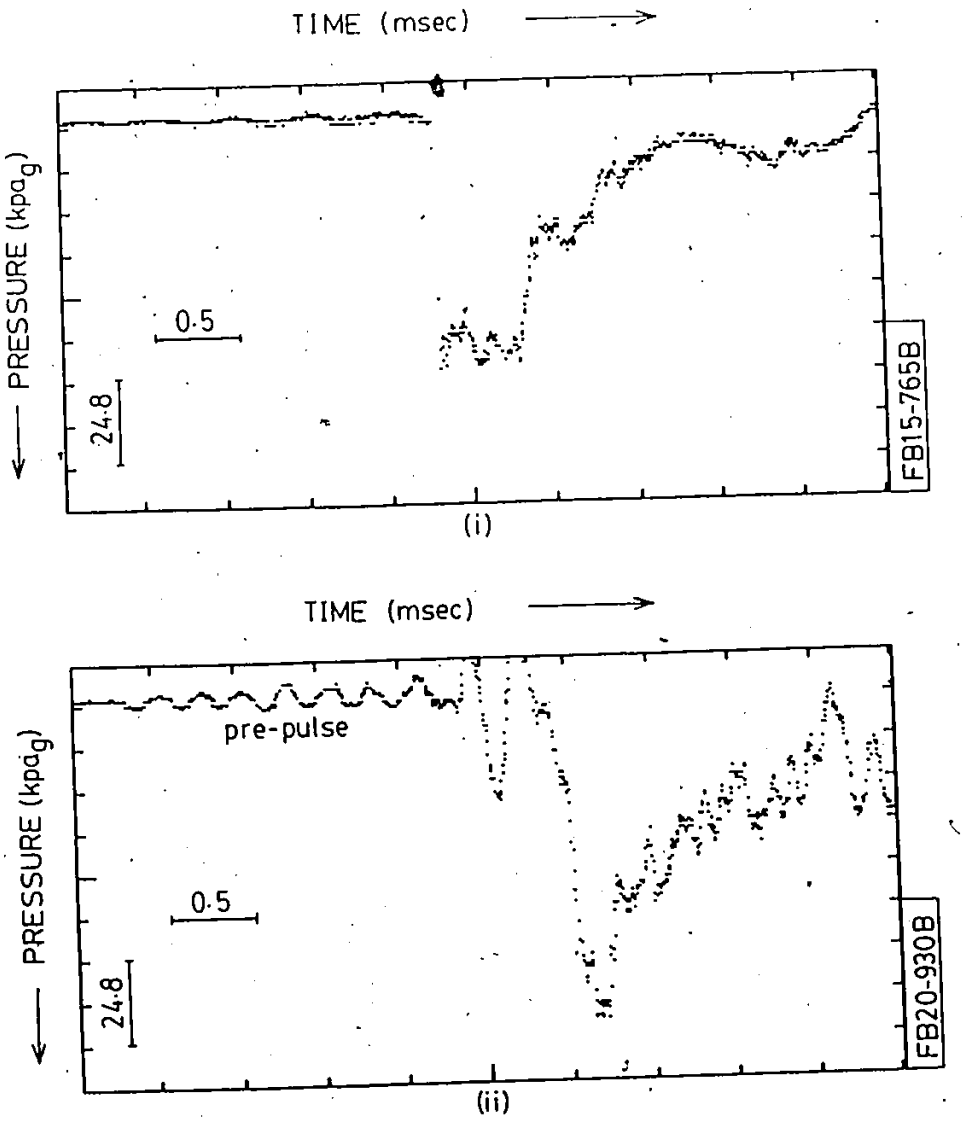

Fig. 5.9: Pressure profiles inside 37-element fuel bundle obtained with 1.90 diaphragm pressure ratio; i) gas phase and ii) liquid phase.

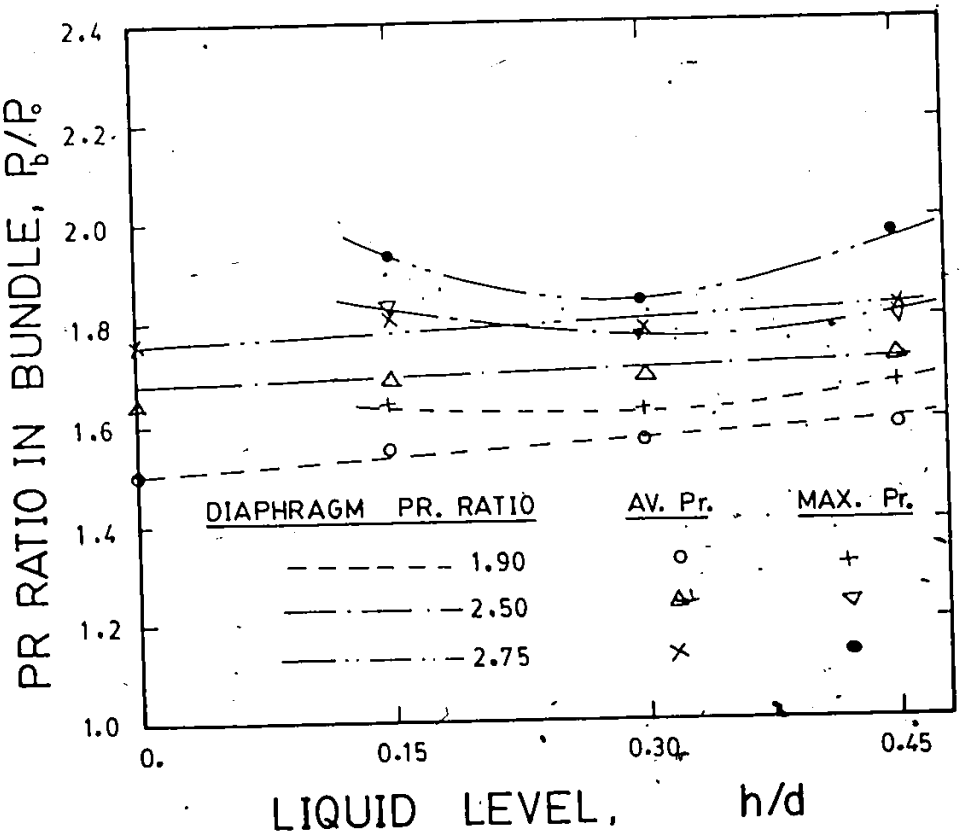

Fig. 5.10: Effect of liquid level on the overpressure (gas phase) inside 37-element fuel bundle.

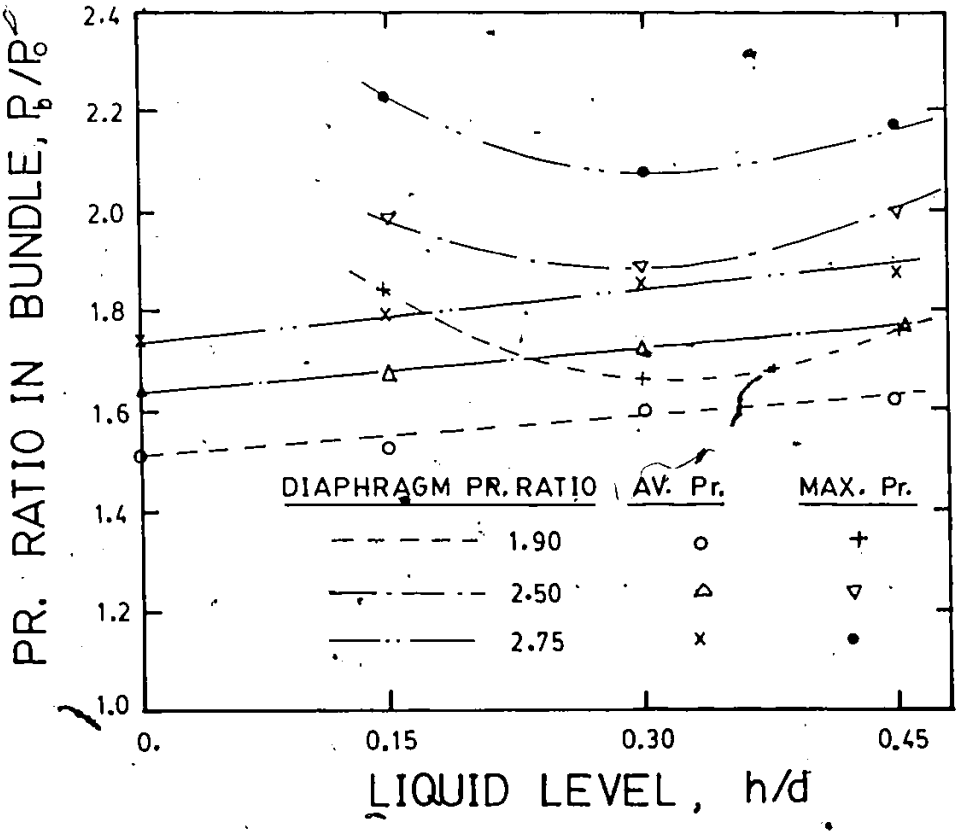

Fig. 5.11: Effect of liquid level on the overpressure (liquid phase) inside 37-element fuel bundle.

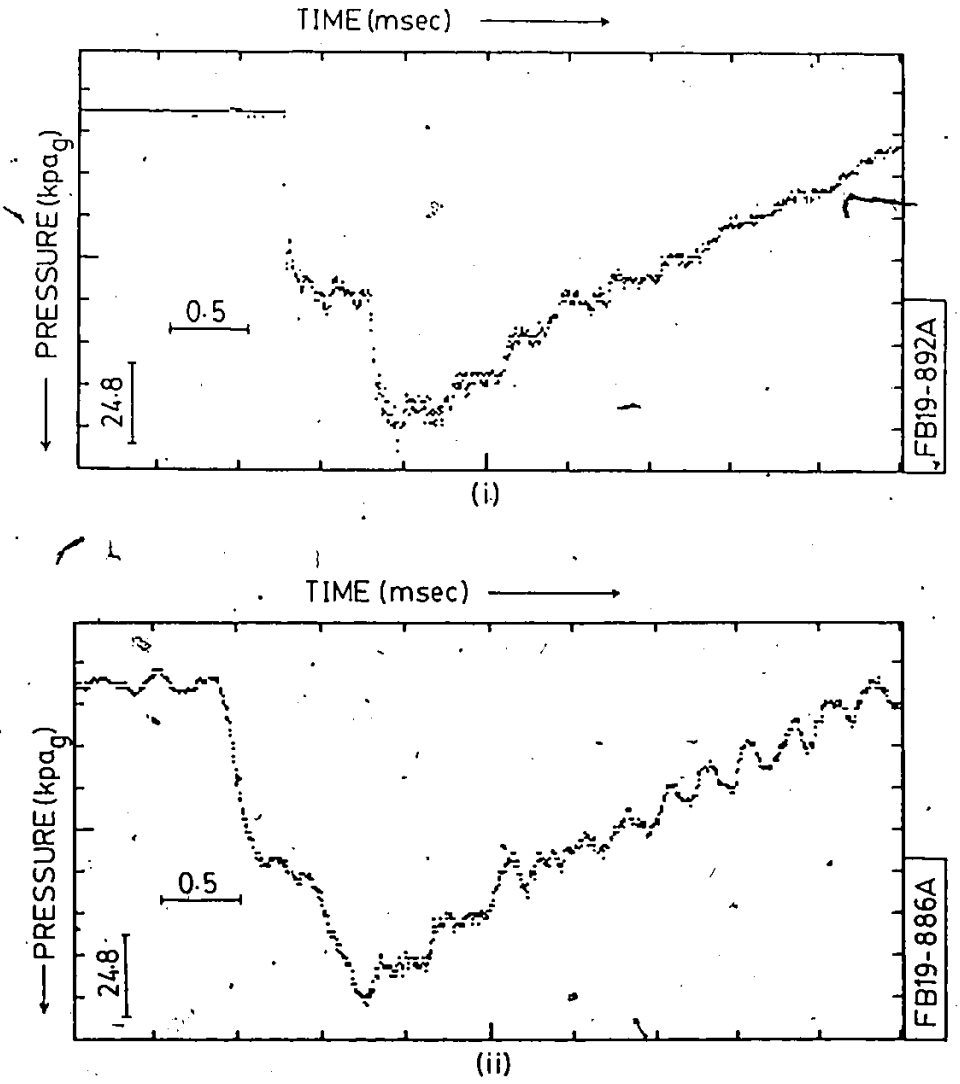

Fig. 5.12: Reflected shock strength from 37-element fuel bundle in 30 mm of liquid with 1.90 diaphragm pressure ratio; i) gas phase and ii) liquid phase.

reflected waves. In fact the strengths of the incident shock waves are found to be increasing due to the reduction in the cross sectional area of the compressible phase. This stronger wave when reflected by a fuel bundle shows a significant increase in the magnitude of the overpressure. Although the presence of liquid does not change the effective flow area of the fuel bundle, however, it reduces the effective cross sectional area of the gas phase. The increase in the strength of the shock wave may be attributed to the reduction in the area of the compressible phase. As shown in Figure 5.14, the non-linear increase in the strengths of the reflected waves at higher liquid levels is an indication of the effect of the liquid level reducing the gas phase area. However, the reduction in the flow area is observed to have more and more predominent effect on the waves transmitting through the bundle as a result of the occurrence of choking inside the bundle. Figure 5.15 depicts the effect of the choking on the transmitted wave where its strength downstream of the bundle is observed to have diminishing value for the higher liquid levels.

In evaluating the strengths of the reflected shock waves in a two-phase system, the theoretical procedures discussed earlier in this chapter may be used here. For a certain diaphragm pressure ratio and liquid level, the strengths of the incident shock waves up to the point of fuel bundle are calculated following the theoretical procedures outlined in Chapter 4. This increased strength of the incident shock wave is used to determine the strength of the reflected shock wave (considering only the gas phase system) from the theoretical plot of the reflected shock wave versus the incident shock wave. If the position of

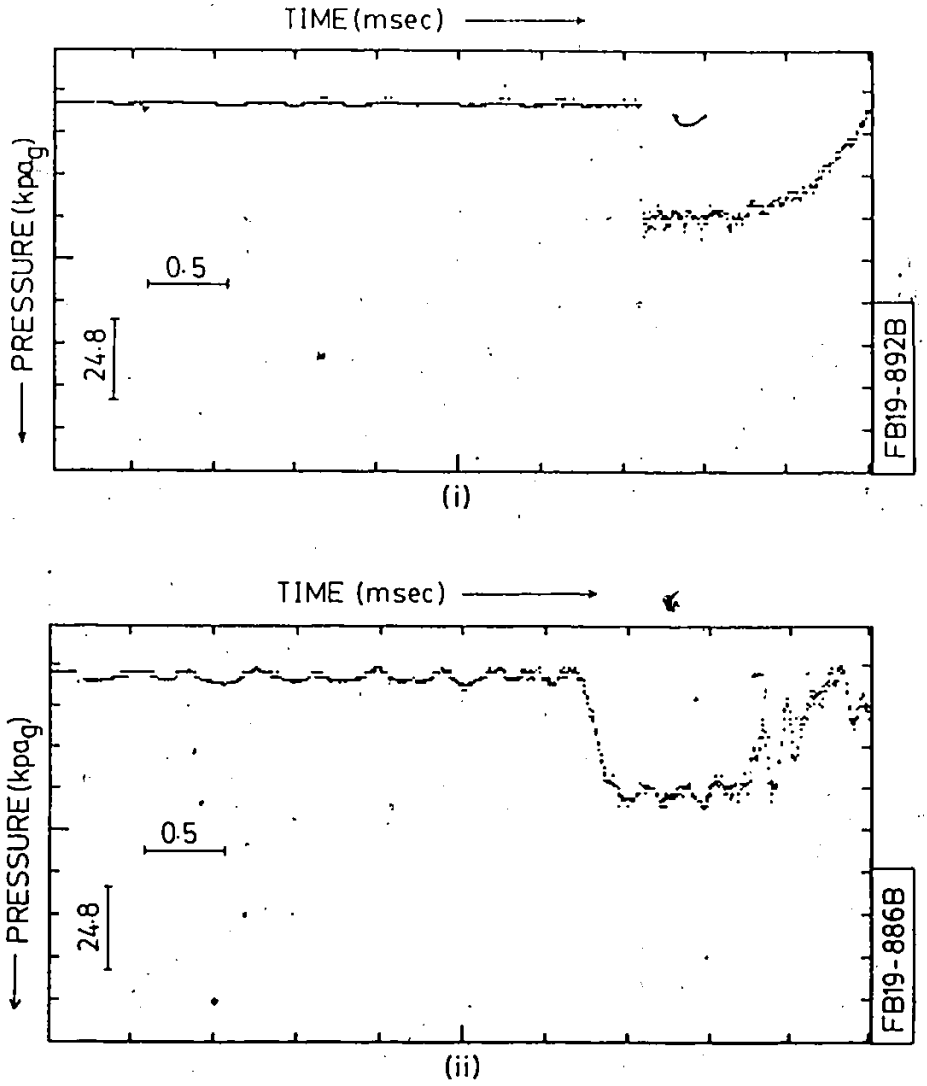

Fig. 5.13: Transmitted shock strength through 37-element fuel bundle in 30 mm of liquid with 1.90 diaphragm pressure ratio; i) gas phase and ii) liquid phase.

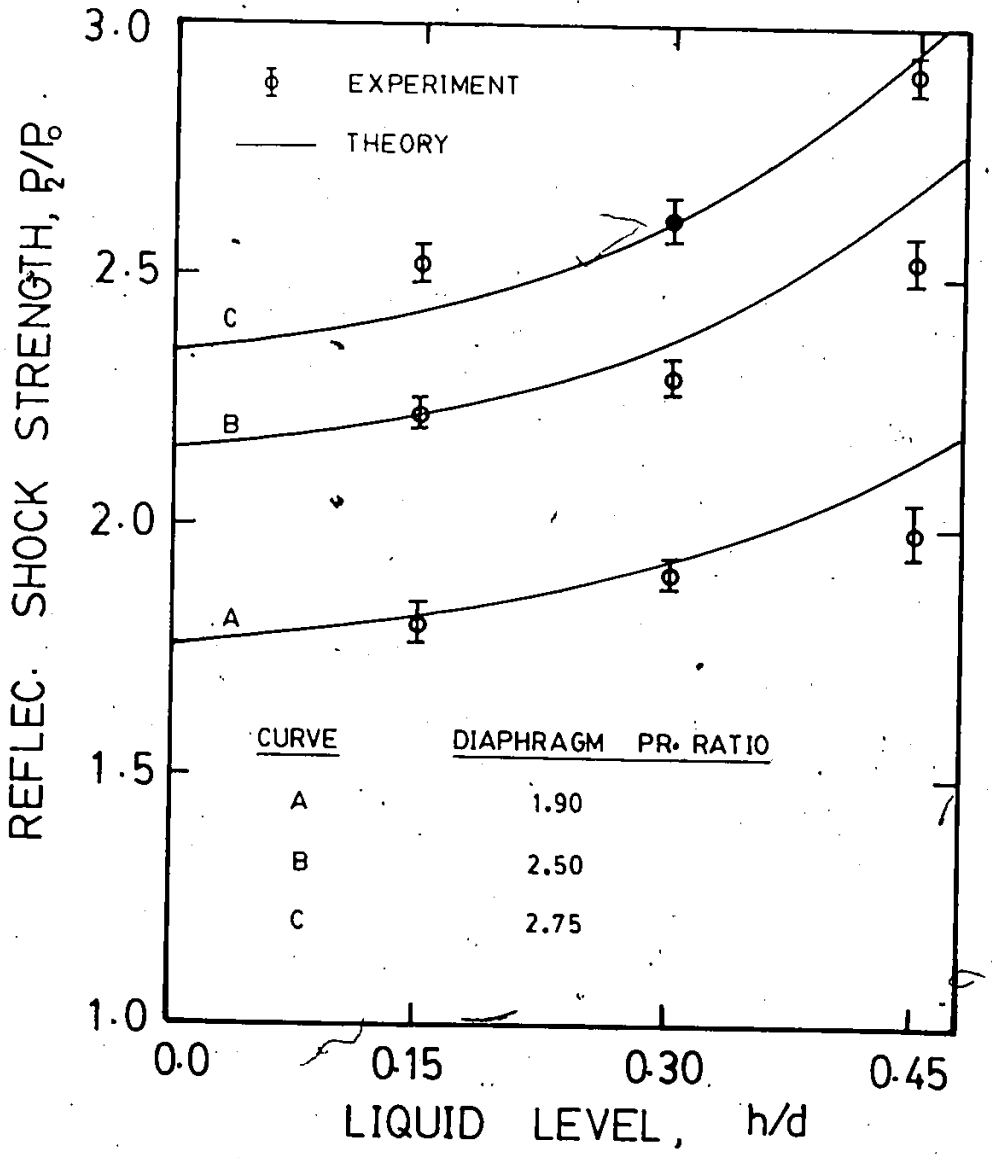

Fig. 5.14: Two-phase reflected shock strength vs. liquid level for 37-element fuel bundle.

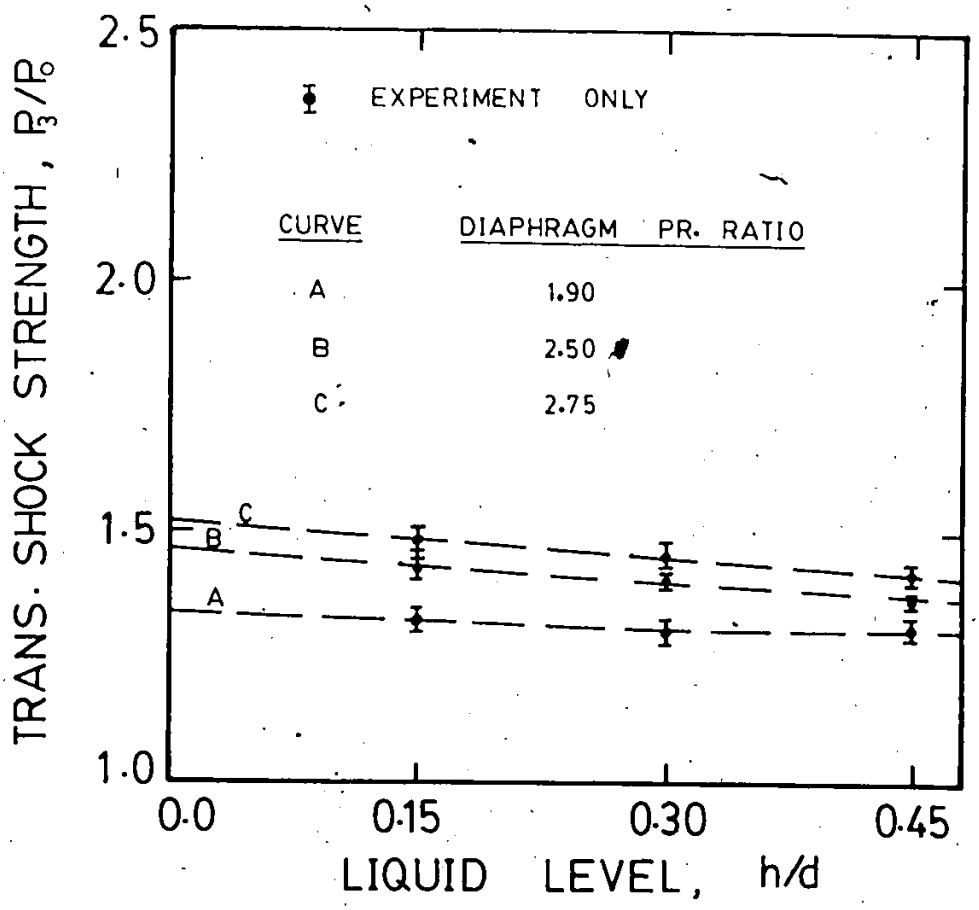

Fig. 5.15: Two-phase transmitted shock strength vs. liquid level for 37-element fuel bundle.

the transducer intercepting the reflected shock wave is far away from the face of the fuel bundle, then the calculated shock wave strengths have to be modified in a fashion similar to the proposed model mentioned in Chapter 4. The theoretical and the experimental results provided in Figure 5.14 show the effect of the increased liquid level on the strengths of the reflected waves. At higher liquid levels, the dispersion effect is high and the theoretical results over-estimate the strength of the reflected shock waves in a two-phase system.

CHAPTER 6

BRANCHED PIPE SYSTEMS

6.1 Introduction

The branched pipe system is an inevitable application in almost all the industrial sectors of the modern world. In the primary heat transport (PHT) system of CANDU-type nuclear reactors, the various pipe joints and connections make the system more complicated for the propagation of pressure waves and the subsequent effect of these waves on the stratification inside the pressure tubes has to be carefully studied. Once a shock wave is produced in the horizontal pipes, these waves make their way through the various pipe joints and connections. The complexity of the piping networks and the discontinuities in flow area render the theoretical evaluation of the behaviour of the pressure wave a difficult task.

In this chapter, the experimental evidences concerning the speed of propagation of a shock wave through the joints, effect of tap and distilled water (Appendix D) and the transverse structure of the waveforms are considered. It is observed that, the propagation of a shock wave is not affected by the presence of any network system and in the case of a stratified system, this can be predicted by the equation

used in connection with a straight pipe system. The tap water produces high oscillations in a pressure wave as it propagates through the liquid phase. Particularly, the maximum pressure peaks measured with tap water has high amplitudes. The use of distilled water, on the other hand, has mild oscillations on the overpressure. The time-averaged magnitude of the overpressure in both the tap and distilled water are very identical in all the cases of the experimental study. Also, the transverse structure of the pressure profiles is calculated from the experimental results. The plots of the experimental results suggest that although the waveforms in the gas phase follow a steady state characteristics, those in the liquid phase do not follow any particular pattern with respect to time. This indicates high pressure fluctuations in the liquid phase compared to those in the gas phase. These fluctuations have severe effects when the air bubbles are present in water, however, in the presence of the distilled water, the time dependent fluctuations are observed to be milder in character.

6.2 Shock Waves in Branched Pipes

6.2.1 Propagation in Two-Phase Systems

The single phase (gas) propagation speed downstream of the branched pipe systems is estimated from the knowledge of the time taken by the shock wave to travel a specified distance along the shock tube. The speed is calculated under normal temperature and pressure assuming that for the range of the overpressures generated by the shock waves in this work, these shock waves may be termed as weak shock waves. The

two-phase propagation speed normalized by the single phase propagation speed can be obtained using the theoretical formula of Henry et al (1968) which is presented below.

$$\frac{a_T}{a_g} = \left[1.0 + \frac{1.0 - \alpha}{\alpha} \left(\frac{\rho_g}{\rho_l}\right)\right]^{1/2} \qquad (6.1)$$

Here, a_T and a_g are respectively the propagation speeds in two-phase and gas phase systems, ρ_g and ρ_l are the densities in the gas and liquid phases respectively and α is the void fraction of the system. In stating the above formula of Henry et al (1968), the liquid phase is assumed as an highly incompressible one. Theoretically, the propagation speed in a two-phase stratified case can very well be predicted by the propagation speed in the gas phase alone. However, from the point of view of the increase in the phasic overpressure, the propagation speed should also increase, though by a very small amount. If the pressure rise in the two-phase system is neglected and the liquid is assumed incompressible, then the propagation velocity should remain the same. Anyway, the verification of this idea needs more sophisticated experimental set ups and measurements. For an increase in the incident shock wave strength from 1.5 to 1.7, the change in the propagation speed is calculated only to be about 4%. The experimental measurements of the shock wave speed downsteam of the branched pipe system is shown in Figure 6.1 and the comparison of the theoretical results of Henry et al (1968) are also shown in this figure.

6.2.2 Tap Water Vs. Distilled Water

The experimental points are selected around the junctions of

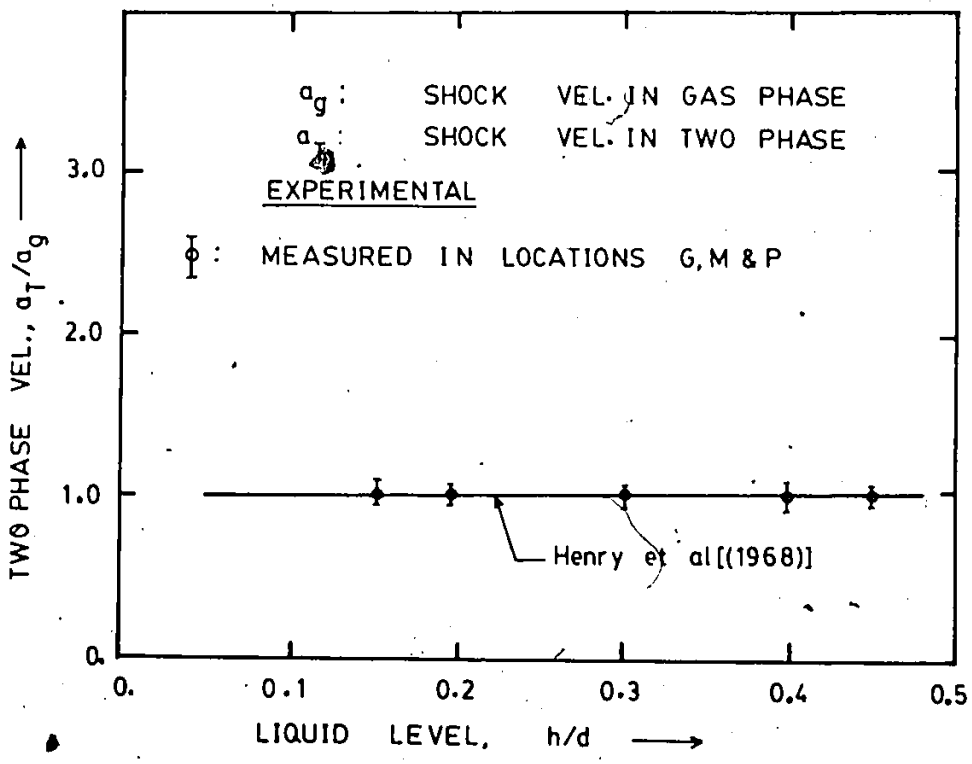

Fig. 6.1: Two-phase propagation velocity around a junction as a function of liquid level.

both symmetric and asymmetric 'TEE' joints. For the symmetric 'TEE', the transducers are located at E, G and H, and for the asymmetric case, the selected points are K, M and P. Measurements are done in both the gas and liquid phases with tap water and distilled water. In the case of tap water, the parameter of prime consideration is the magnitude of the maximum overpressure and the high frequency oscillations of the overpressure in the liquid phase. The oscillations are observed both in the incident and reflected shock waves. The results in Figure 6.2 show the maximum pressure rise as a function of liquid level upstream of the 'TEE' junction for both symmetric and asymmetric cases together with those in a straight pressure tube (location D). Similar tests are conducted for other locations in and around the junctions and in those cases, the pressure rise in gas phase is observed to be very mild whereas that in the liquid phase shows higher magnitudes of the over-pressures. The typical waveform for a two-phase system with tap water as the liquid medium are shown in Figure 6.3(i) for the gas phase; and in Figure 6.3(ii) for the liquid phase. The oscillations in the gas phase is almost absent whereas the liquid phase exhibits high frequency oscillations with sharp peaks in the overpressure. Although the experimental results are not shown here, this trend is observed in the case of tap water for all the points along the straight shock tube as well as around the 'TEE' junctions. The air bubbles with higher degree of compressibility deposited at the inner wall of (liquid phase) the shock tube act as cushions and induce oscillations as the pressure waves move through the liquid phase. Figures 6.4(i) and 6.4(ii) show the pressure traces obtained for a two-phase system with distilled water. In the liquid phase however, the oscillations are substantially reduced and

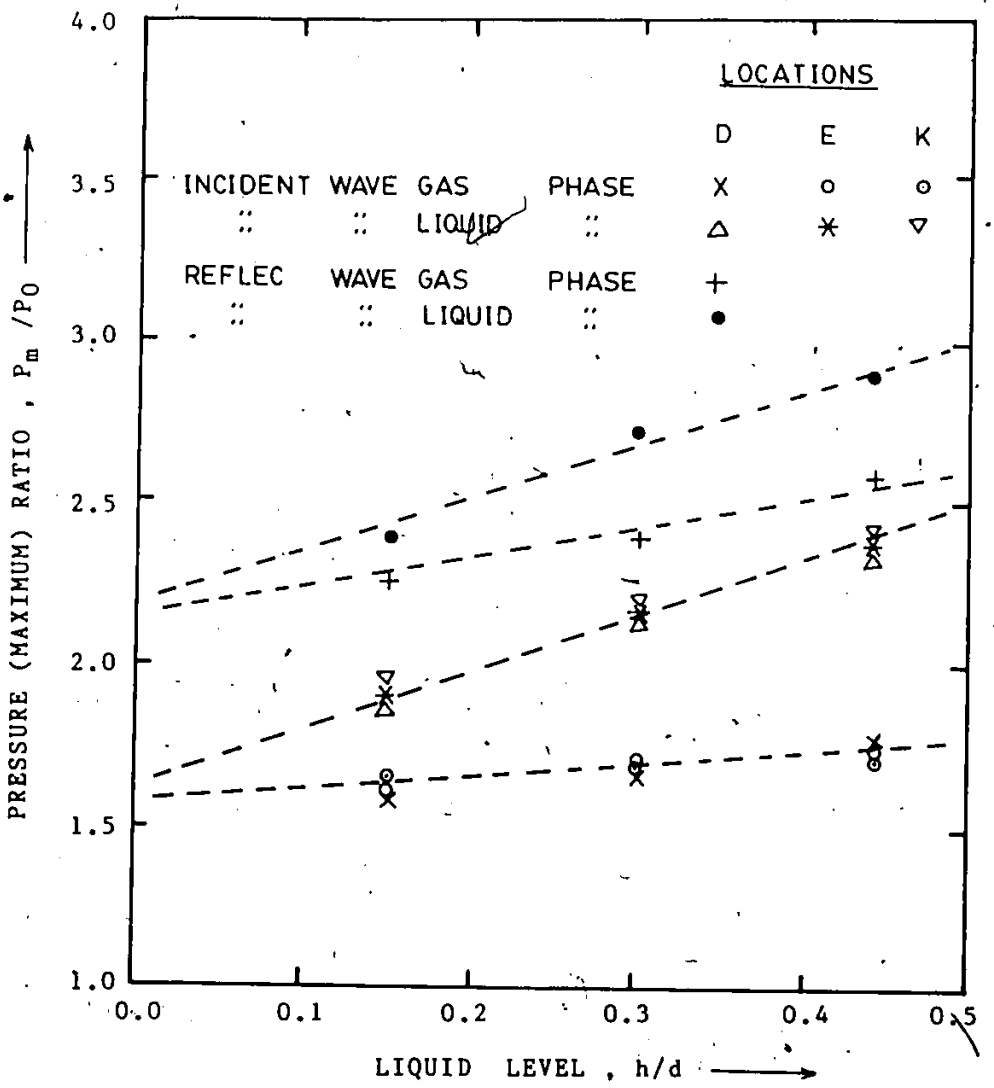

Fig. 6.2: Maximum pressure rise at locations D, E and K as a function of liquid level.

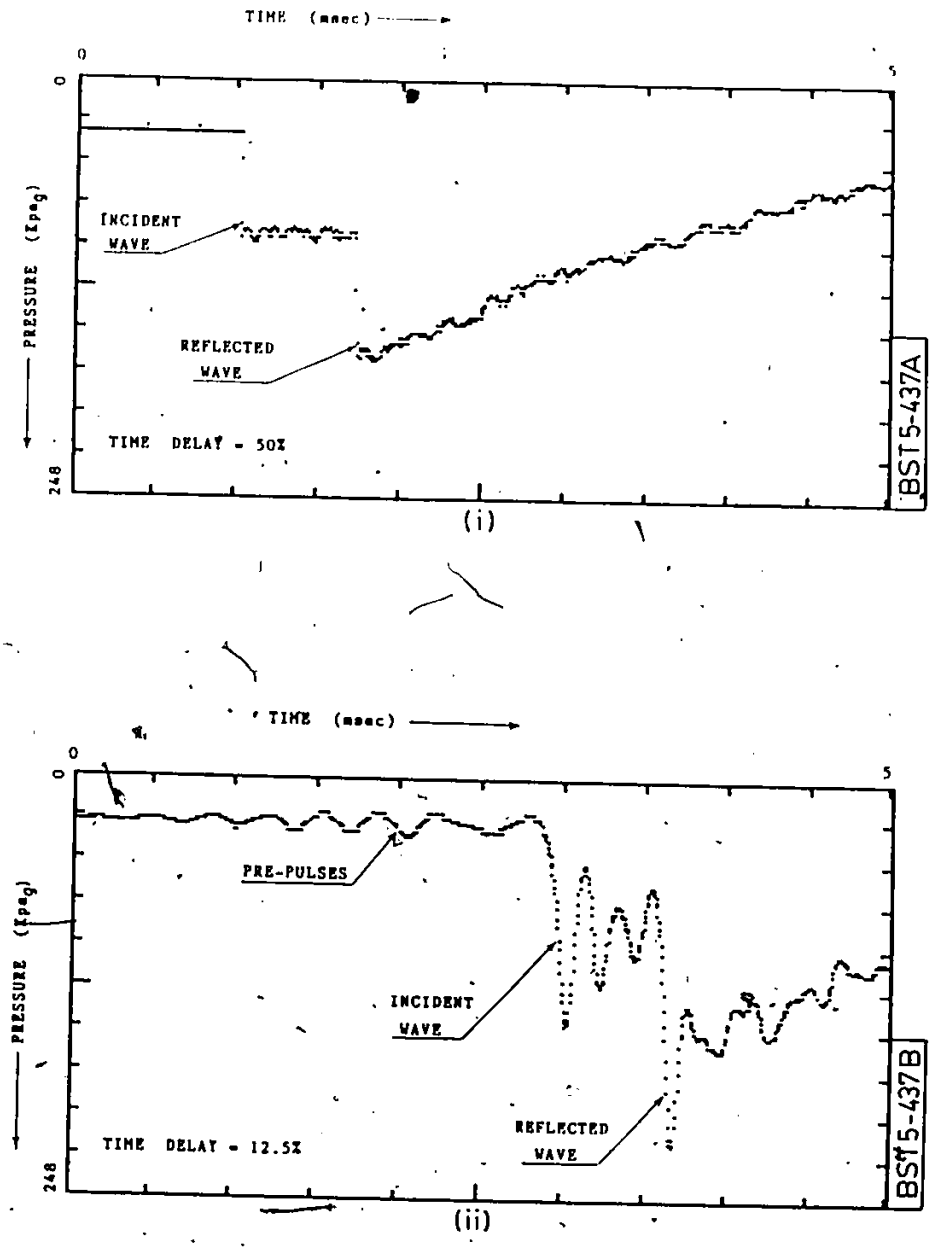

Fig. 6.3: Pressure profiles in i) gas and ii) liquid phases at location D for 30 mm liquid (tap water) level.

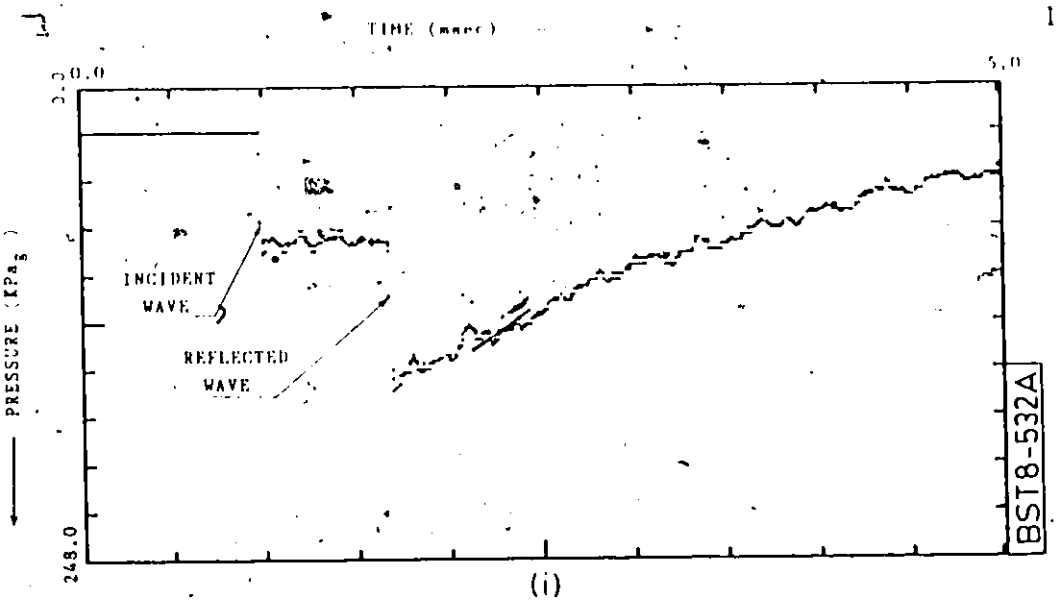

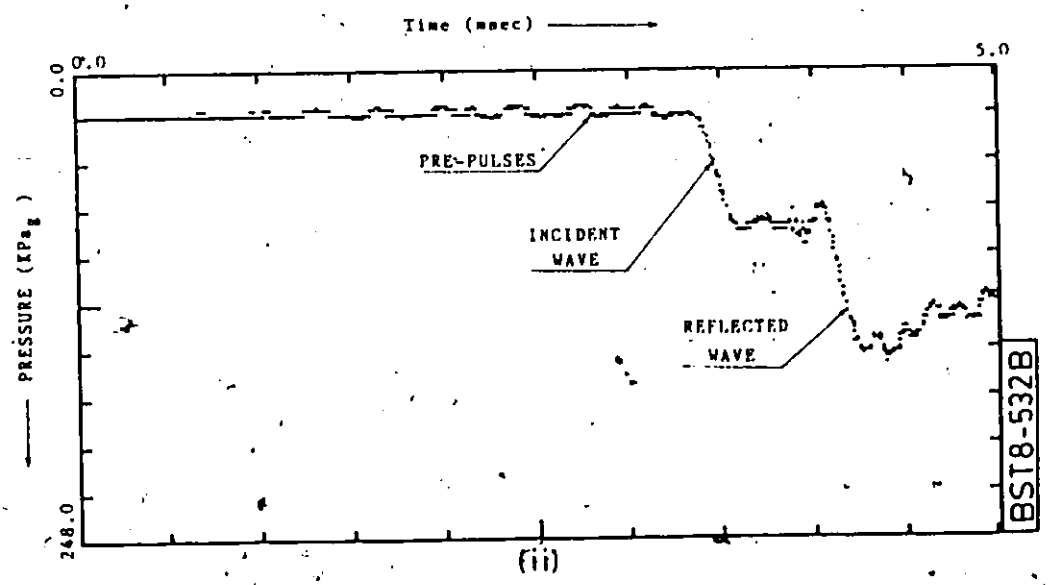

Fig. 6.4: Pressure profiles in i) gas and ii) liquid phases at location D for 30 mm liquid (Distilled water) level.

the pressure profiles in the gas phase maintain flat-topped characteristics. Similarly, the results presented in Figures 6.5(i) and 6.5(ii) for location E also show the effects of deaerated water in a two-phase stratified system. For location E, the expansion waves are also noticeable in the pressure plots. At location D the pre-pulses in liquid phase may reflect from the end plate, whereas at location E, the reflection is not present. Hence, the basic waveform is observed to have changed, though moderately because of the non-reflection of the pre-pulses at this location of the tube. The plots of the analyzed data for the overpressures only in the liquid phase for different systems with both tap and deaerated types of water are shown in Figures 6.6 to 6.9 for a diaphragm pressure ratio of 1.9. The peak pressures both in tap water and deaerated water vary significantly, however, the averaged pressures are close in these two cases at all the points along the shock tube. Also in the asymmetric 'TEE' junction, the average pressures at location M are observed to be higher than those at location P. This, though seems usual qualitatively, that at P the losses due to the turning of the flow around the junction reduces the magnitude of the overpressure.

6.3 Transverse Profile and Pre-Pulses in Pressure Tubes

6.3.1 Tap Water Case

The examination of the vertical structures of the shock waves both in single and two-phase systems reveals the fact that these waves keep changing vertically as they propagate along the shock tube. In the

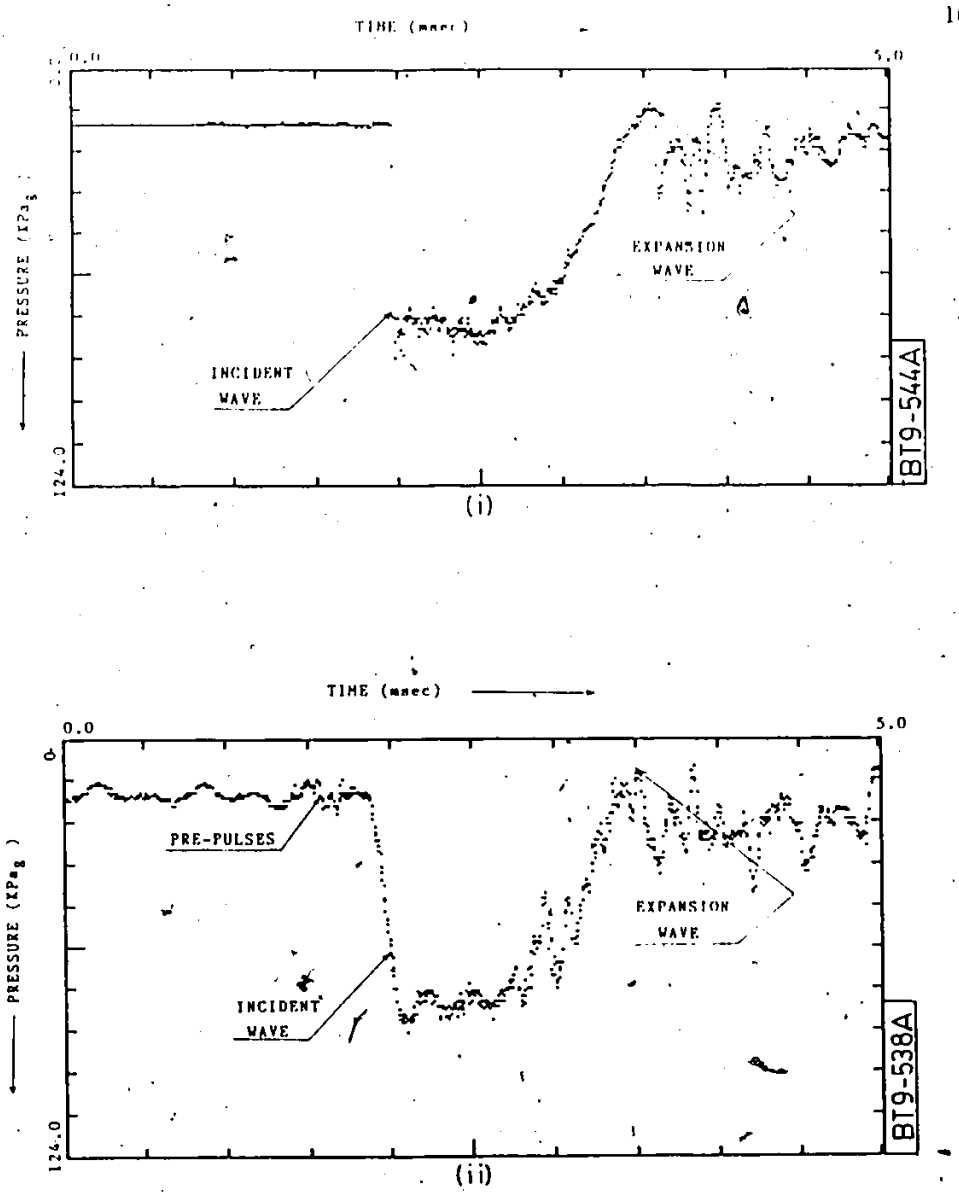

Fig. 6.5: Pressure profiles in i) gas and ii) liquid phases at location E for 30 mm liquid (distilled water) level.

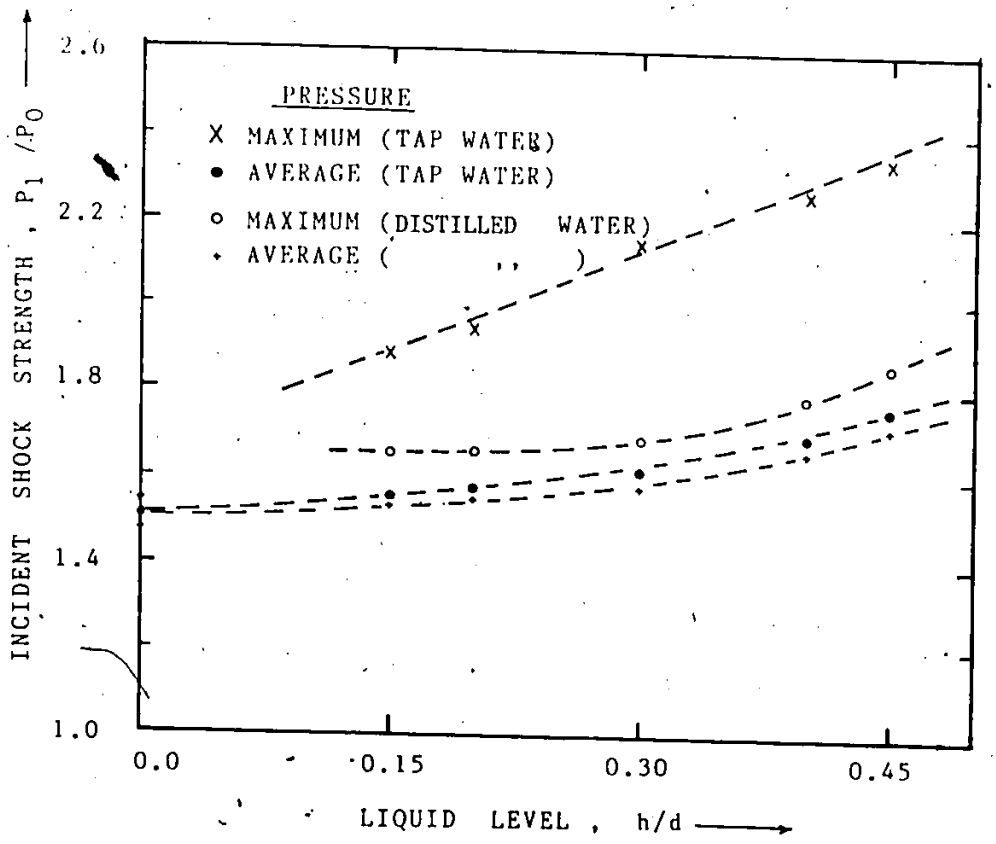

Fig. 6.6: Incident shock strength vs. liquid level at location D for tap and distilled water.

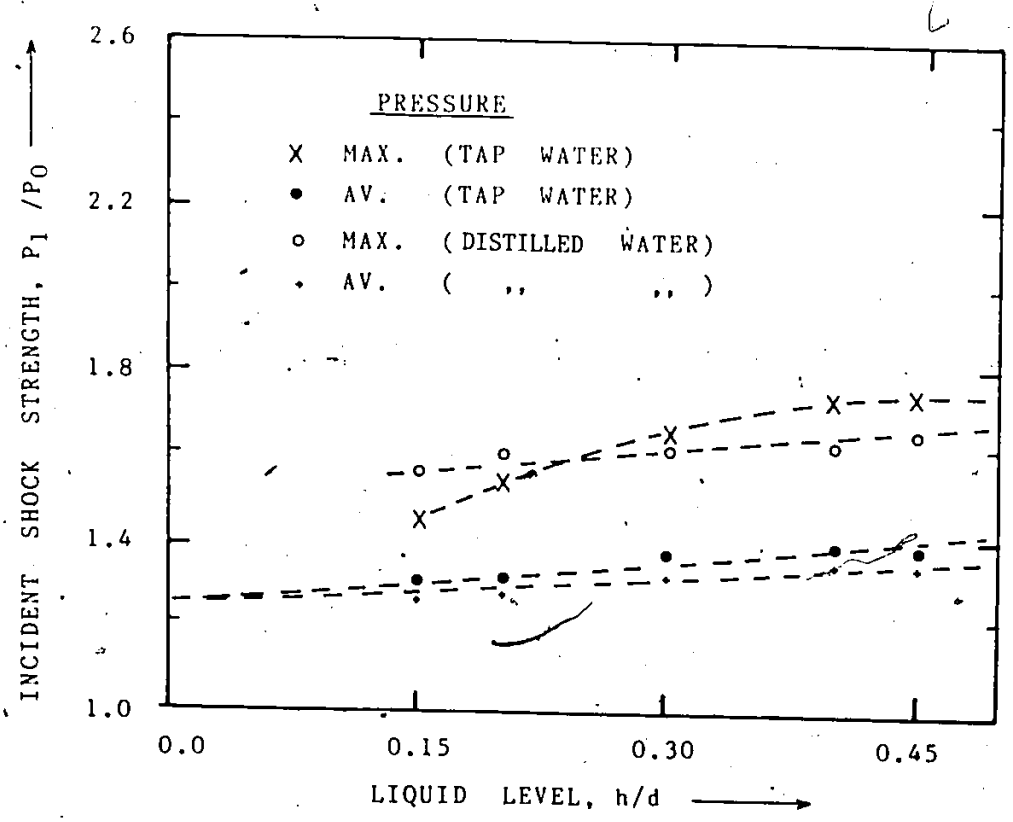

Fig. 6.7: Incident shock strength vs. liquid level at location G for tap and distilled water.

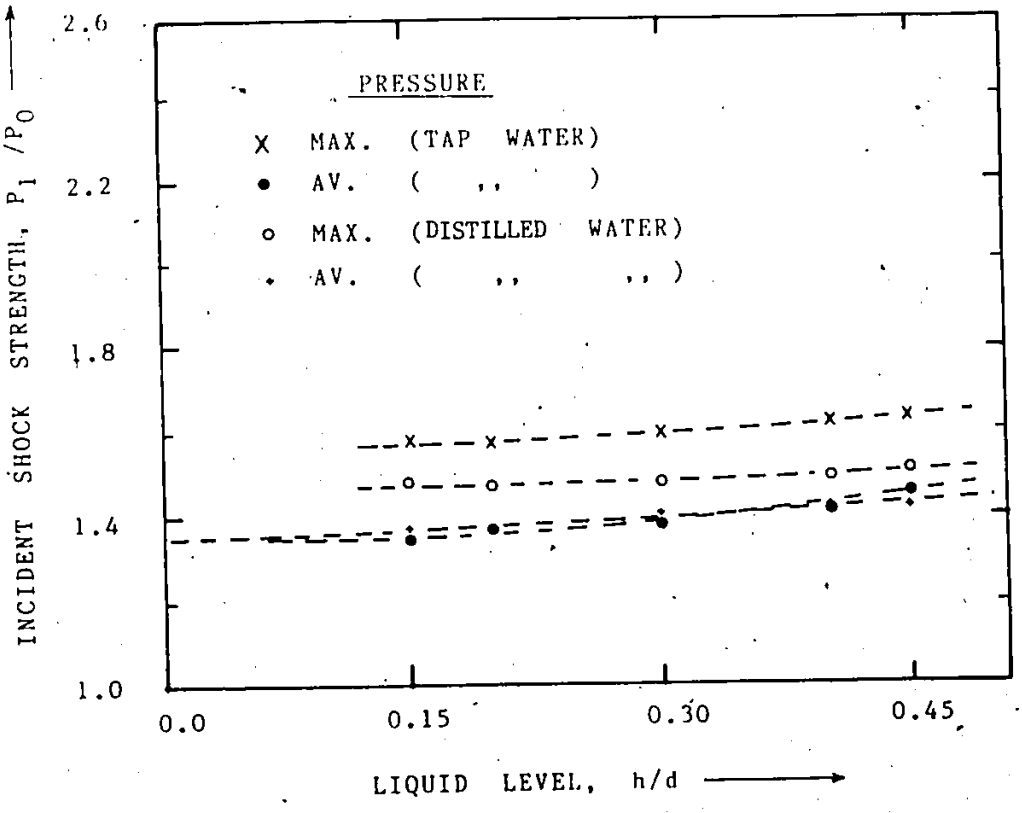

Fig. 6.8: Incident shock strength vs. liquid level at location M for tap and distilled water.

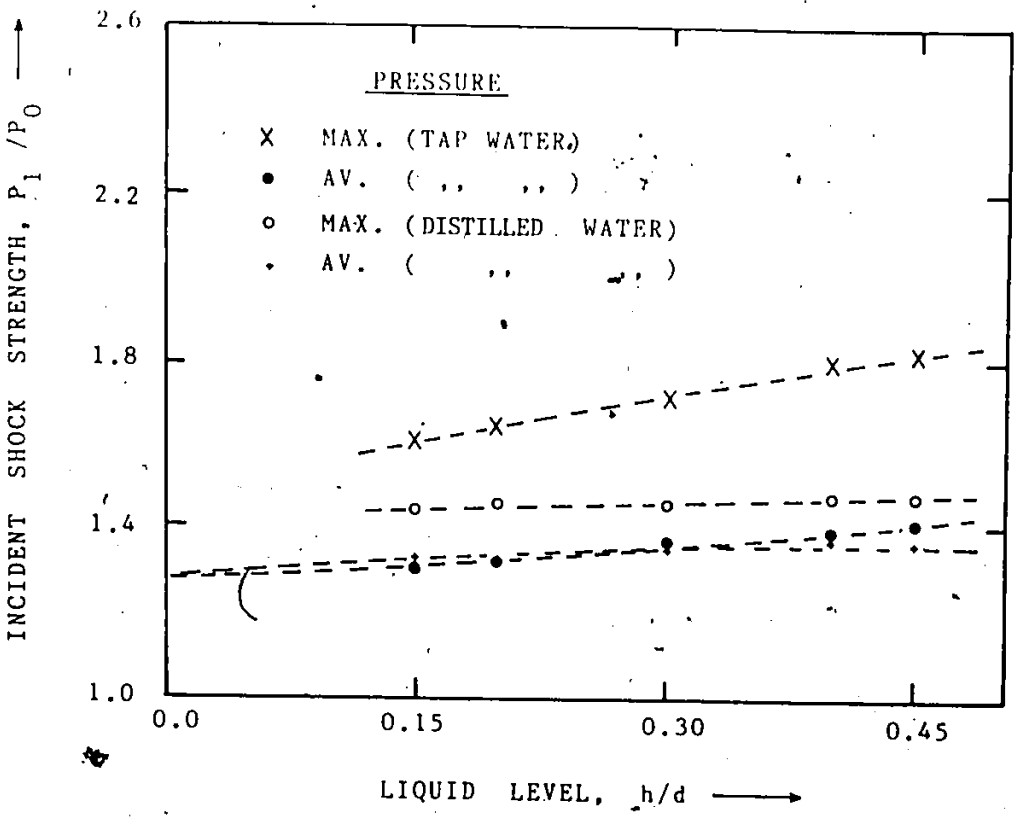

Fig. 6.9: Incident shock strength vs. liquid level at location P for tap and distilled water.

single phase, in most of the cases observed experimentally, it is found that the waves move one-dimensionally whereas in the case of the two-phase system, the vertical profiles do change significantly with time. In Figure 6.10, the vertical pressure profiles at location E for the two-phase case are plotted for different time steps. The transverse structure in the gas phase shows consistency in shape with time, however, the structure in the liquid-phase is observed to be fluctuating in time. Higher order of fluctuations are noticed to be occurring in the liquid phase. The results presented in Figure 6.10 are obtained with a diaphragm pressure ratio of 1.9. The liquid phase is highly dispersive because of the high incompressibility of this phase. When the vertical pressure profile at the junction of a symmetric 'TEE' is evaluated, the results [Sutradhar et al (1983)] show more distorted wave structure in the vertical direction. The multi-dimensional effects at the junction influence the shock wave phenomena and as a result the vertical pressure profiles at the junction of the 'TEE' section show large distortion in character. Unlike the vertical pressure profiles at location E, those at location F show higher order of distortion even under the single (gas) phase condition.

6.3.2 Distilled Water Case

Figures 6.11 and 6.12 provide the transverse pressure profiles at location E for different time intervals. In Figure 6.11, the vertical profiles are evaluated at 0.25 m-seconds interval and those in Figure 6.12, evaluated at 0.1 m-seconds interval. Looking on to the transverse pressure profiles in distilled water, a remarkable difference

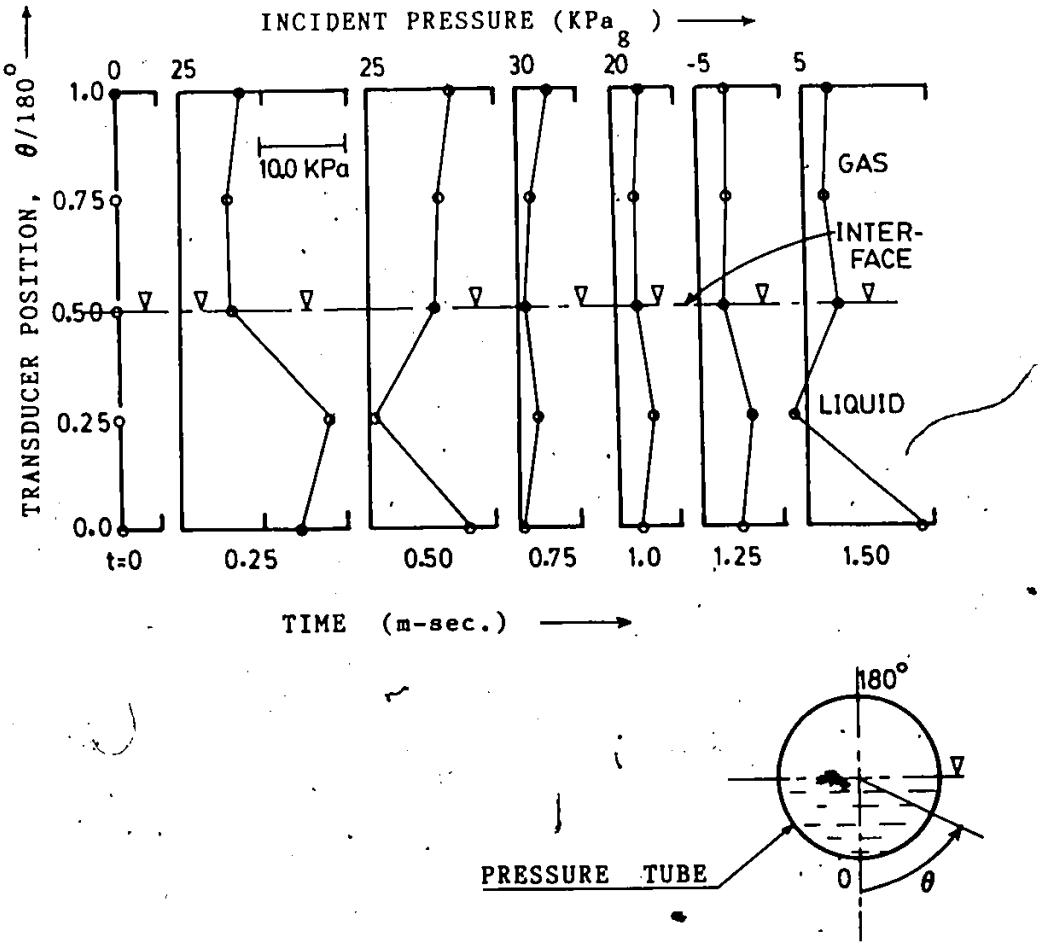

Fig. 6.10: Two-phase vertical pressure profiles at location E with tap water at 0.25 m-sec. interval.

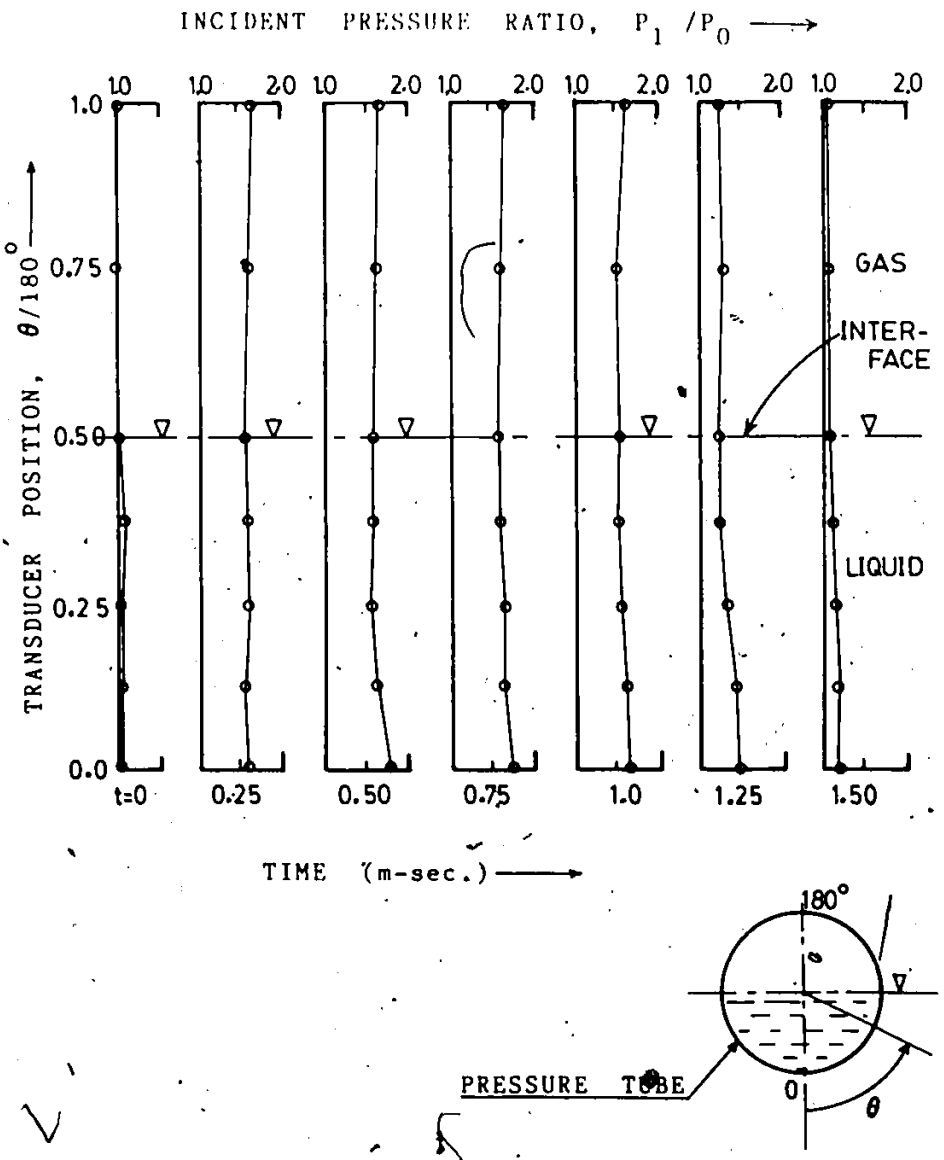

Fig. 6.11: Two-phase vertical pressure profiles at location E with distilled water at 0.25 m-sec. interval.

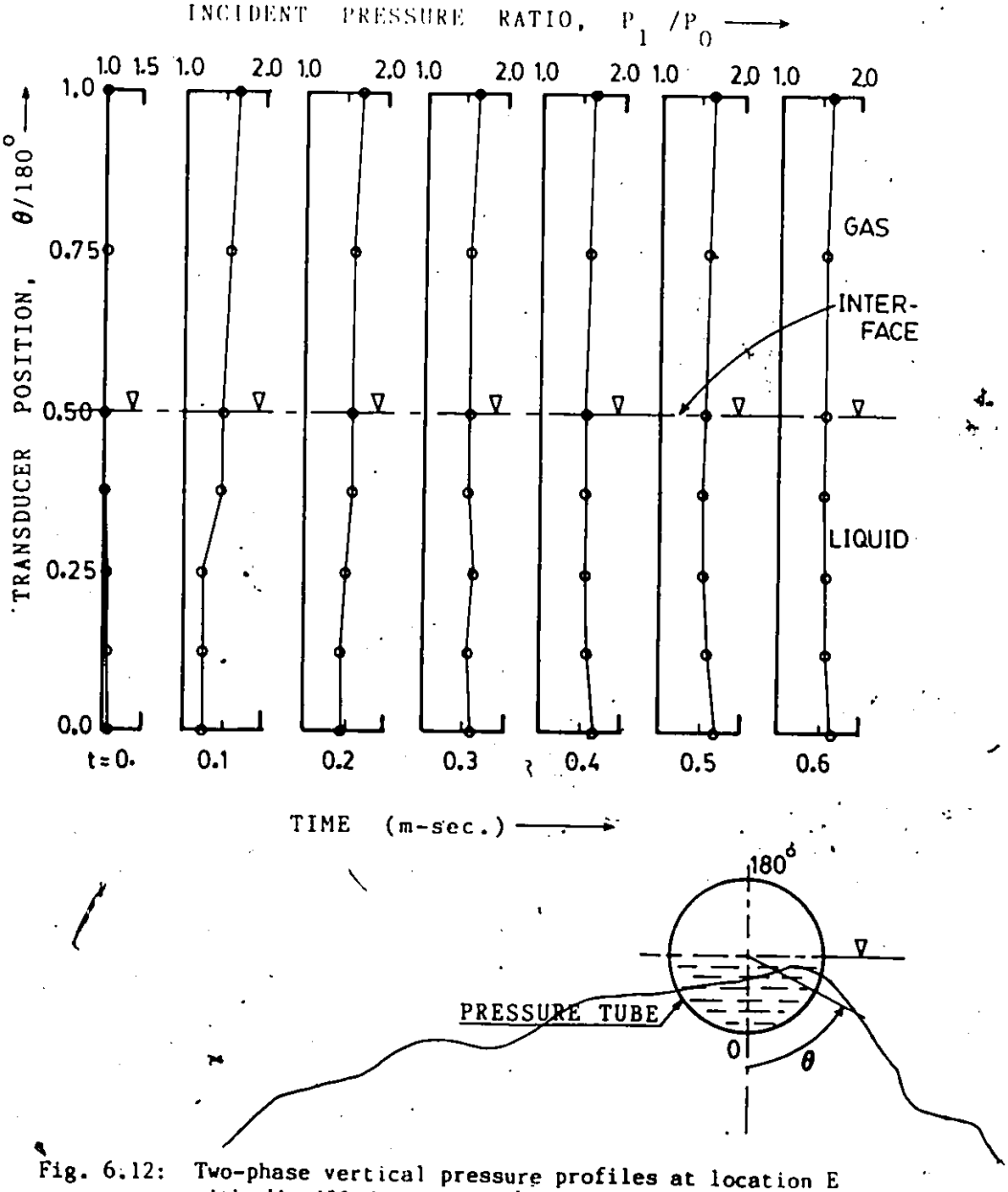

Fig. 6.12: Two-phase vertical pressure profiles at location E with distilled water at 0.10 m-sec. interval.

is noticed, that in the distilled water, the transverse profiles in gas and liquid phases are smooth in shape; the type of fluctuations present in the case of tap water are almost absent here. A comparison of the results in Figure 6.10 and Figure 6.11 confirms the finding that the presence of air bubble in the water makes the system highly unstable. In Figure 6.12, the dispersive nature of the shock wave is clearly shown. In liquid phase, the rise in overpressure is slow. Between t=0.0 and t=0.2 m-seconds, the changes in the shape of the pressure profile are quite remarkable. In the gas phase, the change is very weak in the magnitude of the overpressure.

6.3.3 Pre-Pulses in Tap and Distilled Water

The pre-pulses recorded at location D in the Aluminum pressure tube are shown in Figure 6.13(i) for tap water and Figure 6.13(ii) for distilled water. There are marked differences between these two cases. In tap water, the pre-puleş are observed to grow with the passage of the time until the formation of the shock wave in the system. These pre-pulses travel ahead of the main shock wave, but the amplitude of the pre-pulses are found to be mild in magnitude than those in the tap water case. The pre-pulses in distilled water (Figure 6.13(ii)) are noticed to move with a certain frequency for about 2 m-seconds and after that the frequency of the wave are not well defined. It seems reasonable that the portion beyond 2 m-seconds and up to the start of the shock wave is mainly influenced by the pre-pulses reflecting from the end cover attached to the straight tube. In distilled water, the first positive pulse (marked X) is recorded at about 0.85 m-seconds at

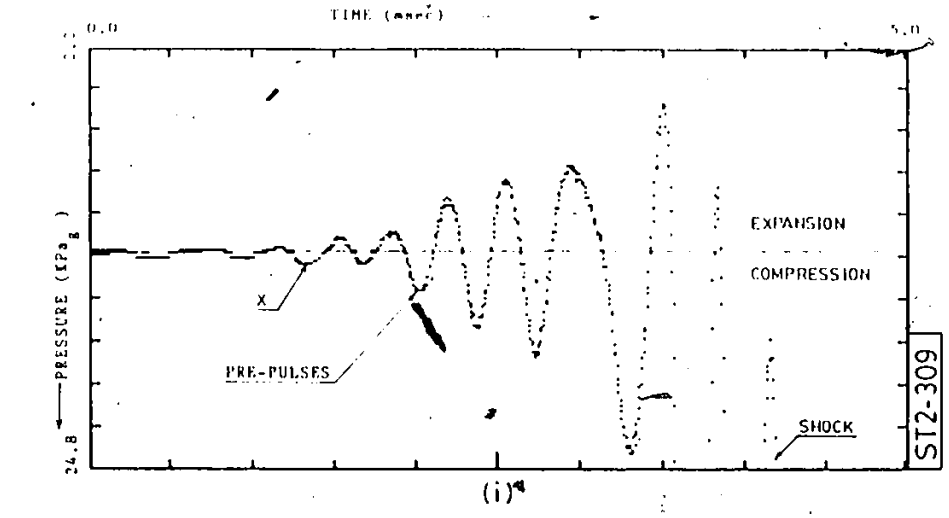

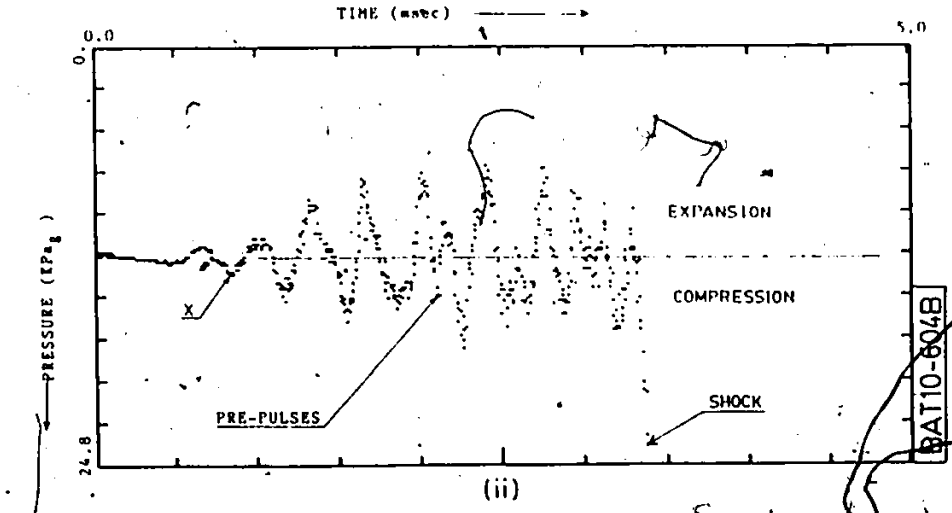

Fig. 6.13: Pre-pulses in liquid phase; i) tap water and ii) distilled water.

location D which is 1.3 meter downstream of the diaphragm separating the two chambers. With this information in hand, the velocity of the pre-pulses is calculated to be about 1530.0 m/second and this velocity is 5.5% more than the standard speed of sound in water. This increase in speed is because of the fact that the shock wave , in this case is stronger than the standard sound wave. However, in the case of tap water, the first well defined peak (marked X) is observed to reach location D much later than that observed under similar condition in the case of distilled water. The presence of air bubbles reduces the resultant propagation speed owing to the fact that the air has lower speed of sound and the combined effect is to reduce the speed of the pre-pulses in the liquid phase. The pre-pulses in both tap and distilled, contain both compression and expansion waves as the pre-pulses move through the liquid phase. This suggests that the wave reflect from the solid surface below and the interface at the top of the liquid phase. This findings are observed to be consistent with those stated by Borisov and co-workers in 1965.

CHAPTER 7

CONCLUSIONS

7.1 Present Work

From the study conducted in perspective of the shock wave propagation in a horizontal stratified two-phase system in straight and branched pipes, the following salient points of practical interest can be summarized.

1. The shock waves travelling through the liquid phase bounded by a free surface generate low amplitude pulses which induce perturbations at the gas-liquid interface ahead of the main shock wave travelling through the system.
2. The high speed gas flow induced by the shock, generates large vortex sheets behind the shock wave. The liquid layer adjacent to the turbulent flow acquires high energy and finally disintegrates into large number of small liquid droplets which are subsequently carried up in the gas phase.
3. The cause of rise in the phasic overpressure due to the presence of the liquid inside the pressure tube can be attributed to the abatement of the cross-sectional area of the compressible phase. The energy distribution in the phases confirms the fact that the interfacial

friction due to the generation of the ripples causes further reduction in the magnitude of the overpressure. However, in the present study, a net increase in the overpressure due to the increase in the liquid level is estimated.

4. The reflection of any shock wave from the fuel bundle produces stronger shock wave and depending on the porosity of the fuel bundles, a strong pulse may be transmitted through the fuel bundle. The oscillatory nature of the transmitted pressure pulse may be treated as a source of vibrations in the fuel elements. A theory is developed to predict the strengths of the reflected and transmitted shock waves from the fuel bundles for the range of the weak shock waves considered in the gas phase.

5. In a two-phase stratified system, the strengths of the reflected shock waves increase with the liquid level whereas, those of the transmitted waves either reduce or remain same with the increase in the liquid levels.

6. Experimental results for the flow around a junction confirms that the propagation speed in a two-phase stratified system can be predicted by the gas phase propagation speed for the weak shock waves.

7. The presence of the gas bubbles in the liquid phase enhances the peak pressure in the liquid phase. However, the averaged pressure in tap water and deaerated water exhibits close values of magnitudes of overpressure in the system.

8. The vertical structures of the pressure profiles show high degree of dispersion in the liquid phase. Near the interface, the vertical pressure profiles show non-linear distributions.

7.2 Practical Application

The application of the findings of this work can be usefully applied for the design of the fuel bundles to counteract the vibrational effects induced by a pressure wave propagating through the fuel bundles during the loss of coolant accidents (LOCA). The increase in the peak pressure due to the presence of the liquid inside the pressure tubes may be of special interest for the design of the flow measuring devices positioned at different critical points in the primary heat transport (PHT) system of the nuclear reactors.

7.3 Future Works

The following studies may be undertaken to understand and complement the present series of works mentioned in this thesis.

1. The mechanism of the instability of the interface and the amount of fluid mass displaced during the propagation of the shock waves through the stratified two-phase system.
2. To understand the mechanisms at the interface, Schlieren or Shadowgraph methods may be adopted to find the structure of the shock waves near the interface.
3. The effects of heat transfer in a two-component two-phase flow with stronger shock waves through the fuel bundles have to be undertaken to predict the flow phenomena in actual loss of coolant accident conditions.
4. Interactions of compression and expansion waves with the fuel

bundles completely submerged in hot liquid inside the pressure tubes should be studied to simulate the conditions of practical interests. Keeping this in mind, the knowledge of the interactions of the expansion waves with the hot fuel bundles will provide the understanding of the physical processes occurring in a real system.

REFERENCES

Anderson, J.D. (1982): "Modern Compressible Flow: With Historical Perspective"; McGraw-Hill Book Company; pp. 39-66.

Banerjee, S. and Chan, A.M.C. (1980): "Separated Flow Models-I, Analysis of the Averaged and Local Instantaneous Formulations"; Int. J. Multiphase Flow, Vol.6; pp. 1-24.

Borisov, A.A., Kogarko, S.M. and Lyubimov, A.V. (1965): "Sliding of Detonation and Shock Waves over Liquid Surfaces"; Comb. Expl. and Shock Waves, Vol. 1, No. 4; pp. 19-23.

Beavers, G.S. and Sparrow, E.M. (1971): "Compressible Gas Flow through a Porous Material"; Int. J. Heat and Mass Transfer, Vol. 14; pp. 1855-1859.

Beavers, G.S. and Matta, R.K. (1972): "Reflection of Weak Shock Waves from Permeable Materials"; AIAA Journal, Vol. 10; pp. 959-961.

Campbell, I.J. and Pitcher, A.S. (1958): "Shock Waves in a Liquid Containing Gas Bubbles"; Proc. Roy. Soc. A, Vol. 243; pp. 534-545.

Carver, M.B., Steward, D.G., Blair, J.M. and Selander, W.N. (1979): "The FORSIM-VI Simulation Package for the Automated Solution of Arbitrarily Defined Partial and/or Ordinary Differential Equation Systems"; AECL-5821, Chalk River Nuclear Laboratories, Chalk River, Canada.

Chakravarti, P.C. (1985): Private Communication, Dept. of Mathematical Sciences, McMaster University, Hamilton, Ontatio.

Chandrashekar, S. (1961): "Hydrodyanmic and Magnetohydrodynamic Stability"; Dover Publications, Inc., New York; pp. 481-507.

Cohen, L.S. and Hanratty, T.J. (1968): "Effects of Waves at a Gas-Liquid Interface on a Turbulent Air-Flow"; J. Fluid Mechanics, Vol. 31, pt. 3; pp. 467-479.

Collins, R.E. (1961): "Flow of Fluids: Through Porous Media"; Reinhold Publishing Corp., New York.

D'Arcy, D.F. (1971): "On Acoustic Propagation and Critical Mass Flux in Two-Phase Flow"; J. Heat Transfer; pp. 413-421.

Davies, P.O.A.L. and Dwyer, M.J. (1964): "A Simple Theory for Pressure Pulses in Exhaust Systems"; Proc. Instn. Mech. Engrs, Vol. 179, pt. I, No. 10; pp. 365-394.

Deckker, B.E.L. and Male, D.H. (1967a): "Unsteady Flow in a Branched Duct"; Proc. Instn. Mech. Engrs., Vol.182, pt.3H; pp. 104-112.

Deckker, B.E.L. and Male, D.H. (1967b): "Fluid Dynamic Aspects of Unsteady Flow in Branched Ducts"; Proc. Instn. Mech. Engrs., Vol. 182, pt. 3H; pp. 167-174.

DeJong, V.J and Firey, J.C. (1968): "Effect of Slip and Phase Change on Sound Velocity in Steam-Water Mixtures and the Relation to Critical Flow"; I & EC Process Design and Development, Vol. 7, No. 3; pp. 454-463.

Duffey, R.B., Tobin, R., Banerjee,S. and Stone, T. (1983): "Wave propagation in idealized separated flow"; In Proc. 3rd CSNI specialists Meeting, Hemisphere Press, Washington; pp. 111-122.

Ellis, S.R.M. and Gay, B. (1959): "the Parallel Flow of Two-Fluid Streams: Interfacial Shear and Fluid-Fluid Interaction"; Trans. Instn. Chem. Engrs., Vol. 37; pp. 206-213.

Ellison, T.S. (1957): "Turbulent transport of heat and momentum from an infinite rough plane"; J. Fluid Mechanics, Vol. 2, pt. 5; pp. 456-466.

Emanuel, G and Jones, J.P. (1968): "Compressible Flow through a Porous Plate"; Int. J. Heat and Mass Transfer, Vol. 11; pp. 827-836.

Evans, R.G., Gouse, S.W. and Bergles, A.E. (1970): "Pressure Wave Propagation in Adiabatic Slug-Annular-Mist Two-Phase Gas-Liquid Flow"; Chem. Engg. Sci., Vol. 25; pp. 569-582.

Franklin, P. (1978): "Geometry and Mansuration"; in Mark's Standard Handbook for Mechanical Engineers, Eighth Edition; Ed. T. Baumeister, McGraw-Hill Book Company., New York; pp. 2-7 to 2-15.

Hammitt, A.G. and Carpenter, H.J. (1964): "Unsteady Flow Past Junctures in Ducts"; AIAA Journal, Vol. 2, No. 12; pp. 2224-2226.

Henry, R.E. (1970): "Pressure Wave Propagation in Two-Phase Mixtures"; Chem. Engg. Progress Symposium Series on Heat Transfer, Minneapolis, Vol. 66, No. 102; pp. 1-10.

Henry, R.E. and Fauske, H.K. (1971): "The Two-Phase Critical Flow of One Component Mixtures in Nozzles, Orifices, and Short Tubes"; J.J. Heat Transfer; pp. 179-187.

Henry, R.E., Grolmes, M.A. and Fauske, H.K. (1968): "Propagation Velocity of Pressure Waves in Gas-Liquid Mixtures"; Proc., Intl. Symposium on Research in Cocurrent Gas-Liquid Flow; Ed. E. Rhodes and D.S. Scott, Plenum Press, N.Y.; pp. 1-18.

Isbin, H.S., Moy, J.E. and DaCruz, A.J.R. (1957): "Two-Phase Steam-Water Critical Flow"; A.I. Ch. E. Journal, Vol. 3, No. 3; pp. 361-365.

Ishii, M. (1976): "Thermo-Fluid Dynamics Theory of Two-Phase Flow"; Eyrolles Press, Paris.

Levy, S. (1965): "Prediction of Two-Phase Critical Flow Rate"; J. Heat Transfer; pp. 53-58.

Liepmann, H.S. and Roshko, A. (1957): "Elements of Gasdynamics"; John Wiley & Sons, Inc., New York.

Lighthill, J. (1978): "Waves in Fluids"; Cambridge University Press, Cambridge, London.

Lilleleht, L.U. and Hanratty, L.J. (1961): "Measurement of interfacial structure for cocurrent air-water flow"; J. Fluid Mechnics, Vol. 11, pt. 1; pp. 65-81.

Matsui, G. (1975): "Pressure wave propagation through a separated gas-liquid system in a duct"; Paper presented at The Annual Meeting of the ASME on Non-Equilibrium Two-Phase Flow, Houston; pp. 55-61.

Mallock, A. (1910): "Damping of Sound by Frothy Liquid"; Proc. Roy. Soc. A, 84; pp. 391-395.

Moody, F.J. (1965): "Maximum Flow Rate of a Single Component, Two-Phase Mixture"; Trans. of ASME; pp. 134-142.

Moody, F.J. (1969): "A pressure PUlse Model for Two-Phase Critical Flow and Sonic Velocity"; J. Heat Transfer, Trans. of ASME; pp. 371-384.

Mori, Y. and Hijikata, K. (1972): "Propagation of Pressure Waves in Two-Phase Flow"; Int. J. Multiphase Flow, Vol. 2; pp. 139-152.

Morioka, S. and Matsui, G. (1975): "Pressure Wave Propagation through a Separated Gas-Liquid Layer in a Duct"; J. Fluid Mech., Vol. 70, pt. 4; pp. 721-731.

Murdock, J.W. (1978): "Mechanics of Fluids"; in Marks' Standard Handbook for Mechanical Engineers, Eighth Edition; Ed. T. Baumeister, McGraw-Hill Book Comp., New York; pp. 3-53 to 3-57.

Redwood, M. (1960): "Mechanical Waveguides"; Pergamon Press, New York; pp. 57-116.

Rudinger, G. (1955): "Nonsteady Duct Flow: Wave-Diagram Analysis"; Dover Publications, Inc., New York; pp. 46-49.

Scheidegger, A.E. (1974): "The Physics of Flow through Porous Media"; 3rd. Edition, University of Toronto Press, Toronto.

Seeger, R.J. and Polachek, H. (1951): "On Shock-Wave Phenomena: Water-like Substances"; J. Appl. Phys., Vol. 22, No. 5; pp. 640-654.

Sha, W.T., Chao, B.T. and Soo, S.L. (1983): "Time averaging of Volume Averaged Conservation Equations of multiphase Flow"; AIChE Symposium Series, Vol. 79, No. 225; pp. 420-426.

Shapiro, A. (1953): "The Dynamics and Thermodynamics of Compressible Fluid Flow"; Vol. I, The Ronald Press Co., New York.

Skews, B.W. (1967a): "The shape of a diffracting shock wave"; J. Fluid Mechanics, Vol. 29, pt. 2; pp. 297-304.

Skews, B.W. (1967b): "The perturbed region behind a diffracting shock wave"; J. Fluid Mechanics, Vol. 29, pt. 4; pp. 705-719.

Sloan, S.A. and Nettleton, M.A. (1971): "The propagation of Weak Shock Waves through Junctions"; Shock Tube Research (Proc. 8th. Int. Shock Tube Symposium), Chapmann and Hall, London; Paper No. 18.

Stone, T.W. (1983): "Pressure Wave Propagation in a Horizontal Air-Water System"; Ph. D. Thesis, McMaster University, Hamilton, Canada.

Sutradhar, S.C., Yoshida, H. and Chang, J.S. (1983): "Shock Wave Propagation in a Horizontal Stratified Gas-Liquid System in Straight and 'TEE' Tubes"; Proc., 14th Intl. Sysmposium on Shock Tubes and Waves; Ed. R.D. Archer and B.E. Milton, New South Wales University Press, Australia, pp. 437-444.

Sutradhar, S.C., Yoshida, H. and Chang, J.S. (1984): "Pressure Wave Propagation in a 2-Phase Flow in Network Branches"; 10th Simulation Symposium on Reactor Dynamics and Plant Control (Canadian Nuclear Society), Saint John, New Brunswick; pp. 1-20.

Sutradhar, S.C., and Chang, J.S. (1985a): "The Role of Interfacial Frictions on the Shock Wave Propagation in Stratified Gas-Liquid Flow inside Pressure Tubes"; Proceedings, Specialists Meeting on Small Break LOCA Analysis in LWRs; Pisa, Italy; Vol. 1, pp. 243-254.

Sutradhar, S.C. and Chang, J.S. (1985b): "Shock Wave Interaction with Nuclear Fuel Bundles in Gas-Liquid Stratified Flow inside Pressure Tubes"; 15th Intl. Symposium on Shock Wave and Shock Tubes, University of California, Berkeley.

Tangren, R.F., Dodge, C.H. and Seifert, H.S. (1949): "Compressibility Effects in Two-Phase Flow"; J. Appl. Phys., Vol. 20, No. 7; pp. 637-645.

Tolstoy, I. and Clay, C.S. (1966): "Ocean Acoustics: Theory and Experiment in Underwater Sound"; McGraw-Hill Book Co., New York; pp. 97-142.

Trengrouse, G.H. and Soliman, M.M. (1966): "Effect of Sudden changes in Flow Area on Pressure Waves of Finite Amplitude"; J. Mech. Engg. Sci.; Vol. 8, No. 2; pp. 198-206.

Ursell, F. (1956): "wave Generation by Wind"; Surveys in Mechanics, Ed. G.K. Batchelor and R.M.Davies; Cambridge University Press, Cambridge; pp. 216-249.

Wade, J.H.T. (1985): Private Communicatin, Dept. of Mechanical Engineering, McMaster University, Hamilton, Ontario.

Wu, J.H.T. and Ostrowski, P.P. (1976): "shock Propagation in a 90-degree Bend"; Canadian Aeronautics and Space Journal; Vol.23, No. 5; pp. 230-242.

Yoshida, H., Tazawa, M. and Honma, H. (1980): "Reflection and Transmission of Weak Shock Waves Incident Upon a Porous material"; 58th National Meeting of JSME, Hokkaido University, Japan.

Yoshida, H., Sutradhar, S.C. and Chang, J.S. (1985): "Pressure Wave Propagation through a Horizontal Stratified Gas-Liquid system in a Straight Rectangular Duct"; To be submitted in the journal.

Zemansky, M.W. (1968): "Heat and Thermodynamics"; McGraw-Hill Book Co., New York; pp. 1-50.

APPENDIX A

Program listings of the Data Acquisition and Analysis of the data using the BASIC computer language.

```
  1  REM  THIS PROGRAM IS USED TO A
       CQUIRE DATA FOR THE SHOCK TU
       BE EXPERIMENT TOGETHER WITH
       THE MACHINE LANGUAGE PROPGRA
       M  "SHOCK-MACH".
  2  REM  THIS PROGRAM LOADED ON AU
       GUST 19, 1983.
  5  HIMEM: 35000
 10   CALL 35100
 100   HGR
 105   HCOLOR= 3
 107 SS = 125
 110   FOR I = 0 TO 1023
 115 IS = I * 279 / 1023
 117 A =   PEEK (35302 + I)
 120 B =   PEEK (36326 + I)
 123 A1 = (A - SS) * 159 / 127
 125 B1 = (B - SS) * 159 / 127
 127   IF A1 < 0 THEN A1 = 0
 128   IF B1 < 0 THEN B1 = 0
 129   HPLOT IS,A1
 130   HPLOT IS,B1
 131   NEXT I
 135   HPLOT 0,0 TO 279,0 TO 279,15
       9 TO 0,159 TO 0,0
 140 IX = 0:IY = 0
 145   FOR I = 1 TO 10
 150 IX = IX + 27.9
 155 IY = IY + 15.9
 160   HPLOT IX,0 TO IX,3
 165   HPLOT IX,159 TO IX,156
 170   HPLOT 0,IY TO 3,IY
 175   HPLOT 279,IY TO 276,IY
 180   NEXT I
 185   HPLOT 0,79.5 TO 6,79.5
 190   HPLOT 139.5,153 TO 139.5,159

 200   INPUT "DO YOU WISH TO SAVE O
       N DISK?(YES=1, NO=0)";C
 205   IF C = 1 THEN  GOTO 211
 207   HIMEM: 38400
 210   STOP
 211 D$ =  CHR$ (4)
 220   INPUT "FILENAME? ";N$
 223   PRINT D$;"BSAVE ";N$;",A3530
       2,L2048"
 225   HIMEM: 38400
 230   STOP
```

```
5  REM  THIS PROGRAM IS USED TO R
     EPLOT THE SHOCK DATA AND ALS
     O TO GET THE HARD COPY.  LOA
     DED ON DEC. 12, 1983 BY S.SU
     TRADHAR.
10  DIM A%(1023)
15 D$ =  CHR$ (4)
20  INPUT "DATA FILE NAME? ";N$
25  PRINT D$;"OPEN";N$
30  PRINT D$;"READ";N$
35  FOR I = 0 TO 1023
40 INPUT A%(I)
45  NEXT I
50  PRINT D$;"CLOSE";N$
100  HGR
105  HCOLOR= 3
110  FOR I = 0 TO 1023
115 X% = I * 279 / 1023
117 SS = 110
120 Y% = (A%(I) - SS) * 159 / 127

121  IF Y% < 0 THEN Y% = 0
122  IF Y% > 159 THEN Y% = 159
125  HPLOT X%,Y%
130  NEXT I
132  GOSUB 135
133  GOTO 200
135  HPLOT 0,0 TO 279,0 TO 279,15
     9 TO 0,159 TO 0,0
140 IX = 0:IY = 0
145  FOR I = 1 TO 10
150 IX = IX + 27.9
155 IY = IY + 15.9
160  HPLOT IX,0 TO IX,3
165  HPLOT IX,159 TO IX,156
170  HPLOT 0,IY TO 3,IY
175  HPLOT 279,IY TO 276,IY
180  NEXT I
185  HPLOT 0,79.5 TO 6,79.5
190  HPLOT 139.5,153 TO 139.5,159

195  RETURN
200  GOTO 400
201 INPUT "EXPAND WAVEFORM(YES=1
     , NO=0)? ";E
205 IF E = 1 THEN  GOTO 220
210  STOP
```

```
220  INPUT "LOWER BOUND % TIME? "
     ;LB
225  INPUT "UPPER BOUND % TIME? "
     ;UB
230 XL = LB * 1023 / 100
235 XU = UB * 1023 / 100
240 XE = XU - XL
243  HGR : HCOLOR= 3
245  FOR I = 0 TO XE
250 XI = XL + I
255 Y = (A%(XI) - SS) * 159 / 127

260 X = I * 279 / XE
265  HPLOT X,Y
270  NEXT I
273  GOSUB 135
275  GOTO 200
400  INPUT "DO YOU WISH HARDCOPY(
     1=YES, 0=NO)? ";H
405  IF H = 1 THEN  GOSUB 500
410  GOTO 201
500  PR# 1: PRINT  CHR$ (9);"GRD"

505  PR# 3: RETURN
```

```
5  REM  REPLOTTING SHOCK DATA AND
      ALSO FOR ANALYSING THE SHOC
     K DATA.
10  DIM A%(1024)
15 D$ =  CHR$ (4)
20  INPUT "DATA FILE NAME? ";N$
25  PRINT D$;"BLOAD";N$
30  INPUT "WHICH CHANNEL (A OR B)
     ? ";G$
31  IF G$ = "A" THEN MA = 35302
32  IF G$ = "B" THEN MA = 36326
35  FOR I = 0 TO 1023
40 A%(I) =  PEEK (MA + I)
45  NEXT I
100  HGR
105  HCOLOR= 3
110  FOR I = 0 TO 1023
115 X% = I * 279 / 1023
117 SS = 120
120 Y% = (A%(I) - SS) * 159 / 127

121  IF Y% < 0 THEN Y% = 0
122  IF Y% > 159 THEN Y% = 159
125  HPLOT X%,Y%
130  NEXT I
132  GOSUB 135
133  GOTO 200
135  HPLOT 0,0 TO 279,0 TO 279,15
     9 TO 0,159 TO 0,0
140 IX = 0:IY = 0
145  FOR I = 1 TO 10
150 IX = IX + 27.9
155 IY = IY + 15.9
160  HPLOT IX,0 TO IX,3
165  HPLOT IX,159 TO IX,156
170  HPLOT 0,IY TO 3,IY
175  HPLOT 279,IY TO 276,IY
180  NEXT I
185  HPLOT 0,79.5 TO 6,79.5
190  HPLOT 139.5,153 TO 139.5,159

195  RETURN
200  INPUT "EXPAND WAVEFORM (YES=
     1, NO=0)? ";E
205  IF E = 1 THEN 220
206  IF E = 0 THEN 650
210  STOP
220  INPUT "LOWER BOUND % TIME? "
     ;LB
225  INPUT "UPPER BOUND % TIME? "
     ;UB
230 XL = LB * 1023 / 100
235 XU = UB * 1023 / 100
```

```
240 XE = XU - XL
243  HGR : HCOLOR= 3
245  FOR I = 0 TO XE
250 XI = XL + I
255 Y = (A%(XI) - SS) * 159 / 127

256  IF Y < 0 THEN Y = 0
257  IF Y > 159 THEN Y = 159
260 X = I * 279 / XE
265  HPLOT X,Y
270  NEXT I
273  GOSUB 135
275  GOTO 200
301  DIM Y1(1024)
302  INPUT "WANT TO ANALYSE(YES=1
     ,NO=0)?";W1
305  IF W1 = 1 THEN 311
310  STOP
311  INPUT "LOWER LIMIT OF TIME %
     ?";L1
312  INPUT "UPPER LIMIT OF TIME %
     ?";U1
313 L2 = L1 * 1023 / 100
314 U2 = U1 * 1023 / 100
315 L3 =  INT (L2)
316 U3 =  INT (U2)
317  FOR I = L3 TO U3
320 Y1(I) = A%(I) - 127
325  NEXT I
330 YL = Y1(L3)
332 L4 = L3 + 1
335  FOR K = L4 TO U3
340 Y1(K) =  ABS (Y1(K))
345  IF YL = Y1(K) GOTO 375
350  IF YL > Y1(K) GOTO 375
355  IF YL < Y1(K) THEN YL = Y1(K
     )
360 N1 = K
375  NEXT K
385  PRINT "LARGEST VALUE IS  ";Y
     L
390  PRINT "SERIAL NO. IS  ";N1
395  INPUT "WANT TO CALCULATE MAX
      PR AND      TIME(YES=1,NO=0
     )?";F
400  IF F = 1 THEN  GOTO 410
405  STOP
410  INPUT "VALUE OF TM SENSITIVI
     TY?";S1
415 P1 = YL * 5.0 * S1
420 P2 = 127.0 * 5.0 * 0.058
425 P3 = (P1 * 6.8947) / P2
430  INPUT "VALUE OF TM CLOCKRATE
     ?";CR
435 T1 = CR * N1 / 1023
440  REM  D1 IS THE TM DELAY IN %
```

```
445  REM  T2 IS THE TIME FROM TRI
     GGER POSITION AT STATION "A"
     .
450  INPUT "VALUE OF TM DELAY?";D
     1
455 T2 = T1 + CR * D1 / 100
456  INPUT "INCIDENT SHOCK TIME %
     ?  ";X1
457 T5 = (D1 + X1) * (CR / 100)
460  INPUT "ANY REFLECTION WAVE(Y
     ES=1,NO=0)?";A1
465  IF A1 = 1 THEN 475
470  IF A1 = 0 THEN 560
475  INPUT "LOWER LIMIT OF TIME %
     ?  ";L1
480  INPUT "UPPER LIMIT OF TIME %
     ?  ";U1
485 L2 = L1 * 1023 / 100:U2 = U1 *
     1023 / 100
490 L3 =  INT (L2):U3 =  INT (U2)

495  FOR I = L3 TO U3
500 Y1(I) = A%(I) - 127
505  NEXT I
510 Y2 = Y1(L3):L4 = L3 + 1
515  FOR K = L4 TO U3
520 Y1(K) =  ABS (Y1(K))
525  IF Y2 = Y1(K) GOTO 540
530  IF Y2 > Y1(K) GOTO 540
535  IF Y2 < Y1(K) THEN Y2 = Y1(K
     )
536 N2 = K
540  NEXT K.
550 P4 = (Y2 * S1 * 6.8947) / (12
     7 * 0.058)
555 T3 = CR * N2 / 1023 + CR * D1
      / 100
558  INPUT "REFLECTION SHOCK TIME
      %? ";X2
559 T6 = (D1 + X2) * (CR / 100)
560  GOTO 700
561  PR# 1
570  PRINT N$; TAB( 12);G$
575  PRINT "AVERAGE PRESSURE
     ";P6
585  PRINT
586  PRINT
587  PRINT
600  PR# 0
605  STOP
```

```
650  POKE -16303,0
700  INPUT "AVERAGE PR (YES=1,NO=
     0)?";V1
705  IF V1 = 1 THEN 715
710  IF V1 = 0 THEN 790
715  INPUT "LOWER LIMIT  %?   ";L
     1
720  INPUT "UPPER LIMIT  %?   ";U
     1
725 L2 = L1 * 1023 / 100
730 U2 = U1 * 1023 / 100
735 L3 =  INT (L2)
740 U3 =  INT (U2)
745 Y5 = 0.0
750  FOR J = L3 TO U3
755 Y5 = Y5 + (A%(J) - 127)
760  NEXT J
765 R1 = U3 - L3
770 Y6 = Y5 / R1
775  INPUT "VALUE OF SENSITIVITY?
       ";S5
780 P6 = (Y6 * S5 * 6.8947) / (12
     7 * 0.058)
785  GOTO 561
790 P6 = 0.0
795  GOTO 561
```

APPENDIX B

Program listings for the calculation of the Shock strength using FORSIM-VI Simulation package and the overpressure in the gas and liquid phases.

```
*       ROUTINE FOR SOLUTION OF COMPRESSIBLE FLOW EQUATIONS
*
*       SUBROUTINE UPDATE
*
*****************************************************************
*       THIS SUBROUTINE IS USED TO SOLVE THE TIME DEPENDENT     *
*       NON-LINEAR HYPERBOLIC EQUATIONS DESCRIBING THE SHOCK    *
*       WAVE PHENOMENON IN A SINGLE (GAS) PHASE SYSTEM USING    *
*       "FORSIM-VI" SIMULATION PACKAGE.                         *
*****************************************************************
*
*       COMMUNICATION COMMON BLOCKS
*
        COMMON/RESERV/T,DT/CNTROL/IOUT
        COMMON/INTEGT/U(71),P(71),R(71)
        COMMON/DERIVT/UT(71),PT(71),RT(71)
        COMMON/DERIVX/UX(71),PX(71),RX(71)
        COMMON/PARTX/NCUP,NPOINT,XL,XU,AUX,AUXX,NDX,DX,X(71)
        COMMON/PARTB/BC(4,2,3)
        COMMON/PARS/PR,ALF,BET
*
        REAL RG,C(71),Q(71),QX(71),F(71)
        LOGICAL AUXX
*       DATA INPUT SECTION
        DATA RG,TT,PA,PSF,GA/287.,293.,101.325,1000.,1.4/
        DATA GC,DH,EG/9.8,0.105,1.00/
*
*
*       INITIAL CONDITION SECTION
        IF (T) 100,100,200
*
100     AUXX=.F.
        NMAX=71
        BC(4,2,1)=0
        BC(4,2,2)=BC(4,2,3)=-2
        PO=PA*PSF
        PB=PO*PR
        PV=.5*(PO+PB)
        GAA=(GA-1.)/(2.*GA)
        RV=PV/(RG*TT)
        RB=PB/(RG*TT)
        DO 120 I=1,NPOINT
           U(I)=0.
           Q(I)=0.
           P(I)=PO
        R(I)=P(I)/(RG*TT)
120     C(I)=SQRT(ABS(GA*P(I)/R(I)))
*
*
        BC(3,1,2)=PV
        BC(3,1,3)=RV
*
*
*       DYNAMIC ION TO ESTABLISH B.CS FOR IN & OUT FLOWS
*
*
200     PRS=(P(1)/PO)**GAA
        BC(4,1,2)=BC(4,1,3)=0
        BC(4,1,1)=-2
        BC(3,1,1)=AMAX1(0.,2.*C(1)*(ABS(PRS-1.))/(GA-1.))
*
*
*       CALL FORSIM ROUTINES TO APPLY B.CS AND
*       DISCRETISE DERIVATIVES
```

```
*       DEFINE EQUATIONS
        CALL PARSET (3,NMAX,U,UT,UX,UXX)
        DO 240 I=1,NPOINT
          Q(I)=-0.5*BET*DX*DX*UX(I)*ABS(UX(I))*R(I)
          IF (UX(I).GT.0.) Q(I)=0.
240     F(I)=0.5*ALF*U(I)*ABS(U(I))*F(I)/(DH*EG)
        CALL PUPX(Q,QX,X,NCUP,NPOINT,NDX)
        CALL PUPW(R,RX,U,NPOINT,DX,2)
*
        DO 260 I=1,NPOINT
          UT(I)=-U(I)*UX(I)-(PX(I)+QX(I)+F(I))/R(I)
          RT(I)=-R(I)*UX(I)-U(I)*RX(I)
          PT(I)=-GA*P(I)*UX(I)-U(I)*(PX(I)+QX(I)+F(I))
260     C(I)=SQRT(ABS(GA*P(I)/R(I)))
*
        CALL PARFIN(3,NMAX,U,UT,UX,UXX)
*
*       PRINT OUT SECTION
        IF (IOUT.EQ.0) RETURN
*
*
        CALL RITER(X,10HCOORDINATE)
        CALL RITER(U,2H U)
        CALL RITER(P,2H P)
*       CALL RITER(C,2H C)
*       CALL RITER(Q,2H Q)
*       CALL RITER(F,2H F)
        CALL PLOTS(1,1,P(30))
*
        DO 360 I=1,NMAX
        P(I)=P(I)/PO
        WRITE(8,400) X(I),P(I),U(I)
400     FORMAT(F10.3,5X,F10.3,5X,F10.3)
360     CONTINUE
        ENDO=99999
        WRITE(8,400) ENDO,ENDO,ENDO
*
        END
```

```
      SHOCK TUBE PROBLEM
*PLOTS*
 P30

*CONS*
XDTOUT      0.0001    XTFIN       0.002     XNPOINT     71.0     XMETHOD
XEMAX       0.001     XJPLOT      0.0       XICHEK      1.

*PARS*
PR          1.30      ALF         0.02      BET         10.0

*FINIT*
```

```
      PROGRAM SHTPH
C*****************************************************************
C*                                                               *
C*          THIS PROGRAM IS USED TO FIND THE VALUES OF THE       *
C*     STRENGTHS OF THE INCIDENT SHOCK WAVES IN THE PRESENCE     *
C*     OF THE LIQUID LEVEL INSIDE THE CIRCULAR PRESSURE TUBE     *
C*     USING THE FRICTIONAL EFFECT OF THE INTERFACE.  THE        *
C*     PROGRAM IS LOADED BY S.C. SUTRADHAR ON JULY 20, 1984.     *
C*                                                               *
C*****************************************************************
C
      COMMON/AMBI/PO,TO,RC,GAM,ROW,AW,AO
      COMMON/VALUE/VISC,DIAP,DIST,ETA
      COMMON/CONST/G1,G2,G3,G4,G5,G6
         PO=101325.0
         TO=293.0
         RC=287.0
         GAM=1.4
         ROW=1000.0
         AW=1440.0
         AO=343.0
C
         VISC=0.0000185
         DIAP=101.5
         DIST=1.3
         ETA=0.0034
C
C
      OPEN(5,FILE='INPUT')
      OPEN(6,FILE='OUTPUT')
      OPEN(1,FILE='SHLIQ')
      REWIND (1)
C
      G1=1./GAM
      G2=2.0*GAM/(1.0+GAM)
      G3=(GAM-1.0)/(GAM+1.0)
      G4=(GAM-1.0)/(2.0*GAM)
      G5=(GAM+1.0)/(2.0*GAM)
      G6=(2.0*GAM)/(GAM-1.0)
C
C
      DELH=1.00
      DELP=10.00
      HALF=50.0
C
      PISH=1.48
      PIN=PISH*PO
      WRITE(6,100) PISH,PIN
100   FORMAT(1H0,10X,F8.4,10X,F14.2)
C
      CALL GASD1(PIN,UGO)
      PROD=PIN*UGO
C
      HTL=0.0
      PRAV=PIN
30        CALL GVOID(HTL,VOID,DHYD,CON)
C
10        CALL GASD2(PRAV,UG,UL,RGG)
C
          CALL FRICN(PRAV,DHYD,UG,F)
C
C
      VAR1=UG-UL
      D1=DHYD/1000.0
      VAR2=F*CON*ROG*UG*VAR1*DIST/(2.0*D1)
      FRWK=VAR2*UG
```

```
      VOIDL=1.0-VOID
      PRWK=PRAV*(UG*VOID+UL*VOIDL)
      TOTWK=PRWK+FRWK
      DIFF=(PROD-TOTWK)/PROD
*
     IF (DIFF.LE.0.0) GOTO20
*
      PRAV=PRAV+DELP
        GOTO 10
20    RAT=PRAV/PO
      WRITE (1,150) HTL,RAT
      WRITE (6,110) HTL,VOID,RAT,PRAV
      WRITE(6,120) DHYD,F
      ENDPLOT=99999
*
      BRK=HTL-HALF
         IF (BRK.GE.0.0) GOTO 40
*
      HTL=HTL+DELH
        GOTO 30
150   FORMAT (5X,2F10.3)
110   FORMAT(1H0,3F10.3,F12.2)
120   FORMAT(1H ,2F20.4)
*
40    WRITE (1,*) ENDPLOT,ENDPLOT
*     PRINT *,*  *  *  *  *  *  *  *  *  *
*     PRINT *,*  *  *  *  *  *  *  *  *  *
*        IF (PISH.GT.2.6) GOTO 50
*     GOTO 5
*     STOP
*
      END
*
*
*
      SUBROUTINE GASD1(PI,UG1)
      COMMON/AMBI/PO,TO,RC,GAM,ROW,AW,AO
      COMMON/VALUE/VISC,DIAP,DIST,ETA
      COMMON/CONST/G1,G2,G3,G4,G5,G6
*
      PRI=PI/PO
      VA=SQRT(G2/(PRI+G3))
      UG1=AO*VA*(PRI-1.0)/GAM
      RETURN
      END
*
*
      SUBROUTINE GASD2(PI,UG1,UL1,ROSH)
      COMMON/AMBI/PO,TO,RC,GAM,ROW,AW,AO
      COMMON/VALUE/VISC,DIAP,DIST,ETA
      COMMON/CONST/G1,G2,G3,G4,G5,G6
      PRI=PI/PO
      VA=SQRT(G2/(PRI+G3))
      UG1=AO*VA*(PRI-1.0)/GAM
      UL1=PI/(ROW*AW)
      RO=PO/(RC*TO)
      ROSH=RO*((PRI+G3)/(1.0+PRI*G3))
*
      RETURN
      END
*
```

```
*
*
      SUBROUTINE GVOID(H1,VOIDG,DHY,CON1)


      COMMON/VALUE/VISC,DIAP,DIST,ETA
*
*
      PII=4.0*ATAN(1.0)
      CIL=2.0*(SQRT(H1*(DIAP-H1)))
      AREA=PII*(DIAP**2.0)/4.0
***
      ACS=ACOS((DIAP-2.0*H1)/DIAP)
***
      PERIL=DIAP*ACS
      VAR1=DIAP*(PERIL-CIL)/2.0+CIL*H1
      AGAS=AREA-VAR1/2.0
      VOIDG=AGAS/AREA
      PERIG=(PII*DIAP-PERIL)+CIL
      DHY=4.0*AGAS/PERIG
      CON1=CIL/DHY
*
      RETURN
      END
*
*
*
      SUBROUTINE FRICN(PAV,DHY,UG1,F)
      COMMON/AMBI/PO,TC,RC,GAM,ROW,AW,AO
      COMMON/VALUE/VISC,DIAP,DIST,ETA
      COMMON/CONST/G1,G2,G3,G4,G5,G6
*
      PRS=PAV/PO
      RE=(UG1*DHY)/(VISC*1000.0)
      TOLER=1.E-5
* IF DIAP IN METER THEN ETA ALSO BE IN METER
      ET1=ETA/(DIAP*1.25)
      ET=ET1*PRS
*
*
      FOO=.05
      FO=FOO
*
        DO 10 ITER=1,100
      VAR1=ET/3.7
      VAR2=2.51/RE
      VAR3=VAR2/SQRT(FO)
      VAR4=VAR1+VAR3
*
      F1=1.0/(-2.0*LOG10(VAR4))**2.0
*
      ERROR=ABS(F1-FO)
        IF (ABS(F1).GT.1.E-10) ERROR=ERROR/ABS(F1)
        IF (ERROR.LT.TOLER) GOTO 20
*
      FO=F1
*
10    CONTINUE
20    F=F1
      RETURN
      END
```

APPENDIX C

Program listings for the estimation of the strengths of the reflected and transmitted shock waves through CANDU Fuel bundles.

```
      PROGRAM WAVES
*
*****************************************************************
*     THIS PROGARM IS USED TO CALCULATE THE STRENGTHS OF        *
*     THE REFELECTED AND TRANSMITTED SHOCK WAVES UNDER          *
*     SINGLE (GAS) PHASE SYSTEM.  THE PROGRAM IS LOADED         *
*     BY S.C. SUTRADHAR ON NOVEMBER 15, 1984.                   *
*****************************************************************
*
      COMMON/VALUE/E,EDD,DIA
      COMMON/SET/G,DIST,DIAH,FRIC
      PO=101325.0
      TO=293.0
      AO=343.0
      RO=1.205
      RC=287.0
      G=1.4
      TOLER=1.E-5
      DIA=0.105
      DIST=0.5
      EDD=1.5E-6
      VISC=16.8E-6
      OPEN(5,FILE='INPUT')
      OPEN(6,FILE='OUTPUT')
*
      OPEN(1,FILE='REFLEC')
      OPEN(2,FILE='TRANS')
      OPEN(3,FILE='AMACH')
      OPEN(4,FILE='BMACH')
      REWIND (1)
      REWIND (2)
      REWIND (3)
      REWIND (4)
*
      G1=(G-1.)/(2.0*G)
      G2=1.0/G1
      G3=(G+1.0)/(2.0*G)
      G4=1.0/G3
      G5=(G-1.0)/(G+1.0)
      G6=1.0/G5
      E=0.2
      WRITE (6,45)
45    FORMAT (1HL,'SHOCK WAVE WITH FUEL BUNDLE ANALYSIS')
      WRITE (6,55)
55    FORMAT (1H0,10X,'INCID. PR.',6X,'REFL. PR.',5X,'TRANS. PR.')
3     D=(1.0-E)/(1.0+E)
      WRITE(6,50) E
50    FORMAT(1H0,'THE POROSITY =    ',F10.3)
      PRINT *,'
      PRINT *,'
      PI=1.0
      P2=1.0
      PT=1.0
5     C1=2.0*(PI**G1)-1.0
      P5=C1**G2
        IF (E.LE.0.0) THEN
      PR2=P5
      PTT=0.0
      WRITE (6,60) PI,PR2,PTT
      ELSE
          IF (PI.LE.1.0) THEN
      P2=1.0
      PT=1.0
      AMB=0.0
      AMEX=0.0
```

```
      WRITE (6,60) PI,P2,PT,AMB,AMEX
            IF ((E.GT.0.239.AND.E.LT.0.241).OR.
     +          (E.GT.0.289.AND.E.LT.0.291).OR.
     +          (E.GT.0.319.AND.E.LT.0.321)) THEN
      WRITE(1,60) PI,P2
      WRITE(2,60) PI,PT
      WRITE(3,60) PI,AMB
      WRITE(4,60) PI,AMEX
            ENDIF
*     PRINT *,'          '
*     PRINT *,'          '
         ELSE
      R1=RO*(1.0+G6*PI)/(G6+PI)
      C2=SQRT(G4/(PI+G5))
      U1=AO*(PI-1.0)*C2/G
      T2=PI*RO/R1
      T3=SQRT(T2)
      A1=AO*T3
      DO 10 ITER=1,100
        P3=P2/PI
      R2=(1.0+G6*P3)/(G6+P3)
      R3=1.0/R2
      C4=(1.0-R3)
      V1=SQRT(G1+G3*P3)*A1
      C5=(V1+U1)
      C6=C4*R1*(C5**2.0)
*
*
      GP1=P2-PI+P2*D*(P5/P2-1.0)-C6/PO
      P2=P2+TOLER
      PP3=P2/PI
      RR2=(1.0+G6*PP3)/(G6+PP3)
      RR3=1.0/RR2
      CC4=(1.0-RR3)
      VV1=SQRT(G1+G3*PP3)*A1
      CC5=(VV1+U1)
      CC6=CC4*R1*(CC5**2.0)
*     CC7=CC6/PO
*     CC8=P2*D*(P5/P2-1.0)
      GP2=P2-PI+P2*D*(P5/P2-1.0)-CC6/PO
      P2=P2-TOLER
      DGP=(GP2-GP1)/TOLER
      DELTAP=-GP1/DGP
      ERROR=ABS(DELTAP)/ABS(P2)
        IF (ERROR.LT.TOLER) GO TO 20
      P2=P2+DELTAP
   10  CONTINUE
   20  CONTINUE
      U4=R3*U1-V1*C4
      R4=R2*R1
      DIAH=DIA*SQRT(E)
      TRAT=P3/R2
      ACS2=A1*SQRT(TRAT)
      AMA2=U4/ACS2
      ATAS1=(2.0/(G+1.0)+AMA2**2.0/6.0)
      ATAS=ATAS1**3.0/AMA2
      ABAS=E*ATAS
        CALL AMBI(ABAS,AMB)
      XCON1=1.0+AMB**2.0/5.0
      TEMB=TO/XCON1
      ACSB=SQRT(G*RC*TEMB)
      VELB=AMB*ACSB
      XCON2=1.0+AMA2**2.0/5.0
      XCON3=XCON2**3.5
      PTO2=XCON3*P2*PO
```

```
      PRESB=PTO2/(XCON1**3.5)
      RODB=PRESB/(RC*TEMB)
      REY=VELB*DIAH/VISC
        CALL FRICTN(REY,FRIC)
        CALL FANNO(P2,AMB,AMEX,DF2,PFAN)
      DRAG=FRIC*RODB*(VELB**2.0)*DIST/(2.0*DIAH)
      DRAG=0.0
      Q2=R4*(U4**2.0)
        DO 15  ITER1=1,100
        C8=SQRT(G4/(PT+G5))
      U5=AO*(PT-1.0)*C8/G
      Q3=Q2*(1.0-U5/U4)
      GPT1=PT-PFAN+D*(PFAN-1.0)-Q3/PO+DRAG/PO
      PT=PT+TOLER
      C8=SQRT(G4/(PT+G5))
      U5=AO*(PT-1.0)*C8/G
      Q3=Q2*(1.0-U5/U4)
      GPT2=PT-PFAN+D*(PFAN-1.0)-Q3/PO+DRAG/PO
      PT=PT-TOLER
      DGPT=(GPT2-GPT1)/TOLER
      DELTAPT=-GPT1/DGPT
      ERROR=ABS(DELTAPT)/ABS(PT)
        IF (ERROR.LT.TOLER) GOTO 40
      PT=PT+DELTAPT
15    CONTINUE
40     WRITE (6,60) PI,P2,PT,AMB,AMEX
*     WRITE (6,60) VELB,DIAH,REY,FRIC,RODB
*     WRITE (6,60) ABAS,ACSB,AMA2,PRESB
*     WRITE (6,60) PTO2,PFAN,DF2,DRAG
*     PRINT *,
*
            IF ((E.GT.0.239.AND.E.LT.0.241).OR.
     +          (E.GT.0.289.AND.E.LT.0.291).OR.
     +          (E.GT.0.319.AND.E.LT.0.321)) THEN
      WRITE(1,60) PI,P2
      WRITE(2,60) PI,PT
      WRITE(3,60) PI,AMB
      WRITE(4,60) PI,AMEX
          ENDIF
        ENDIF
      ENDIF
60     FORMAT (1H ,5X,5F13.3)
      PI=PI+0.10
        IF (PI.LE.2.1) GOTO 5
      E=E+0.10
      ENDPLOT=99999
          IF ((E.GT.0.249.AND.E.LT.0.251).OR.
     +        (E.GT.0.299.AND.E.LT.0.301).OR.
     +        (E.GT.0.329.AND.E.LT.0.331)) THEN
      WRITE(1,*) ENDPLOT,ENDPLOT
      WRITE(2,*) ENDPLOT,ENDPLOT
      WRITE(3,*) ENDPLOT,ENDPLOT
      WRITE(4,*) ENDPLOT,ENDPLOT
        ENDIF
        IF (E.LE.0.5) GOTO 3
      STOP
      END
*
*
*
      SUBROUTINE AMBI(ABAS,AMB)
      G=1.4
        IF (ABAS.LE.1.0) THEN
      AMB=1.0
      ELSE
```

```
      BMB=0.01
    5   CON1=(2.0/(G+1.0))+BMB**2.0/6.0)
      CON2=(CON1**3.0)/BMB
      CON3=ABAS-CON2
        IF (CON3.GE.0.0) GOTO 10
      BMB=BMB+0.01
      GOTO 5
   10   AMB=BMB
      ENDIF
      RETURN
      END
*
*
*
      SUBROUTINE FRICTN(REY,FRI)
      COMMON/VALUE/E,EDD,DIA
        IF (E.LE.0.0) THEN
      FRI=0.0
      ELSE
*     DIAH=DIA*SQRT(E)
*     ETAD=EDD/DIAH
      TOLER=1.E-5
      FOO=0.001
      FO=FOO
        DO 10 ITER=1,100
*     VAR1=ETAD/3.7
*     VAR2=2.51/REY
*     VAR3=VAR2/SQRT(FC)
*     VAR4=VAR1+VAR3
      VAR4=REY*SQRT(FO)
*     F1=1.0/(-2.0*LOG10(VAR4))**2.0
*     F1=1.0/(2.0*LOG10(VAR4)-0.8)**2.0
      FO=FO-TOLER
      ERROR=ABS(F1-FO)
        IF (ABS(F1).GT.1.E-10) ERROR=ERROR/ABS(F1)
        IF (ERROR.LT.TOLER) GOTO 20
      FO=F1
   10   CONTINUE
   20 FRI=F1
      ENDIF
      RETURN
      END
*
*
*
      SUBROUTINE FANNO(PP2,AAMB,AAMEX,DF2,PFANNO)
      COMMON/SET/G,DIST,DIAH,FRIC
      ALF=(G-1.0)/2.0
      DFE=FRIC*DIST/DIAH
*  TO FIND THE MACH NUMBER AT INLET
      CXM1=LOG(1.0+ALF)-LOG(1.0+ALF*(AAMB**2.0))
      CXM2=0.5*(1.0+ALF)*CXM1
      CXM3=0.5*(1.0-1.0/(AAMB)**2.0)
      CXM4=(1.0+ALF)*(LOG(1.0)-LOG(AAMB))
      CXM5=2.0*(CXM2-CXM3-CXM4)/G
      DF1=CXM5
      DF2=DF1-DFE
        IF (DF2.LE.0.0) THEN
      AAMEX=1.0
        ELSE
      TOL=1.0E-05
      A=AAMB
      B=1.0
*
      F2=CXM5-DF2
```

```
      F3=0.0-DF2

      PROD1=F2*F3
        IF (PROD1.LE.0.0) GOTO 1
      AAMEX=1.0
      GOTO 20
1     ERROR=ABS(B-A)
5     ERROR=ERROR/2.0
        IF (ERROR.LE.TOL) THEN
      XI=(A+B)/2.0
      AAMEX=XI
        ELSE
      XM=(A+B)/2.0
      XMTOL=XM+TOL
          IF (XMTOL.EQ.XM) THEN
      XI=(A+B)/2.0
      AAMEX=XI
          ELSE
      AMS=XM
      CXMM1=LOG(1.0+ALF)-LOG(1.0+ALF*(AMS**2.0))
      CXMM2=0.5*(1.0+ALF)*CXMM1
      CXMM3=0.5*(1.0-1.0/(AMS)**2.0)
      CXMM4=(1.0+ALF)*(LOG(1.0)-LOG(AMS))
      CXMM5=2.0*(CXMM2-CXMM3-CXMM4)/G
      FUNM=CXMM5-DF2
      PROD2=F2*FUNM
        IF (PROD2.LE.0.0) GOTO 10
      A=XM
      F2=FUNM
      GOTO 5
10      B=XM
      GOTO 5
*     AAMEX=(A+B)/2.0
          ENDIF
      AAMEX=(A+B)/2.0
        ENDIF
      ENDIF
20    CONTINUE
*
*
*   TO FIND THE PRESSURE AT THE EXIT OF THE BUNDLE
      CXP2=LOG(AAMB*SQRT(1.0+0.2*(AAMB**2.0)))
      PSTAR2=EXP(0.0911607-CXP2)
      CXP3=LOG(AAMEX*SQRT(1.0+0.2*(AAMEX**2.0)))
      PSTAR3=EXP(0.0911607-CXP3)
      PREX=PSTAR3/PSTAR2
*
*
      PFANNO=PREX*PP2
      RETURN
*
      END
```

APPENDIX D

Solubility of air in water at normal temperature and pressure

The solubility coefficient, α [Baldwin and Daniel (1952)] is defined as the volume of gas reduced to 0-degree celsius and 760 mm pressure of Hg, which is absorbed by the unit volume of solvent under a gas pressure of 760 mm of Hg. In general, the solubility may be stated as follows [Battino and Clever (1966)]

$$\alpha = (V_g \frac{273.15}{T} \frac{p_g}{760})(\frac{1}{V_s})(\frac{760}{p_g}) \qquad (D1)$$

where p_g is the partial pressure of the gas above the solution, T is the absolute temperature, V_g is the volume of gas absorbed (at T and the total pressure of the measurement) and V_s is the volume of the absorbing solvent. For the system at atmospheric pressure, Equation D1 may be reduced to the following [Battino and Clever (1966)]

$$\alpha = \frac{V_g}{V_s}(\frac{273.15}{T}) \qquad (D2)$$

The solubility coefficient for air in water at 20-degree celsius is 0.0186 [Baldwin and Daniel (1952)] and this is very close to the value stated in the International Critical Tables (1928). The solubility of gases in water, in general, are always decreased as the temperature is increased and this statement may also be realized from Equation D2. Solubility of gases does not depend on pressure and referring Markham and Kobe (1941) it can be stated that under equal circumstances of temperature, water takes up, in all cases , the same volume of condensed gas as of gas under ordinary pressure.

In the experiment performed in this dissertation, the tap water was at a temperature of about 12-14 degree celsius. The distilled water did not show any temperature difference with the ambient condition. Using Equation D2, it can be shown that the solubility coefficient for both tap and distilled water varies only about 2%. As the distilled water was at a higher temperature than the tap water, the solubility was less by 2% than that of the tap water. This value is very well within any experimental measurement.

The presence of gas bubbles in the tap water may be attributed to the fact that, unlike the distilled water, the tap water contains a considerable amount of dissolved minerals. Such solutes may react with the metalic tube containing the water and produce gas bubbles. Also the tap water was at a lower temperature than that of the surrounding air. In that case, the gas bubbles trapped at the troughs of the roughness of the inner surface may be enlarged at the equilibrium temperature.

REFERENCES

Baldwin, R.R. and Daniel, S.G. (1952): J. Appl. Chemistry, 2; pp.161-165

Battino, R. and Clever, H.L. (1966): Chem. Rev., 66; pp.395-463.

International Critical Tables (1928), Volume 3 by National Research Council of U.S.A.

Markham, A.E. and Kobe, K.E. (1941): Chem. Rev., 28; pp.519-588.